Columbia University

Doctoral Thesis

Interaction and Disorder in Novel Condensed Matter Systems

Yonah Lemonik

A thesis submitted in fulfilment of the requirements
for the degree of Doctor of Philosophy
in the Graduate School of Arts and Sciences

2015

COLUMBIA UNIVERSITY

Abstract

Interaction and Disorder in Novel Condensed Matter Systems

by Yonah Lemonik

Despite almost a century of exploration, we continue to discover new systems where quantum mechanics, strong interactions and disorder combine in novel ways. These systems test the capabilities of our strongest theoretical tools. In this thesis I discuss work on three of these systems: bilayer graphene, disordered conductors and cold atom systems. In bilayer graphene I show that the large number of degenerate bands leads to a plethora of possible spontaneous symmetry breaking ground state. In disordered conductors I discuss how quantum interference can lead to arbitrarily long lived responses, so called memory effects. I also consider whether a novel spontaneous symmetry breaking state can be created in cold atomic gasses using non-equilibrium perturbations.

Contents

List of Figures

List of Tables

Acknowledgements

"Disorder, that hath spoil'd us, friend us now!"

William Shakespeare, *Henry V*

I gratefully acknowledge the support and guidance of Igor Aleiner, from whom I learned almost all of my physics.

I would also like to acknowledge Allan Blaer and Andy Millis, who have been present throughout my long time at Columbia, and who played pivotal roles in my development.

The work on graphene was done jointly with Vladimir Fal'ko. The work on cold atom systems was done with Boris Altshuler.

This work is dedicated to my wife Rachel.

Chapter 1

Introduction

Condensed matter should be a solved field. By 1965, fifty years ago, the theories of Fermi-liquid, Anderson localization, the Landau classification of phase transitions and the BCS mechanism had already been established and the basic tenets of band-theory and transport were already over a generation old. Nonetheless, novel condensed matter systems continue to be discovered at a brisk pace. In the last ten years we have been introduced to cold atomic gasses, exfoliated 2D crystals, new ultrathin films, a plethora of semi-conductor hetero-structures and topological materials. These new systems challenge the basic paradigms of the field and present difficult challenges to theoretical technique.

The root of the difficulty and promise of these novel systems is disorder and strong interaction. Both of these take us away from the simple picture of band theory that has served so well. In this thesis we discuss three systems where interaction and disorder play a large role: bilayer graphene, disordered metallic films and RF pumped atomic gasses. The difficulty posed by each of these systems is a reminder that we really have no handle on the general problem of interacting, disorder fermions. Instead we must grope our way forward on a case by case basis.

In Chapter 2 we analyze the phase diagram of bilayer graphene (BLG) at zero temperature and zero doping. A very large number of spontaneous symmetry breaking ground states are a priori possible. We therefore attempt to determine the ground state in an unbiased way by using a controlled approximation to the renormalization group flow. The phase diagram is determined to be dependent on the the short distance physics, which we parameterize by phenomenological constants. We explore the plausible space of these constants and find that three ground states are the most likely: nematic, anti ferromagnetic and spin flux (a.k.a quantum spin Hall).

In Chapter 3 we propose a novel effect in disorder conducting systems. We show that a memory effect in the conductivity of metallic systems can be produced by the same two level systems that are responsible for the $1/f$ noise. Memory effects are extremely long-lived responses of the conductivity to changes in external parameters such as density or magnetic field. Using quantum transport theory, we derive a universal relationship between the memory effect and the $1/f$ noise. Finally, we propose a magnetic memory effect, where the magneto-resistance is sensitive to the history of the applied magnetic field.

In Chapter 4 we propose a novel effect in cold atom systems. Cold atom systems consist of $> 10^5$ neutral atoms which are trapped and cooled to sub-microKelvin temperatures. These systems have attracted interest because of the possibility of simulating many-body physics in a highly controlled environment. We show that by applying a weak radio frequency perturbation in a two-dimensional cold atomic gas we may induce a novel instability. The instability may be understood as transmuting the Bose-Einstein condensate (BEC) to Bardeen-Cooper-Schriffer state (BCS) transition into a non-equilibrium phase transition. The instability leads to a supersolid state that spontaneously breaks translational symmetry. The transition would provide an interesting arena to study non-equilibrium phase transitions, the kinetics of first-order quantum phase transitions, the properties of the supersolid as well as illuminating the properties of the underlying BEC-BCS transition.

Chapter 2

The Ground State of Bilayer Graphene

2.1 Introduction

Bilayer graphene[1, 2] (BLG) is a crystal which consists of two monolayers of honeycomb carbon lattice arranged according the Bernal stacking known from bulk graphite [2]. In a Bernal stacked lattice, one out of the two sites on the upper monolayer resides directly over a site on the lower lattice, and the the other carbon atoms are on/under the centers of the hexagons (see Fig. 2.1). Such a crystal has a very high symmetry with symmetry group $\mathcal{D}_{3d}$.

This high symmetry may be lifted by the formation of correlated states of electrons. There is a plethora of ways the symmetry can be lifted, some of which have been discussed in the recent literature: the ferroelectric-layer asymmetric state [3, 4], the layer polarized antiferromagnetic state[5–8], the quantum anomalous Hall state [4, 7, 9], the "spin flux"/ quantum spin Hall state[4, 7], the charge density wave state[7, 10, 11], the loop current state[12] and an anisotropic nematic liquid[13, 14]. Some of the proposed phases above have a gap in the electronic spectrum (ferroelectric, antiferromagnetic, spin-flux, CDW), whereas in the other phases (nematic, ferromagnetic) no gap is formed. This large variety of possibilities makes the theory of electronic properties of BLG a very interesting and challenging subject. The complexity of the theoretical problem is compounded by two factors. One is a lack of precise information about the relevant interaction constants which determine the electronic phase in undoped pristine BLG. The other issue is the competition between exchange energy contributions for a large number of candidate phases which makes the determination of the ground state non-trivial, even with precise knowledge of the interaction constants.

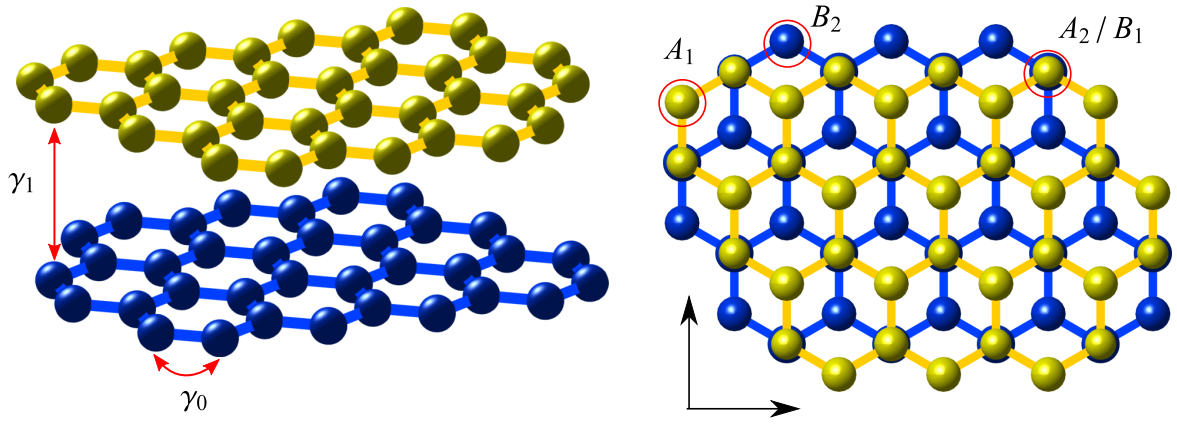

FIGURE 2.1: Left panel: 3D view of bilayer graphene. The sites that sit on top of each other, connected by dotted lines, hybridize strongly and form bands with a gap of $\gamma_1 \approx 0.4eV$. The low energy electron live on the half of the carbon atoms that sit over/under the centers of the hexagons. Right panel: top-down view of the lattice.

On the experimental side, several contradicting observations have been reported based on interpretations of the measured transport properties of suspended samples in terms of a gapful or gapless spectrum of electronic excitations[15–21]. At the moment the preponderance of experiments point to a gapped state, but a lack of consistency between samples and between experiments means there is not a yet a clear understanding of the situation. However, all of these works as well as optical studies of BLG [22–27] indicate that the high-energy properties (but below $0.2eV$) of BLG are well described by the two band model [1] without interactions. This makes a comprehensive theoretical treatment of the problem starting from the weak coupling even more timely. In this paper, we employ the previously developed RG approach [13] to identify the possible scenarios of symmetry breaking phase transition in BLG at low temperature and zero carrier density.

The tendency to form a state with spontaneously broken symmetry is encoded in the system response to local symmetry breaking fluctuations, in particular in their mutual interaction,

$$H_{int} \sim \int d^2 r \sum_{\mathcal{A} \in IrReps} g_{\mathcal{A}} \delta\hat{\rho}_{\mathcal{A}}(r) \cdot \delta\hat{\rho}_{\mathcal{A}}(r). \tag{2.1}$$

Here $\delta\hat{\rho}_{\mathcal{A}}$ are operators creating local density fluctuations breaking lattice symmetry, with $\delta\hat{\rho}_{\mathcal{A}} = \psi^\dagger \hat{M} \psi$ expressed in terms of electron annihilation and creation operators ψ and $\psi^\dagger$, and $g_{\mathcal{A}}$ are coupling constants. Each of the fluctuations $\delta\hat{\rho}_{\mathcal{A}}$ belong to one of the irreducible representations $\mathcal{A}$ (IrReps) of the symmetry group of the lattice. (A precise definition of the densities can be found in Sec. 2.2).

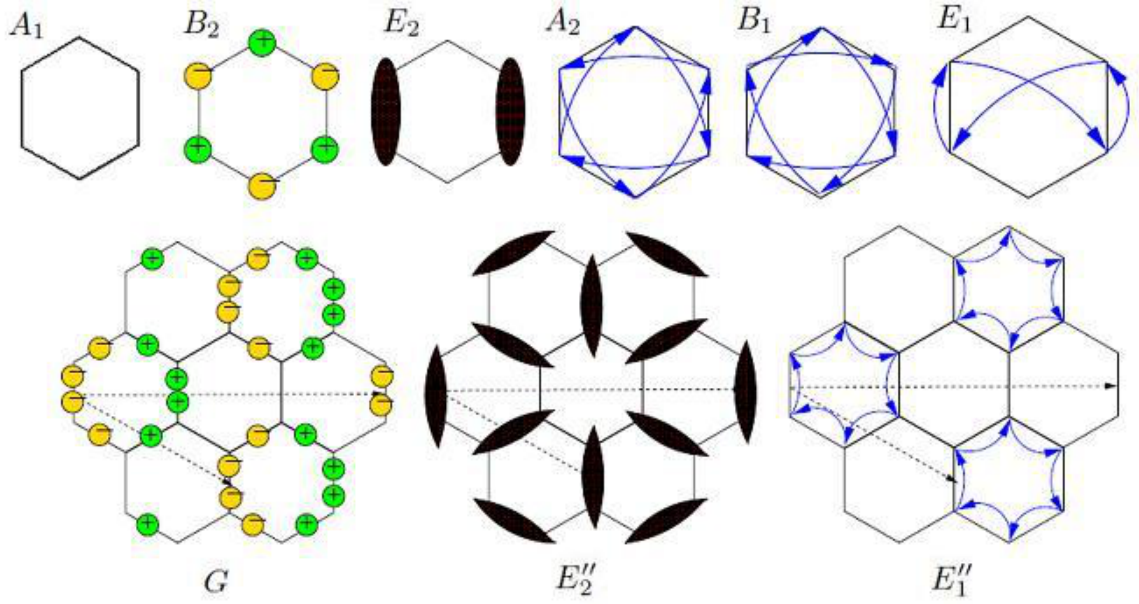

FIGURE 2.2: Sketches of the density and currents transforming according representations of the group $\mathcal{D}_{3d}''$. In the case of a spin singlet symmetry breaking, the plus and minus signs represent charges, the blue lines persistent currents and the black bars represent bonds. The G, E_2 and E_2'' order parameters triple the unit cell; the new Bravais lattice vectors are given by the dashed arrows. The representations are given in terms of Pauli matrices in Eqs. (2.13) and (2.12).

If Hamiltonian (2.1) is dominated by one term with negative constant $g_{\mathcal{A}}$, we would expect it to be energetically favorable for a state with a non-zero expectation value of $\delta\hat{\rho}_{\mathcal{A}}$ to form, with the symmetry of the ground state determine by the corresponding IrRep, $\mathcal{A}$. However if the coupling constant in the dominant term is positive, then the ground state is determined by the exchange energy, which can be negative for not only for magnetic (ferro/antiferro) but also for non-magnetic orderings, because of the sublattice/valley matrix structure. Because of the large number of IrReps, this can result in a competition between many phases. Therefore, to determine the ground state of BLG we must know all the interaction constants $g_{\mathcal{A}}$ sufficiently well, especially when the dominant ones are positive. The situation is actually even more intriguing since attraction may result in a superconducting phase with non-trivial Cooper pair structure.

To add to the complexity of the problem, the values of the "constants" $g_{\mathcal{A}}$ are not fixed. They change as a function of the energy scale $\mathcal{E}$ within which the electrons establish the symmetry breaking correlations. The energy scale dependence, $g_{\mathcal{A}}(\mathcal{E})$, may be calculated using the renormalization group (RG) approach. In the RG approach the highest energy electron states are eliminated and their effects incorporated into a redefinition of the parameters of the theory. The renormalization of BLG parameters starts at the energy scale $\gamma_1/2 \approx 0.2eV$ which limits the

applicability of the two-band model with parabolic spectrum and initial conditions $g_{\mathcal{A}}(\gamma_1/2)$. Then it is iterated until the lowest energy scale $\mathcal{E}$ is reached. This energy scale $\mathcal{E}$ is determined when the interaction energy in at least one of the the channels becomes of the order of kinetic energy. After this scale is reached the mean field theory can be used to establish the electronic ground state. The necessary RG equations for the constants $g_{\mathcal{A}}$ and their interplay with Coulomb interaction,

$$H_C \sim \int d^2r d^2r' \frac{\psi^\dagger(r)\psi(r)\psi^\dagger(r')\psi(r')}{|r-r'|}, \tag{2.2}$$

have been derived for the full set of eight constants in Refs. [13]. (Similar in spirit treatment of Ref. [8] replaced Eq. (2.2) with the short range weak interaction.)

Calculating $g_{\mathcal{A}}(\gamma_1/2)$ requires detailed knowledge of the microscopic orbitals which is not available at present. Therefore, in this paper we explore a wide variety of initial conditions $g_{\mathcal{A}}(\gamma_1/2)$ for the RG to find possible electronic ground states for BLG. We can make some arguments to constrain the values of the $g_{\mathcal{A}}(\gamma_1/2)$. The coupling g_{B_2} which describes the interaction of dipoles oriented perpendicular to the bilayer (see Fig. 2.2) must be positive at high energy scales. The four "current-current" interactions g_{A_2}, g_{B_1}, g_{E_1} and $g_{E_1''}$ are only generated by virtual processes because of time reversal symmetry. Therefore we will set them to be zero at $\gamma_1/2$.

Also, it is interesting to note that in the value of $g_{\mathcal{A}}(\gamma_1/2)$ one has to take account of the interactions between electrons via polarization of the lattice. Particularly, the in-plane TO-LO phonons at the Γ-point and TO phonons at the Brillouin zone corner have energies comparable to $\gamma_1/2$, so that they mediate an attractive interaction via their virtual creation/absorption. These would give negative contributions to the bare values of g_{E_2} and $g_{E_2''}$. Analogously, virtual $LO-LA$ phonons from K - the Brillouin zone corners give negative contribution to the value of g_G. Therefore, we make no assumption about the sign of g_{E_2}, $g_{E_2''}$, and g_G. A set of typical outcomes of the RG flow and the resulting electronic phases is shown in Fig. 2.3.

In Fig. 2.3 we reproduce the earlier reported result[13, 14] that for the initial choice of $g_{\mathcal{A}}=0$ the RG flow leads to a nematic phase. The nematic phase is a state with broken rotational (but intact translational) symmetry corresponding to representation E_2 in Fig. (2.2), mimicking the effect of anisotropic hopping along bonds with different directions on the honeycomb lattice. This breaks the six-fold rotational symmetry by selecting one of axes of the lattice. In this state the electronic spectrum remains gapless but is significantly reconstructed from the unbroken symmetry state with two four-fold degenerate Dirac cones at low energy. The state has the same symmetry and spectrum as uniaxial strain[28], and we expect that strain will, all else equal, favor the nematic phase. Figure 2.3 shows that the nematic phase is the preferred ground state not only when $g_{\mathcal{A}}(\gamma_1/2)=0$, but in a significant section of the $g_{\mathcal{A}}(\gamma_1/2)$ parameter space. In

particular, the nematic phase always emerges from the part of the parameter space where bare electron-electron couplings causing intervalley scattering are zero ($g_G = g_{E_2''} = g_{E_1''} = 0$).

In other parts of the parameter space explored in this work and illustrate in Fig. 2.3, the ground state appears to be anti-ferromagnetic (AF), with the A_1 and B_2 sublattices of two layers, see Fig. 2.1, are spin polarized in opposite directions. In the AF state the electronic excitations are gapped (though neutral spin wave excitations are gapless). Although the AF state prevails over a significant section of the parameter space, the combinations of high energy couplings which produce the AF state are not intuitive. For example, increasing the bare coupling g_{B_2} does not necessarily introduce the AF phase. However increasing the bare coupling g_G makes the ground state AF. The reason for this counter-intuitive behavior is in the complexity of the RG flows. Since there are eight non-linearly coupled variables in the RG equations [8, 13], the RG flow is quite complicated, and the connection between the couplings at low energy and the bare couplings at high energy is not obvious.

Exploring a broader parameter space further we find more phases. A spin flux phase is found in a significant sector of the parameter space $g_{\mathcal{A}}(\gamma_1/2)$, as seen in Fig. 2.3. This spin flux phase is a state with a persistent spin current circling the honeycomb lattice rings, corresponding to the spin triplet form of representation B_1 in Fig. 2.2. It may be viewed as the spontaneous formation of a strong spin-orbit coupling. It therefore leads to a gapped electronic spectrum and possibly a quantum spin Hall effect.

There are two more phases which appear to some degree in the phase space explored. One is a ferroelectric phase (FE). The FE phase a trivial band gap insulator where the bilayer becomes spontaneously charged like a capacitor. It is a completely gapped phase. It corresponds to representation B_2 precisely the same representation as AF but spin singlet, rather than spin triplet. Therefore, positive g_{B_2} suppresses the ferroelectric phase, which appears in Fig. 2.3 only in the fine tuned corners corresponding to the applicability of the weak-coupling theory.

We also found other phase a new superconducting phase (not shown in figure, see Fig. 2.9 for more details) which has the energy tantalizingly close to the nematic and ferro-electric states. It is a triplet superconductor with a nontrivial Cooper pairing. Cooper pairs are formed between pairs of electrons with opposite valleys and opposite layer. The pairing is symmetric in exchange of valleys, but antisymmetric in exchange of layers.

As usual, the singlet superconductivity appears only for the attractive interaction. From the first panel on Fig. 2.3, we see that it requires quite siginificant attraction in two channels $g_{E_2''}, g_G < 0$.

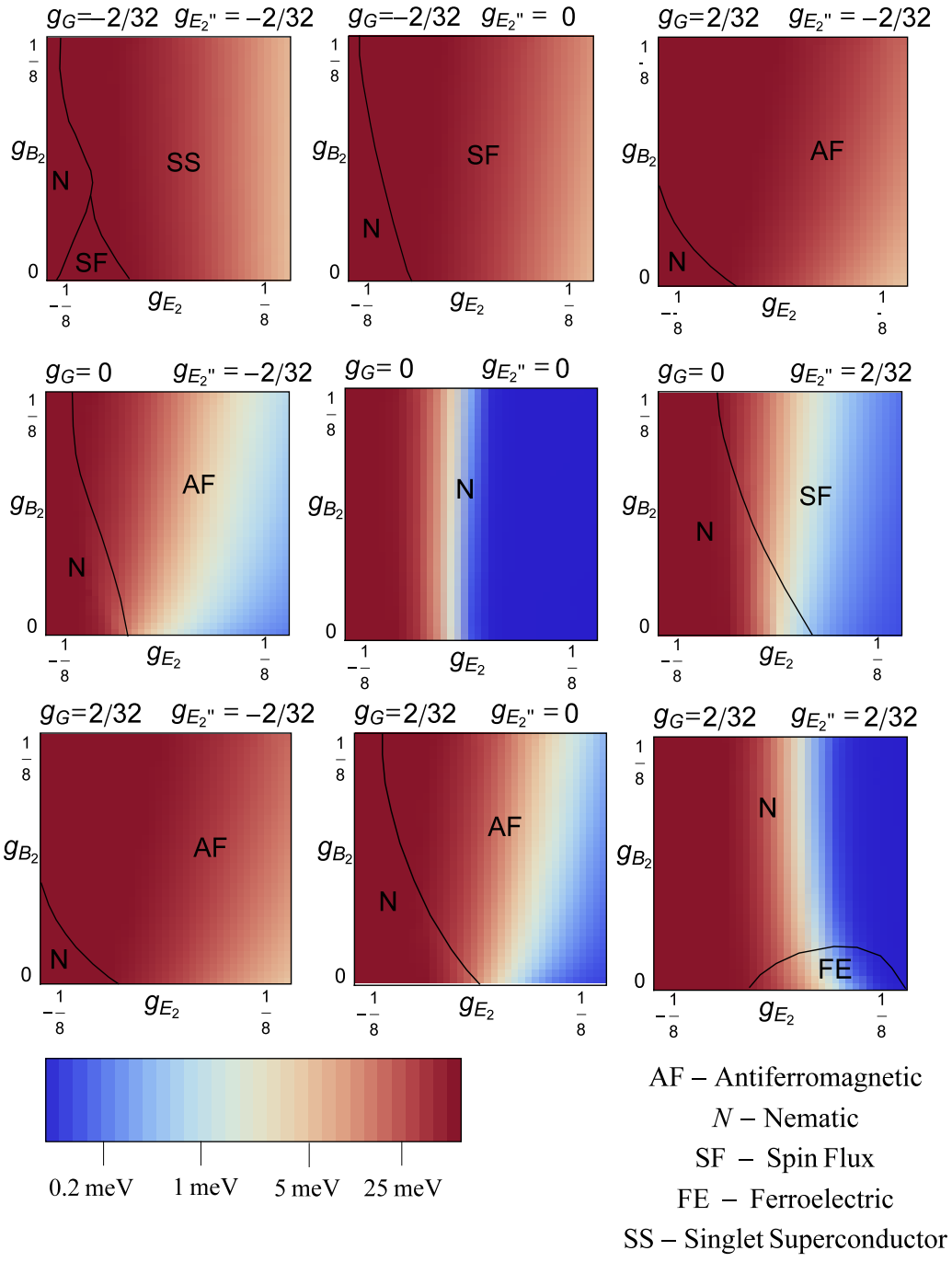

FIGURE 2.3: Four cuts through the possible parameter space of BLG. The predicted gap (or saddle point energy for only gapless nematic phase) is indicated by the color scale and the predicted phase is indicated. N is a nematic, AF is an antiferromagnetic phase, SF is a spin flux phase and FE is a ferroelectric. A fifth predicted superconducting phase is in a range parameters not shown, see Fig. 2.9 for more details. The g are coupling constants of BLG, with the subscript labeling the irreducible representations in accordance with Fig. 2.2, and defined in Sec. 2.2. All boundaries are the first order phase transitions.

Below we describe how the conclusions listed above have been reached. In Sec. 2.2 we review the structure of BLG, it's symmetry group and the low energy Hamiltonian. Section 2.3 describes the resummation of the Coulomb interactions in the $1/N$ expansion[13, 29–31], where $N = 4$ is the degeneracy of the single particle spectrum. We then derive the RG equations that connect the couplings at low and high energy scales. In Sec. 2.4 the results of the RG flow equations are analyzed and augmented by a self-consistent mean field theory which produces a possible phase. Section 2.5 discusses the properties of the emerging phases. In Appendix A we describe the group-theoretic analysis of the phases of the BLG. diagram.

2.2 Model

The top view of the BLG lattice with Bernal stacking is shown on the right panel of Fig. 2.1. Here we label the two layers 1 and 2 and the four inequivalent lattice sites A_1, B_1, A_2, B_2, with A_2 directly over B_1.

Calculation based on the minimal tight-binding model has established the following BLG band structure [1]. The A_2 and B_1 sites hybridize strongly and host states from the high energy bands with excitation energies $> \gamma_1 \approx 0.4eV$. The low energy fermionic excitations in BLG belong to a four-component representation of the group $\mathcal{D}_{3d}$, exactly as in monolayer graphene. The four fermionic fields ψ are conveniently joined into a 4-vector as follows

$$\vec{\psi}^t \equiv \left\{(\psi_K^A, \psi_K^B)^{AB}, (\psi_{K'}^B, -\psi_{K'}^A)^{AB}\right\}_{KK'}, \tag{2.3}$$

where the ψs are true spinors including real electron spin. This four dimensional space can be written as the direct product of the (AB) and (KK') spaces. We will use this to write all operators as the sum of direct products $\tau_a^{AB}\tau_b^{KK'}\sigma_c$ of Pauli matrices in each space. We define $\{\tau_i^{AB}, \tau_i^{KK'}, \sigma_i\}$ as the Pauli matrices acting on layer, valley and spin, respectively, and define $\tau_0 \equiv \hat{1}$, $\tau_\pm \equiv (\tau_x \pm i\tau_y)/2$.

The symmetries of the BLG lattice consist of the two independent lattice translation $\hat{t}_1$ and $\hat{t}_2$, a $\hat{C}_3$, rotation by $2\pi/3$ around one of the lattice sites; and two independent reflections: $\hat{R}_h$, reflection across the y-axis, and $\hat{R}_v$, reflection across the x-axis together with reflection through the plane midway between the graphene sheets, see right panel of Fig. 2.1. The reflections and rotations form the point group $\mathcal{D}_{3d}$. The groups $\mathcal{D}_{3d}$ and $\mathcal{C}_{6v}$ are isomorphic and have precisely the same action on the plane. We also ignore the spin-orbit interaction which gives an additional $SU(2)$ symmetry from the independent rotation of the spin. We will be concerned with the physics about K and K' points which are inequivalent in the Brillouin zone but are

connected by $\hat{R}_h$. Rather than dealing with two degenerate but inequivalent points we can triple the unit cell, which maps K and K' onto the Γ point. In this view, the point group D_{3d} is expanded to $\mathcal{D}''_{3d} = \mathcal{D}_{3d} + \hat{t}_1\mathcal{D}_{3d} + \hat{t}_2\mathcal{D}_{3d}$ with the translation operator $\hat{t}_1$ with $\hat{t}_1^2 = \hat{t}_2$ and $\hat{t}_1^3 = \hat{1}$ (see *e.g.* Ref. [32]).

Ignoring the spin structure, the vector ψ transforms as follows under the action of the symmetry operators:

$$\begin{aligned}
\hat{t}_1\psi(\boldsymbol{r}) &= e^{\frac{2\pi i}{3}\tau_z^{KK'}}\psi\left(t_1\boldsymbol{r}\right), \\
\hat{C}_3\psi(\boldsymbol{r}) &= e^{\frac{4\pi i}{3}\tau_z^{AB}}\psi\left(C_3\boldsymbol{r}\right), \\
\hat{R}_h\psi(\boldsymbol{r}) &= \tau_y^{AB}\tau_y^{KK'}\psi\left(R_h\boldsymbol{r}\right), \\
\hat{R}_v\psi(\boldsymbol{r}) &= \tau_x^{AB}\tau_z^{KK'}\psi\left(R_v\boldsymbol{r}\right),
\end{aligned} \tag{2.4}$$

There is also the time reversal symmetry operation given by

$$\psi \to \psi^\dagger\hat{\mathcal{T}}; \quad \hat{\mathcal{T}} \equiv i\hat{\tau}_y^{AB}\hat{\tau}_y^{KK'}\hat{\sigma}_y. \tag{2.5}$$

2.2.1 Single particle spectrum

We write the Hamiltonian for this model as

$$H \equiv H_0 + H_C + H_{int}. \tag{2.6}$$

The single-particle part of the Hamiltonian in the two band model[1] reads (we will put $\hbar = 1$ in all the subsequent formulas)

$$H_0 \equiv \sum_k \psi^\dagger \left[\frac{1}{2m}\tau_z^{KK'}(\tau_+^{AB}k_+^2 + \tau_-^{AB}k_-^2)\right]\psi. \tag{2.7}$$

Here we ignore the "warping term" [1] caused by the small skew hopping (γ_3) since it would have a negligible effect on the RG. We have defined $k_\pm = k_x \pm ik_y$, and $m = \frac{2\gamma_1}{gr_{AB}^2\gamma_0^2}$ where γ_0 is the the interlayer integral and r_{AB} is the interatomic distance. (Effect of the electron-electron interaction on the warping was studied in Ref. [13].) The Hamiltonian in Eq. (2.7) has the eigenvalue spectrum

$$\varepsilon(\boldsymbol{k}) = \pm\frac{k^2}{2m}, \tag{2.8}$$

where each branch is four-fold (spin and valley) degenerate. The system described by Hamiltonian (2.7) has a higher symmetry than the underlying lattice. This larger symmetry is described by the $SU(4) \otimes U(1)$ group whose sixteen generators M_{ij} are given by

$$M_{ij} = \sigma_i \tilde{\tau}_j^{KK'} \quad (i,j = 0,x,y,z), \tag{2.9}$$

$$\begin{aligned} \tilde{\tau}_0^{KK'} &= \tau_0^{KK'}; \quad \tilde{\tau}_z^{KK'} = \tau_z^{KK'}, \\ \tilde{\tau}_x^{KK'} &= \tau_z^{AB}\tau_x^{KK'}; \quad \tilde{\tau}_y^{KK'} = \tau_z^{AB}\tau_y^{KK'}. \end{aligned} \tag{2.10}$$

An additional rotational $U(1)$ symmetry extends the discrete rotation $\hat{C}_3$ to a continuous transformation given by $\psi(\boldsymbol{r}) \to \exp(-2i\theta\sigma_z^{AB})\psi(\hat{R}(\theta)\boldsymbol{r})$, where $\hat{R}(\theta)$ is the real space rotation by an angle θ

The preceding discussion actually undercounts the symmetry algebra of the single particle Hamiltonian greatly, since they do not include the continuous particle hole symmetry rotations [33]. Including these rotations, the total symmetry group is $Sp(8)$. However these extra rotations are not necessary for the following analysis.

2.2.2 Electron-electron interactions

The Coulomb interaction

$$H_C \equiv \frac{e^2}{2}\int \frac{d^2\mathbf{r}d^2\mathbf{r}'}{|\mathbf{r}-\mathbf{r}'|}\left[\left(\psi^\dagger\psi\right)_{\mathbf{r}}\left(\psi^\dagger\psi\right)_{\mathbf{r}'}\right], \tag{2.11}$$

is the largest interaction energy in the system. The strength of Coulomb interaction on the length scale L is e^2/L. The electron kinetic energy related to the same energy scale is $1/(mL^2)$ so the Coulomb interaction will dominate at the scale $L = 1/(me^2)$, which is comparable to Bohr radius. However due to the generation of electron-hole pairs, the Coulomb interaction is screened, leading to the reduction of interaction energy $e^2/L \to 1/(mNL^2)$. This screened interactions respects all the symmetries of the system and does not scale; therefore by itself it does not induce any spontaneous symmetry breaking of the lattice symmetry group. We will return to the quantitative description of the screened Coulomb interaction in Sec 2.3.

Any lattice symmetry breaking is captured by the scaling of the marginal short range interactions. These interactions also reduce the symmetries of the low energy model almost down to the crystal

group[13, 30, 31, 34],

$$H_{int} \equiv \frac{2\pi}{m} \int d^2\mathbf{r} \sum_{ij} g_{ij} \left[\psi^\dagger \hat{\tau}_i^{AB} \hat{\tau}_j^{KK'} \psi\right]_{\mathbf{r}}^2, \tag{2.12}$$

where have included a factor of $\frac{2\pi}{m}$ to make the couplings dimensionless. The $\mathcal{D}''_{3d}$ symmetry of the two band BLG model forces various relations among the g_{ij}:

$$\begin{aligned} &g_{xx} = g_{xy} = g_{yx} = g_{yy} \equiv g_G \\ &g_{xz} = g_{yz} \equiv g_{E_2};\ g_{zx} = g_{zy} \equiv g_{E_2''} \\ &g_{x0} = g_{y0} \equiv g_{E_1};\ g_{0x} = g_{0y} \equiv g_{E_1''} \\ &g_{z0} \equiv g_{B_1};\ g_{0z} \equiv g_{A_2};\ g_{zz} \equiv g_{B_2} \end{aligned} \tag{2.13}$$

Here we have labeled the couplings by the appropriate representation of D''_{3d} schematically represented in Fig 2.2. We note for future reference that the interaction terms $g_{E_2}(\psi^\dagger \tau_{x,y}^{AB} \tau_z^{KK'} \psi)^2$ and $g_{B_1}(\psi^\dagger \tau_z^{AB} \psi)^2$ are invariant under the entire $U(4)$ (and which can be extended to $Sp(8)$ by including the particle-hole rotations[33]) symmetry of H_0. All other short range interactions, such as those of the form $\sim (\psi_\mu^\dagger \vec{\sigma}_{\mu\nu} \psi_\nu)^2$ or $\sim |\psi_\mu^\dagger \psi_\nu^\dagger|^2$ can be always rearranged into the form of H_{int} by using standard Pauli matrix identity $2\delta_{\mu\nu}\delta_{\mu'\nu'} = \delta_{\mu\mu'}\delta_{\nu\nu'} + \vec{\sigma}_{\mu\mu'}\vec{\sigma}_{\nu'\nu}$.

2.3 Perturbation theory and RG equation

2.3.1 1/N resummation

For the Coulomb interaction we will use $1/N$ as a small parameter, where $N = 4$ is the number of degenerate fermion flavors[13, 29–31]. We achieve this expansion by performing the usual RPA resummation of diagrams (Fig 2.5). Note that the coupling g_{00} has the same matrix structure as the long range Coulomb interaction. We therefore resum the two together,*i.e.* we take the bare interaction in the RPA resummation to be

$$\mathcal{V}^{(0)}(q) \equiv \frac{2\pi e^2}{|q|} + \frac{4\pi g_{00}}{m}. \tag{2.14}$$

Summing up the geometric series of terms in Fig. 2.5(b) we arrive at the resummed propagator,

$$\mathcal{D}(q,\omega) = \frac{\mathcal{V}^{(0)}(q)}{1 + \mathcal{V}^{(0)}(q)\Pi(q,\omega)}, \tag{2.15}$$

(a) 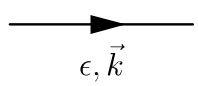 $= -\hat{G}(\epsilon, \vec{k}) = -\dfrac{1}{i\epsilon + \bigcirc}$

(b)  $= -\dfrac{1}{2m}\tau_z^{KK'}\left(\tau_+^{AB} q_+^2 + \tau_-^{AB} q_-^2\right)$

(c) 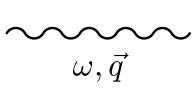 $= -\dfrac{2\pi e^2}{|\vec{q}|};$

(d) 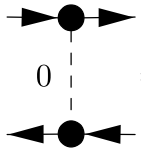 $= -\dfrac{4\pi}{m} g_0^0 \tau_0^{AB} \tau_0^{KK'} \otimes \tau_0^{AB} \tau_0^{KK'}$

(e) 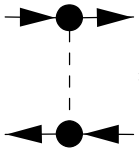 $= -\dfrac{4\pi}{m} \sum_{i,j=0}{}' g_{ij} \tau_i^{AB} \tau_j^{KK'} \otimes \tau_i^{AB} \tau_j^{KK'}$

FIGURE 2.4: Definition of the elements of the diagrammatic expansion. The thick line is the fermion propagator, the circle is the self energy from the single particle of the spectrum. The wavy line is the Coulomb propagator and the dotted line is the contact interaction. We separate the scalar contact interaction g_{00} from the other interactions.

where

$$\begin{aligned} \Pi(q,\omega) &= \frac{mN}{\pi f(\frac{2m\omega}{q^2})}, \\ f(x) &\equiv \left[\log\left(\frac{x^2+1}{x^2+1/4}\right) + \frac{2\arctan x - \arctan 2x}{x}\right]^{-1}. \end{aligned} \tag{2.16}$$

We further take the long wavelength limit, $q \to 0$, where $V^{(0)}(q)\Pi \gg 1$. This gives us the approximate expression for the interaction propagator,

$$\mathcal{D}(q,\omega) \approx \frac{1}{\Pi(q,\omega)} = \frac{\pi}{mN} f\left(\frac{2m\omega}{q^2}\right). \tag{2.17}$$

Since $\mathcal{D} \propto 1/N$ we can use a perturbative expansion in $1/N$. Note that we have neglected the higher-energy bands in considering the resummation of the Coulomb potential. However, the higher energy bands would only change the dielectric constant which cancels out of the final formula.

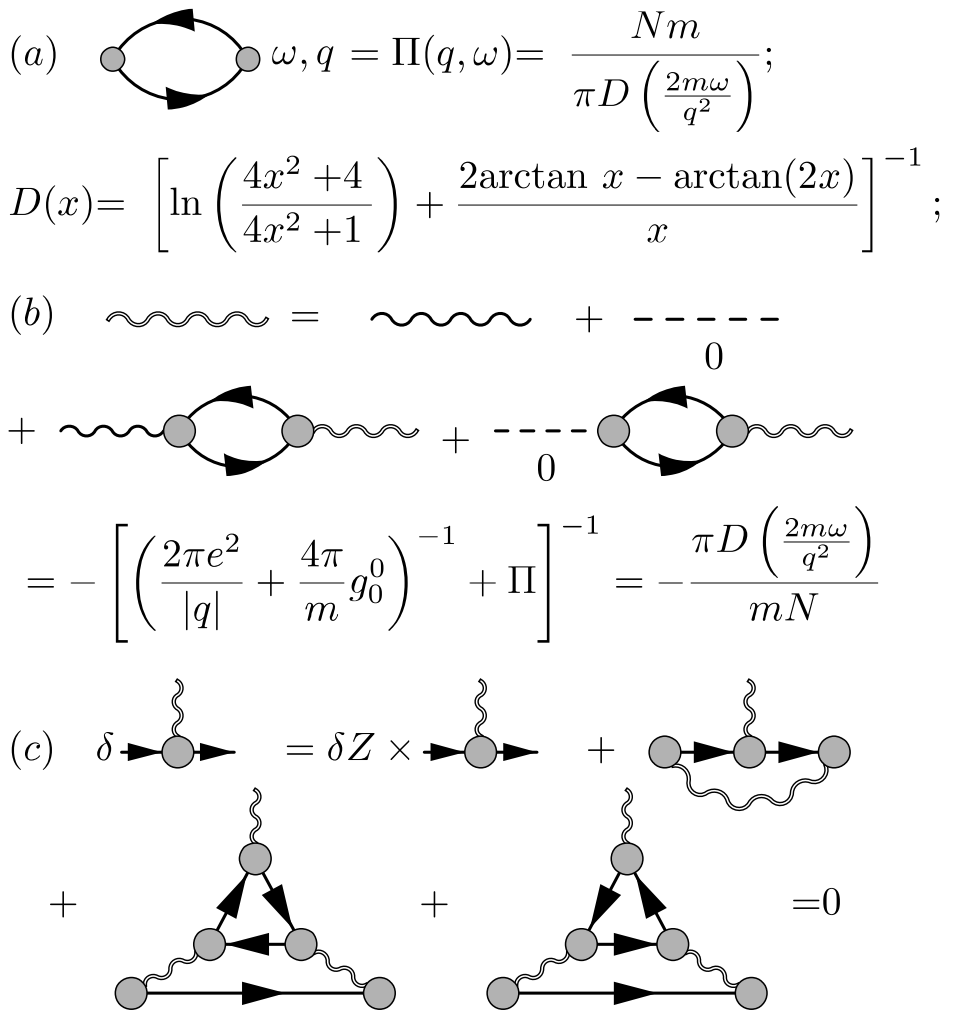

FIGURE 2.5: Resummation of the strong Coulomb interaction in the $1/N$ approximation. a) Evaluation of the polarization loop. b) Definition of the resummed propagator, represented by the double wavy line. The scalar contact interaction is included in the resummation as it has the same matrix structure as the Coulomb interaction. c) The non renormalization of the Coulomb vertex as a result of gauge invariance. (δZ is defined in Fig. 2.6 a).

Now we write the partition function as a path integral in imaginary time t over Grassman fields ψ and $\psi^\dagger$,

$$\begin{aligned} Z &= \int D\psi D\psi^\dagger e^{-S} \\ S &\equiv \int d^2r dt \left(\psi^\dagger \frac{d}{dt}\psi - H\left[\psi^\dagger, \psi\right]\right), \end{aligned} \tag{2.18}$$

where H is defined in equation (2.6). Then, we perform the RG by integrating out all fermionic states with momenta q such that $K > |q| > K\,e^{-\ell}$, where K is some ultraviolet cutoff regardless of ω. We will set K_0 so that $K_0^2/(2m) = \gamma_1/2$, approximately the upper-limit of the applicability of the two band model with the parabolic dispersion. We then rescale $\psi \to (1 + \delta Z/2)\psi$ to keep

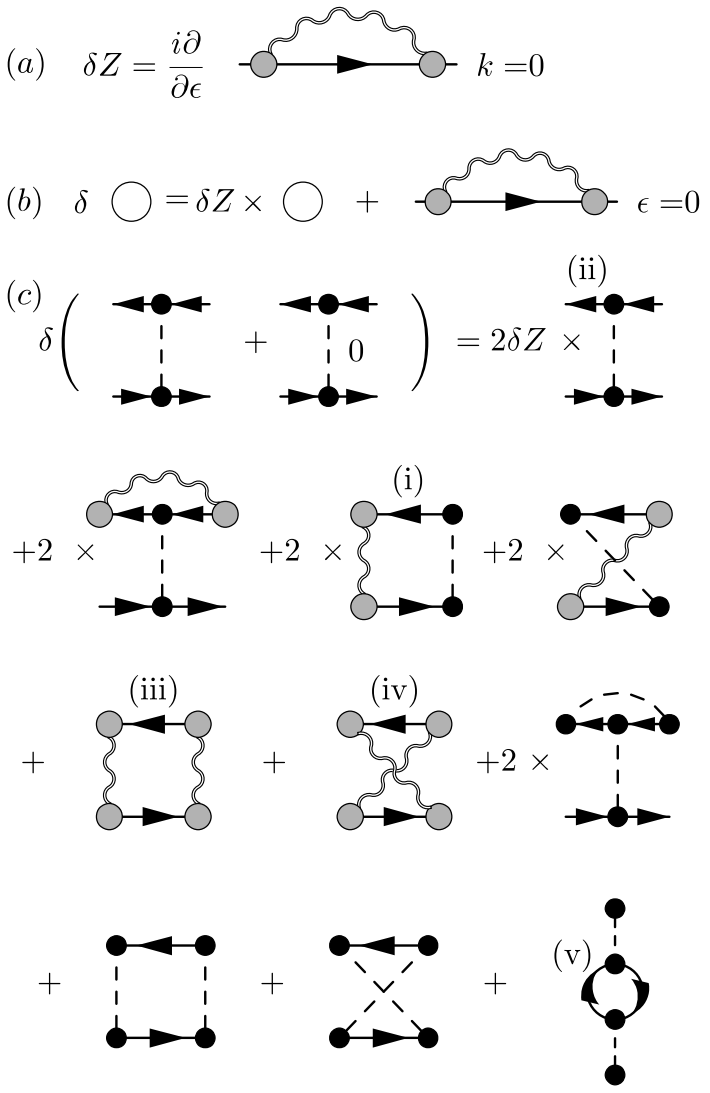

FIGURE 2.6: Diagrams included in RG equations. a) Single-particle particle weight renormalization; b) Renormalization of the mass m. c) Renormalization of the contact interactions.

the term $\int \psi^\dagger \frac{d}{dt} \psi$ unchanged. This procedure has the benefit of not renormalizing the Coulomb vertex because of gauge invariance (see Fig. 2.5(c)). If we assign t an RG dimension 2 then at tree level the operator ψ has RG dimension +1, and m, g_{ij} and the Coulomb interaction are marginal.

There is a subtlety in the $1/N$ treatment of the Coulomb interaction. Because of the behavior of the interaction in the limit $q \to 0$, $\omega \to \infty$, some of the diagrams taken individually diverge faster than logarithmically. For example, the self energy diagram (see Fig. 2.6(a)) gives the

correction to the quasiparticle weight,

$$\begin{aligned}\delta Z &= \frac{\partial}{i\partial\Omega}|_{\Omega=0}\int\frac{d\omega d^2\boldsymbol{k}}{(2\pi)^3}\left(\frac{-\pi}{mN}\right)f\left(\frac{2m\omega}{k^2}\right)\\ &\quad\times\left[\frac{-i(\omega+\Omega)+\hat{\tau}_z^{KK'}(\hat{\tau}_+^{AB}k_+^2+\hat{\tau}_-^{AB}k_-^2)}{(\omega+\Omega)^2+(\frac{k^2}{2m})^2}\right]\\ &= \frac{1}{N}\log K\int_{-\infty}^{\infty}\frac{dx}{2\pi}f(x)\frac{1-x^2}{(1+x^2)^2},\end{aligned}\tag{2.19}$$

where the variable x is defined by the substitution $\omega = xk^2/(2m)$. This integral is formally infinite since $f(x)\to x$ as $x\to\infty$. To understand this divergence, note that it comes from the region where the momentum k through the Coulomb line goes to zero. This corresponds to a spatially constant but time-varying potential $V(t)$. Such a potential is merely a constant shift in energy so that the Green's function are changed as $G(t_1,t_2)\to G(t_1,t_2)\exp\left(ie\int_{t_1}^{t_2}V(t)\,dt\right)$. It is the summation over the fluctuations of this phase that produces the divergence. However, in all observables gauge invariant quantities the fermion lines must come in closed loops which cancels out this phase, and so it cannot appear in any physical quantities. Reassuringly in all our calculations this is the case. Indeed such a divergence cancels out from the correction to the electron mass,

$$\delta\left(\frac{1}{2m}\right)=\frac{1}{2}\frac{\partial^2}{\partial p_+^2}\Sigma-\frac{1}{2m}\delta Z,\tag{2.20}$$

where

$$\begin{aligned}&\frac{\partial^2}{\partial p_+^2}\Sigma=\\ &tr\left\{\frac{1}{2}\hat{\tau}_z^{KK'}\hat{\tau}_-^{AB}\frac{\partial}{\partial p_+^2}|_{p=0}\int\frac{d\omega d^2\boldsymbol{k}}{(2\pi)^3}\frac{\pi}{mN}\left[-f\left(\frac{2m\omega}{k^2}\right)\right]\right.\\ &\left.\times\hat{G}(\omega,\boldsymbol{k}+\boldsymbol{p})\right\}\\ &=-tr\left\{\frac{1}{2}\hat{\tau}_z^{KK'}\hat{\tau}_-^{AB}\frac{\partial}{\partial p_+^2}|_{p=0}\int\frac{d\omega d^2\boldsymbol{k}}{(2\pi)^3}\frac{\pi}{mN}f\left(\frac{2m\omega}{k^2}\right)\right.\\ &\left.\times\frac{-i\omega+\frac{1}{2m}\hat{\tau}_z^{KK'}(\hat{\tau}_+^{AB}(k_++p_+)^2+\hat{\tau}_-^{AB}(k_-+p_-)^2)}{\omega^2+\left[(\frac{(\boldsymbol{k}+\boldsymbol{p})^2}{2m}\right]^2}\right\}\\ &=-\int\frac{d^2k}{(2\pi)^2}\frac{1}{k^4}\int\frac{dx}{2\pi}\frac{\pi f(x)}{mN}\frac{\partial}{\partial p_+^2}|_{p=0}\frac{k_+^2+2k_+p_++p_+^2}{x^2+(1+\frac{k\cdot p}{k^2}+\frac{p^2}{k^2})^2}\\ &=-\frac{1}{2mN}\log K\int\frac{dx}{(2\pi)}f(x)\frac{x^4-3x^2}{(x^2+1)^3}.\end{aligned}\tag{2.21}$$

Although the latter expression is divergent in the limit $x \to \infty$, the sum,

$$\delta\left(\frac{1}{2m}\right) = \frac{1}{2mN} \log K \int_{-\infty}^{\infty} \frac{dx}{2\pi} f(x) \frac{1-3x^2}{(1+x^2)^3}, \tag{2.22}$$

is convergent. Therefore the mass has a logarithmic dependence on cutoff, as expected. This enables us to write down the RG equations for the electron mass m,

$$\frac{d \log m(\ell)}{d\ell} = -\frac{\alpha_1}{2N}; \quad \ell \equiv \log(K_0/K), \tag{2.23}$$

where

$$\alpha_1 \equiv \frac{1}{2\pi} \int dx\, f(x)(1-3x^2)/(1+x^2)^3 \approx -0.078. \tag{2.24}$$

Since $\alpha_1/(2N) < 10^{-2}$ is very small we shall neglect this mass renormalization for the rest of this analysis.

2.3.2 Renormalization of the contact interactions

We now consider the renormalization of the short-range interactions. Based on our assumption that the bare values $g_{\mathcal{A}}$ are small we will work to order g^2 and to lowest order in $1/N$.

The leading logarithmic corrections to the coupling constants of the contact interaction (2.12) are shown on the Fig. 2.6(c). Straightforward calculation of those diagrams yield[35] the set of RG equations for the 8 coupling constants $g_{\mathcal{A}}$

$$\begin{aligned} \frac{dg_{ij}}{d\ell} =& -\frac{\alpha_3}{N^2}\delta(E_2)_{ij} - \frac{\alpha_1 + 2\alpha_2 A_{ij}}{N} g_{ij} \\ & - \sum_{kl}^{\sim} \frac{g_{kl}}{N} \alpha_2 B_{ij}^{kl} - 2N A_{ij} g_{ij}^2 + \sum_{kl}^{\sim} \sum_{mn}^{\sim} C_{klmn}^{ij} g_{kl} g_{mn}, \end{aligned} \tag{2.25}$$

where

$$
\begin{aligned}
A_{ij} \equiv & -\frac{1}{16}\sum_{\gamma=x,y} tr\left(\left[\hat{\tau}_i^{KK'}\hat{\tau}_j^{AB},\hat{\tau}_z^{KK'}\hat{\tau}_\gamma^{AB}\right]^2\right), \\
B_{kl}^{ij} \equiv & \frac{1}{64}\sum_{\gamma=x,y} tr\left(\hat{\tau}_k^{KK'}\hat{\tau}_l^{AB}\left\{\hat{\tau}_i^{KK'}\hat{\tau}_j^{AB},\hat{\tau}_z^{KK'}\hat{\tau}_\gamma^{AB}\right\}\right)^2, \\
C_{klmn}^{ij} = & \\
& \frac{1}{8}\sum_{\gamma=x,y} tr\Big(\hat{\tau}_k^{KK'}\hat{\tau}_l^{AB}\hat{\tau}_i^{KK'}\hat{\tau}_j^{AB}\hat{\tau}_z^{KK'}\hat{\tau}_\gamma^{AB} \\
& \qquad \times\left[\hat{\tau}_k^{KK'}\hat{\tau}_l^{AB},\hat{\tau}_z^{KK'}\hat{\tau}_\gamma^{AB}\right]\hat{\tau}_i^{KK'}\hat{\tau}_j^{AB}\Big) \\
& +\frac{1}{64}\sum_{\gamma=x,y}\Big\{tr\Big(\hat{\tau}_i^{KK'}\hat{\tau}_j^{AB}\Big[\hat{\tau}_k^{KK'}\hat{\tau}_l^{AB}\hat{\tau}_z^{KK'}\hat{\tau}_\gamma^{AB}\hat{\tau}_m^{KK'}\hat{\tau}_n^{AB} \\
& \qquad +\hat{\tau}_k^{KK'}\hat{\tau}_l^{AB}\hat{\tau}_z^{KK'}\hat{\tau}_\gamma^{AB}\hat{\tau}_m^{KK'}\hat{\tau}_n^{AB}\Big]\Big)\Big\}^2 \\
& +\frac{1}{32}\left\{tr\left(\hat{\tau}_i^{KK'}\hat{\tau}_j^{AB}\left[\hat{\tau}_k^{KK'}\hat{\tau}_l^{AB},\hat{\tau}_m^{KK'}\hat{\tau}_n^{AB}\right]\right)\right\}^2.
\end{aligned}
\tag{2.26}
$$

Here $\tilde{\sum}_{ij}$ is a sum over $i,j=\{0,x,y,z\}$ excluding the combination $i=0,j=0$ and the summation convention is not used. The symbol $\delta(E_2)_{ij}$ is 1 when $i=z$ and $j=x,y$ and 0 otherwise. By appearance there are 16 equations contained in Eq. (2.25). However several of these are identical due to the $\mathcal{D}_{3d}''$ symmetry so there are only eight independent equations for the flow of the eight independent coupling constants. The numerical coefficient α_1 is defined in Eq. (2.24) and

$$\alpha_2 \equiv \int \frac{dx}{2\pi}\frac{2f(x)}{(1+x^2)^2} \approx .469, \tag{2.27}$$

$$\alpha_3 \equiv \int \frac{dx}{2\pi}\frac{f(x)^2}{4(1+x^2)^2} \approx .066. \tag{2.28}$$

The term $2NA_{ij}g_{ij}^2$ in Eq. (2.25) corresponding to leading loop diagram (v) in Fig. 2.6(c) is naively the most significant quadratic term in Eq. (2.25), because it is leading in N. This term represents screening of repulsive interactions in the charge channel as expected in a fermionic system (since $A_{ij}\geq 0$). Note that this term is actually zero for the representation E_2'' and A_2, because these interactions commute with the single particle Hamiltonian. Therefore, to lowest order in $1/N$, the interactions E_2'' and A_2 are unscreened and free to grow strongly attractive. We hasten to add that that the higher order terms in Eq. (2.25) are very important and one cannot understand the behavior of the RG flows based only on the leading terms.

The single particle Hamiltonian is off-diagonal so there is a contribution of order $g^0 N^{-2}$ to the coupling g_{E_2} from the two Coulomb line diagram in Fig. 2.6(c)(iii,iv). These may be calculated,

$$\begin{aligned}
&\int \frac{d^2k d\omega}{(2\pi)^3}\left[\frac{\pi f(\frac{2m\omega}{k^2})}{Nm}\right]^2 \hat{G}(k,\omega)\otimes\left(\hat{G}(k,\omega)+\hat{G}(k,-\omega)\right)\\
=&2\int \frac{d^2k d\omega}{(2\pi)^3}(\frac{\pi f(\frac{2m\omega}{k^2})}{Nm})^2(\frac{k^2}{2m})^2\\
&\quad\times\left(\frac{\tau_z^{KK'}\tau_+^{AB}\otimes\tau_z^{KK'}\tau AB_- + hc}{(\omega^2+(\frac{k^2}{2m})^2)^2}\right)\\
=&\frac{\pi}{N^2 m}\int\frac{dk}{k}\int\frac{dx}{2\pi}\frac{f(x)^2}{(1+x^2)}\sum_{\gamma=x,y}\left(\tau_z^{KK'}\tau_\gamma^{AB}\otimes\tau_z^{KK'}\tau_\gamma^{AB}\right)\\
=&\frac{4\pi\alpha_3}{N^2 m}\log K\sum_{\gamma=x,y}\left(\tau_z^{KK'}\tau_\gamma^{AB}\otimes\tau_z^{KK'}\tau_\gamma^{AB}\right).
\end{aligned}\tag{2.29}$$

From this, it follows the that the free field point $g_{\mathcal{A}}=0$ is not a fixed point. Even if the the system starts with all bare couplings $g_{\mathcal{A}}(\gamma_1/2)=0$ it will flow under RG to have finite g_{E_2} and g_{B_1} with the other couplings fixed to zero by the $SU(4)$ symmetry of the single particle Hamiltonian. To demonstrate the behavior in this regime we ignore momentarily g_{B_1} which gives us a single equation for g_{E_2},

$$\begin{aligned}
\frac{dg_{E_2}(\ell)}{d\ell}=&-\frac{1}{N(N+2)}\left(\frac{\alpha_3(N+2)}{N}-\frac{(\alpha_2-\alpha_1)^2}{8N}\right)\\
&-2(N+2)\left(g_{E_2}-\frac{\alpha_2-\alpha_1}{4N(N+2)}\right)^2.
\end{aligned}\tag{2.30}$$

Since the first term on the RHS is negative, there can be no fixed point and g_{E_2} flows to $-\infty$ regardless of the initial conditions. (This holds whether we treat Eq. (2.30) to lowest order in N or simply plug in $N=4$). According to the mean-field theory (see Sec. 2.4), this suggests a nematic ground state[35] with transition at ≈ 100mK.

2.3.3 Applicability of our approximations

Let us turn to the justification of only including the diagrams Fig 2.6(c) in our treatment. Notice that it is different from the conventional $1/N$ approximation, see e.g Ref. [36]. There are two issues: (1) there are two loop diagrams which are leading order in $1/N$ but are not included, Fig. 2.7(c); and (2) there are diagrams that are subleading in N which are taken into account (compare the bubble and ladder diagrams in Fig. 2.6(c).

To address the first issue, let us discuss diagrams of Fig. 2.7 c in more detail. They are non-vanishing only for g_{E_2} and have the form $\delta g_{E_2} \sim \frac{g_{E_2}}{N}\left(C\ln^2(K) + D\ln(k)\right)$. The term $\ln^2$ is produced by two iterations of the the RG equations (by substituting diagrams (iii) and (iv) into diagram (v)) but the second term does contribute to the linear term in the RG equation $2\alpha_2 A_{E_2} \to 2\alpha_2 A_{E_2} + D$. The constant D, however, depends on the cutoff scheme so that the term linear in g_{E_2} in the RG equation for g_{E_2} is not known (for the other constants it is well defined). Fortunately, is does not matter for the divergent behavior at large N. Consider the situation with all other constants except g_{E_2} fixed to zero, keeping only coefficients leading in $1/N$, compare Eq. (2.30),

$$\frac{dg_{E_2}}{d\ell} = -\frac{\alpha_3}{N^2} - \frac{\alpha_1 + 2\alpha_2}{N} g_{E_2} - 2N g_{E_2}^2 \tag{2.31}$$

The quadratic term dominates the constant term when $g_{E_2} \geq N^{-\frac{3}{2}}$ at this point, but then the linear term is smaller by a factor of $1/\sqrt{N} \ll 1$. Thus, contrary to initial appearance, the linear term is of higher order in $1/N$ for g_{E_2} - so that we leave it in Eq. (2.25) only for simplicity. It makes essentially no difference to the evolution of the RG equations.

To address the second question we notice that the bubble diagram Fig. 2.6c(v) contains an extra factor of N in comparison with diagrams (vi, vii,viii). The latter diagrams are not diagonal in terms of the coupling constant, as given by the tensor C^{ij}_{klmn}, whereas the bubble diagram is $\propto N g_{ij}^2$ by construction. The large amounts of constants involved in the non-diagonal term may overcome the factor of N in the diagonal terms; therefore keeping both is legitimate. The higher order terms may be considered as $1/N$ corrections to the tensors A_{ij} and C^{ij}_{klmn} respectively. For example, Fig. 2.7(a) is a leading $1/N$ correction to $A_i j$, whereas Fig. 2.7(b) is a leading $1/N$ correction to C^{ij}_{klmn}, even though the two diagrams do not have the same in order in N.

Finally, we compare our treatment to the existing theoretical contributions. The first attempt at an RG treatment of BLG can be found in Ref. [11], however it does not appear consistent with our results[37]. The work of Vafek and Yang [14] is similar in spirit but contains only the G_1 and B_2 out of the eight possible representations and treats the Coulomb interaction as short range. The later work of Vafek[8]contains the RG equations for the full eight constants but again treats the Coulomb interaction as short ranged. The treatment of Ref. [3] is completely at the mean-field level and corresponds to counting only the diagrams from Fig. 2.6c marked (i) and (ii), which is not a parametrically justified approximation as well as considering only the B_2 representation. Ref. [12] considered a mean field theory of the BLG, however their results appear to depend on an unreaslistically strong next nearest neighbor interaction. Ref. [38] attempted to calculate numerically the functional RG equation keeping the full momentum

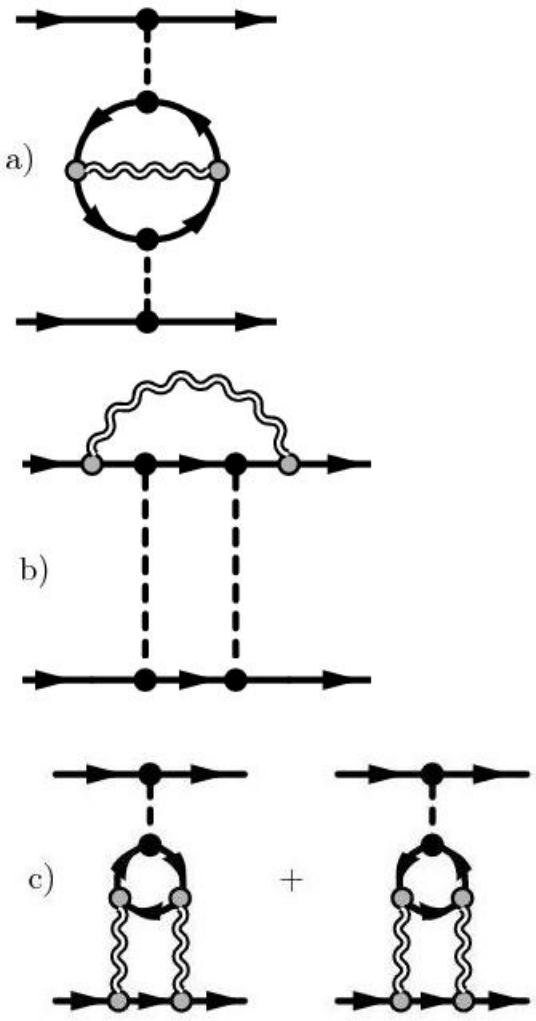

FIGURE 2.7: a) Schematic representation of the "bubble" diagrams where the shaded blob represents all possible connected diagrams, and arbitrary Coulomb propagators may be added. b) Similar representation of the "ladder" diagrams. The leading diagrams from both of these groups are included, even though this is not strictly parametrically correct. c) A second loop contribution to the anomalous dimension of the coupling g_{E_2} which is disregarded.

dependence of the four fermion interaction and calculating the beta function perturbatively - this is not a parametrically justified treatment A Hartree-Fock analysis was performed in Ref. [39].

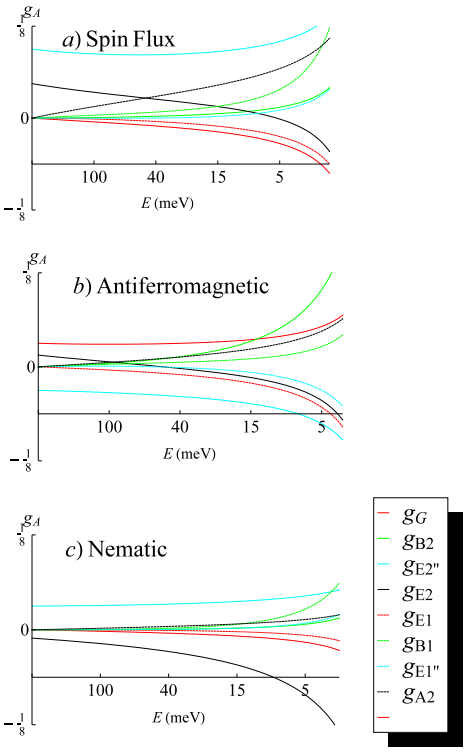

FIGURE 2.8: Plots of the coupling constant as a function the running RG scale $\ell = \log(K_0/K)$. There are eight running couplings labeled by the corresponding representation. The density-density couplings are given by solid lines, the current-current couplings by dashed. The graphs end when the couplings become of order $1/N = 1/4$. They reach a singularity a finite ℓ soon after the graph ends.

2.4 RG Flows, Their Termination and Renormalized Mean Field Treatment of Symmetry Breaking

In this section we describe the numerical analysis of the coupling constant RG flows described by Eq. (2.25) and show that there are no weak coupling fixed points. The divergence of coupling constants in 2D at zero temperature indicates spontaneous symmetry breaking. (Unlike in 1D the quantum fluctuations in 2D are not infrared divergent and do not destroy zero temperature phases.) We analyze the resulting phases within mean-field theory, using the coupling constants renormalized by the RG. This treatment is superior to simply doing mean field start from the high energy scale since in that case the large logarithms are not summed in a controlled fashion.

2.4.1 General structure

If the initial RG conditions are such that $g_{\mathcal{A}}(\gamma_1/2) \neq 0$, then the $SU(4)$ symmetry is absent and we must consider the flow of all the coupling under the RG. Determining if there exist any fixed points cannot be done analytically as it requires solving a polynomial of the 64th order. However, a numerical solution shows that there exist no fixed points. Therefore at least some of the couplings must grow infinitely. At the same time, the leading term quadratic in the couplings in Eq. (2.25) $\sim Ng^2$, always with a non-positive coefficient, so we expect generically that large positive coupling to be driven back to zero. For all positive initial coupling constants, this means that the system will be driven to the free field point until g_{E_2} becomes large and negative. This behavior is confirmed by the numerical evolution of the RG equations (see Fig. 2.8 where g_{E_2} always becomes negative and increases until the other couplings diverge).

Note that although we have set the current-current couplings g_{B_1}, g_{A_2}, g_{E_1} and $g_{E_1''}$ to zero initially, they are generated through renormalization. The examples of the RG equation shown in Fig. 2.8 indicate the current-current couplings become of the same order as the density-density couplings at low energies. Therefore we cannot ignore the current-current interactions when analyzing the ground state, and ignoring them would lead to misleading results.

The coupling g_{B_2} has been given special emphasis in some of the earlier studies[5]. We find that in the RG equations it does not seem to play an exclusive role, as can be seen in Fig. (2.9), where it is screened efficiently - the leading term in the RG flow is $2Ng_{B_2}^2$. Note that large positive initial g_{B_2} does not provoke a phase transition to the AF state on its own (see Fig (2.8)). Once g_{E_2} becomes relatively large the presence of a finite g_{B_2} will change the structure of the flow, especially since it breaks the $SU(4)$, however not in a marked way. For example, starting with all other couplings set to zero except for g_{B_2}, g_{E_2} still becomes the most significant negative coupling, and the nematic phase is the preferred phase. As a result, g_{B_2} is perhaps the least important of the four couplings. This is not a conclusion that can be reached on general grounds, but only by solving the detailed RG equations over a broad range of parameters. Moreover, at least some of the couplings behave non-monotonically. Initially negligible coefficients may end up diverging quickly (e.g. g_{A_2} in Fig(2.8(a)). At the same time a couplings that is not large at the end of the RG flow may change the character of the flow in the initial stages.

The RG equations contain terms up to second order in g. Therefore, it may be easily seen that since there is no fixed point, the couplings always go to infinity as $g_{\mathcal{A}} \sim \lambda_{\mathcal{A}}(\ell_0 - \ell)^{-1}$ where ℓ_0 gives the value of the singularity in the RG flow and the $\lambda_{\mathcal{A}}$ determine how quickly each constant diverges. Mathematically, there are six sets of $\{\lambda_{\mathcal{A}}\}$ that satisfy the RG equations and are stable to perturbation. One might be tempted to determine the ground state, using this

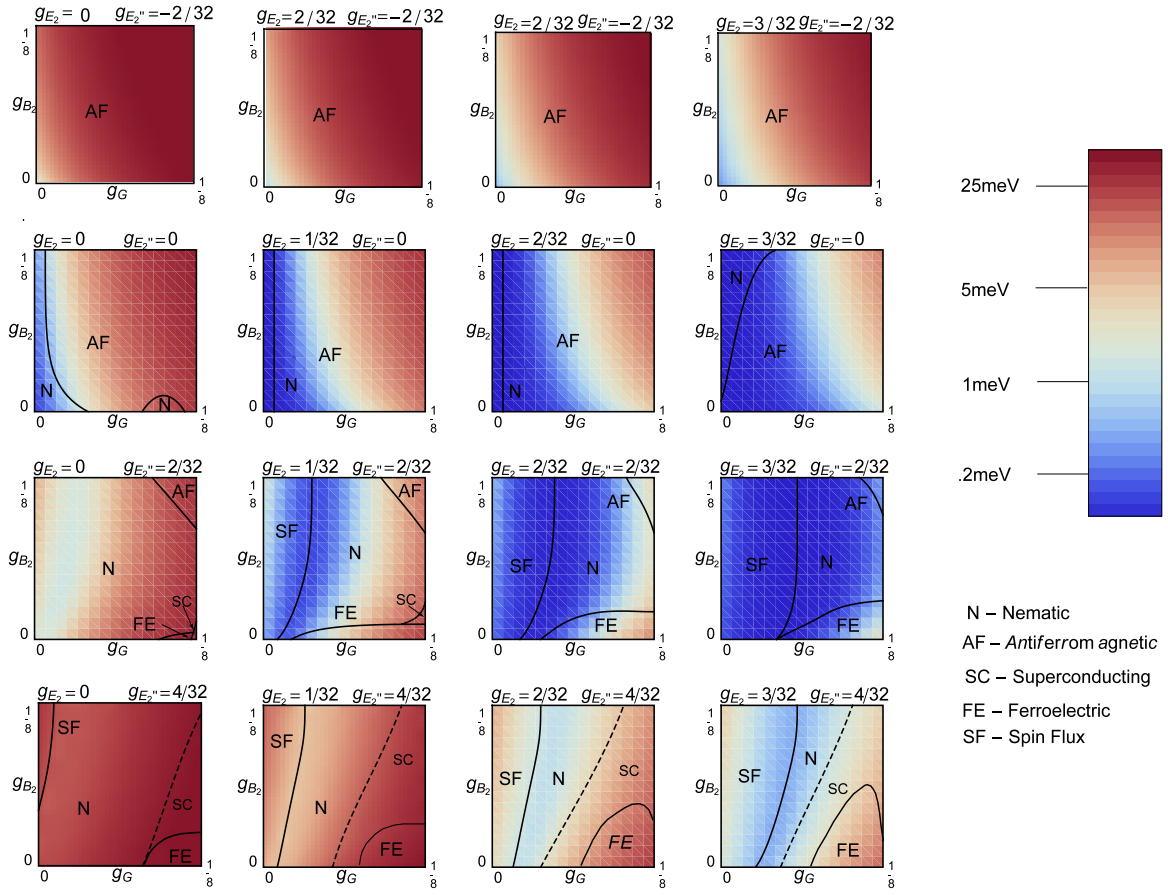

FIGURE 2.9: Plot of the broken symmetry phase and energy scale for BLG as a function of bare coupling constants. When the energy scale is less $E_{LiTr} \approx 1meV$ the broken symmetry state is in competition with the Lifshitz transition and the BLG may remain metallic (with eight Dirac points). Dashed line indicates the region where the triplet superconducting phase (SC) is very close in energy (but slightly above) to normal (nematic or ferroelectric) states.

mathematical feature, via the coefficients $\lambda_{\mathcal{A}}$. However these coefficients are meaningful only for the RG at $g_{\mathcal{A}} \gg 1$ which is outside the range of validity of the proposed theory and the RG equation (2.25). Moreover, $g \to \infty$, indicates an instability towards a broken symmetry states, so that we shall use a mean field theory starting from the energy scale where some of the couplings become sufficiently large.

2.4.2 Ground state energies within renormalized mean-field approach

The unbounded growth of coupling constants in the RG flow generally indicates the development of a spontaneous symmetry breaking and the opening of a gap. To describe the corresponding phase transition we use a self-consistent mean-field theory. The self-consistent mean-field theory

is implemented by replacing all possible pairs of fermions in the quartic interaction terms with their mean values. For this we introduce the Gorkov-Nambu vectors which adjoin the two 8-component vectors ψ and $\psi^\dagger$ as follows,

$$\begin{aligned}\Psi(\boldsymbol{k}) &\equiv \begin{pmatrix} \psi(\boldsymbol{k}) \\ \hat{\mathcal{T}}\left(\psi^\dagger(-\boldsymbol{k})\right)^t \end{pmatrix}_N, \\ \Psi^\dagger(\boldsymbol{k}) &\equiv \begin{pmatrix} \psi^\dagger(\boldsymbol{k}), & -\left(\psi(-\boldsymbol{k})\right)^t \hat{\mathcal{T}} \end{pmatrix}_N,\end{aligned} \tag{2.32}$$

where $\hat{\mathcal{T}} \equiv i\tau_y^{KK'}\tau_y^{AB}\sigma_y$ is the time reversal matrix. We also introduce Pauli matrices $\tau^N_{0,x,y,z}$ acting on the Nambu space. The vectors $\Psi^\dagger$ and Ψ satisfy the condition

$$\Psi^\dagger(\boldsymbol{k}) = i\Psi^t(-\boldsymbol{k})\tau_y^N\hat{\mathcal{T}} \tag{2.33}$$

We rewrite the interaction terms with the help of the Nambu vectors

$$\sum_{ij}\left(\psi^\dagger\tau_i^{KK"}\tau_j^{AB}\psi\right)^2 = \frac{1}{4}\sum_s g_s\left(\Psi^\dagger\cdot\hat{M}_s\cdot\Psi\right)^2. \tag{2.34}$$

Here $M_s \equiv \tau_i^{KK'}\tau_j^{AB}\tau_k^N\sigma_l$ acts on the 16 dimensional space spanned by the Nambu vectors and we write s as a shorthand for the list (ijkl). The couplings g_s are defined as $g_{abz0} = g_{ab}$, $g_{00z0} = g_{00}$, $g_{a000} = g_{a0}$ and $g_{0b00} = g_{0b}$, where $a, b = x, y, z$ and all other constants are zero. The factors of τ_z^N are necessary since we must have

$$(i\tau_y^N\mathcal{T})M_s^t(i\tau_y^N\mathcal{T}) = -M_s \tag{2.35}$$

to satisfy both Eq. (2.33) and fermion anticommutivity.

The mean field approximation consists of replacing pairs of fermionic operators in Eq. (2.34) with their expectation values as follows:

$$\begin{aligned}\frac{1}{4}\sum_s g_s\left(\Psi^\dagger\cdot\hat{M}^s\cdot\Psi\right)^2 \approx \frac{1}{2}\sum_s g_s\Big\{&\Psi^\dagger\cdot\hat{M}^s\cdot\Psi\langle\Psi^\dagger\cdot\hat{M}^s\cdot\Psi\rangle \\ &+2\,\Psi^\dagger\cdot\left(\hat{M}_s\cdot\langle\Psi\otimes\Psi^\dagger\rangle\cdot\hat{M}_s\right)\Psi - \frac{1}{2}\left(\langle\Psi^\dagger\cdot\hat{M}^s\cdot\Psi\rangle\right)^2 \\ &+ tr\left[\left(\langle\Psi\otimes\Psi^\dagger\rangle\cdot\hat{M}_s\right)^2\right]\Big\}.\end{aligned} \tag{2.36}$$

Here we have used the fact that, according to Eqs. (2.33) and (2.35),

$$\Psi^\dagger\cdot\hat{M}^s\cdot\Psi = \Psi^t\cdot(i\tau_y\mathcal{T})\hat{M}_s^t(i\tau_y\mathcal{T})\cdot(\Psi^\dagger)^t = -\Psi^t\cdot\hat{M}^s\cdot(\Psi^\dagger)^t$$

to combine the Cooper and Fock terms.

Now we assume that the there is some nonzero expectation value of the fields which corresponds to a non-zero order in one of the phases classified in Appendix A.

$$\langle \Psi \otimes \Psi^\dagger \rangle \equiv -\frac{1}{2Nc_{\mathcal{A}}} \left(\frac{m}{4\pi}\right) \sum_\alpha \hat{M}^\alpha_{\mathcal{A}} \Delta^\alpha_{\mathcal{A}}, \tag{2.37}$$

where matrices $\hat{M}^\alpha_{\mathcal{A}}$ are specified for each phase $\mathcal{A}$ in Appendix A and $\mathbf{\Delta}_{\mathcal{A}} = \{\Delta^\alpha_{\mathcal{A}}\}$ is the order parameter, which is singlet or multi-component depending on the phase. Below we will use the notation $|\mathbf{\Delta}_{\mathcal{A}}|^2 \equiv \sum_\alpha |\Delta^\alpha_{\mathcal{A}}|^2$. The effective interaction constant $c_{\mathcal{A}}$ are defined for each phase as,

$$c_{\mathcal{A}} \equiv \sum_s g_s \left\{ \delta_{s\mathcal{A}} - \frac{1}{4N^2} tr \left[\left(\hat{M}_s \hat{M}_{\mathcal{A}} \right)^2 \right] \right\}. \tag{2.38}$$

The assumption of a finite expectation value is consistent only if $c_{\mathcal{A}} < 0$. The interaction mean field energy is therefore,

$$H_{sr} = \frac{1}{2} \sum_\alpha \Delta^\alpha_{\mathcal{A}} \left(\Psi^\dagger \cdot \hat{M}^\alpha_{\mathcal{A}} \cdot \Psi \right) - \frac{m}{8\pi c_{\mathcal{A}}} |\mathbf{\Delta}_{\mathcal{A}}|^2. \tag{2.39}$$

Including the effect of the single-particle Hamiltonian $\hat{H}_0$, defined in Eq. (2.7), the total mean field Hamiltonian is,

$$H_{MF} = \frac{1}{2} \sum_k \Psi^\dagger(\boldsymbol{k}) \left[\hat{H}_0 \tau_z^N + \sum_\alpha \Delta^\alpha_{\mathcal{A}} \hat{M}^\alpha_{\mathcal{A}} \right] \Psi(\boldsymbol{k}) - \frac{m|\mathbf{\Delta}_{\mathcal{A}}|^2}{8\pi c_{\mathcal{A}}}, \tag{2.40}$$

for fixed values of the order parameters $\Delta^\alpha_{\mathcal{A}}$.

In the spirit of the Hartree-Fock or BCS theory, we diagonalize Eq. (2.40) to obtain the ground state energy per unit area,

$$E_{MF}\left(\{\Delta_{\mathcal{A}}\}\right) = -N \int_{\frac{k^2}{2m} < \mathcal{E}_c} \frac{d^2k}{2\pi} \varepsilon(k, \mathbf{\Delta}_{\mathcal{A}}) - \frac{m|\mathbf{\Delta}_{\mathcal{A}}|^2}{8\pi c_{\mathcal{A}}(\mathcal{E}_c)}. \tag{2.41}$$

Here $\varepsilon(k, \{\Delta_{\mathcal{A}}\}))$ are the positive eigenvalues of the matrix $\hat{H}_0 \tau_z^N + \sum_\alpha \Delta^\alpha_{\mathcal{A}} \hat{M}^\alpha_{\mathcal{A}}$ and the factor of N comes from the degeneracy. The energy scale $\mathcal{E}_c$ is the energy scale at which we stop the RG. The integral in Eq. (2.41) evaluates to

$$\int_{\frac{k^2}{2m} < \mathcal{E}_c} \cdots = \text{const} + \frac{m|\mathbf{\Delta}_{\mathcal{A}}|^2}{2\pi} \left(\alpha_{\mathcal{A}} + \beta_{\mathcal{A}} \ln \frac{\mathcal{E}_c^2}{|\mathbf{\Delta}_{\mathcal{A}}|^2} \right), \tag{2.42}$$

where $\alpha_{\mathcal{A}}$ and $\beta_{\mathcal{A}}$ are coefficients that depend on the phase $\mathcal{A}$. The coefficients $\alpha_{\mathcal{A}}$ may be explicitly calculated from Eq. (2.41) (the value of $\beta_{\mathcal{A}}$ is irrelevant as we will see). We list here $\alpha_{\mathcal{A}}$ for the states where $\Delta \cdot M$ may be written as $\sum_{ijkl} u_i v_j w_k x_l \tau_i^{AB} \tau_j^{KK'} \sigma_k \tau_l^N$. Because of the symmetry of H_0 there are only three independent coefficients. Labeling the coefficient α by the representation and using the superscript n or s to denote normal or superconducting we have

$$\begin{aligned}
&\alpha^n_{A_1} = \alpha^n_{A_2} = \alpha^n_{E''_2} = \alpha^s_{B_1} = \alpha^s_{B_2} = \alpha^s_{E''_1} = 1, \\
&\alpha^n_{B_1} = \alpha^n_{B_2} = \alpha^n_{E''_1} = \alpha^s_{A_1} = \alpha^s_{A_2} = \alpha^s_{E''_2} = \frac{1}{2} + \log 2 \approx 1.19, \\
&\alpha^n_{E_2} = \alpha^n_{E_1} = \alpha^n_G = \alpha^s_{E_2} = \alpha^s_{E_1} = \alpha^s_G = \frac{1}{4} + \log 2 \approx 0.94.
\end{aligned} \tag{2.43}$$

The coefficients for the spin singlet and spin triplet normal states are the same because of symmetry. These coefficients are sufficiently close to one that we have simply taken $\alpha_{\mathcal{A}} \approx 1$. the term $\beta_{\mathcal{A}} \ln \frac{\mathcal{E}_c^2}{\Delta^2}$ in Eq. (2.42) should be interpreted as the continuation of the RG flow from the scale $\mathcal{E}_c$ down to the energy $|\mathbf{\Delta}|$. Although obtained by using mean-field theory, since the flow of $c_{\mathcal{A}}$ is governed by the RG equation (2.25), we have to replace the logarithmic correction to Eq. (2.42) with the evaluation of $c_{\mathcal{A}}$ at the energy Δ. The mean field energy density is therefore written as,

$$E\left(\Delta_{\mathcal{A}}\right) = \frac{m}{8\pi}\left[-2N - \frac{1}{c_{\mathcal{A}}(|\Delta_{\mathcal{A}}|)}\right]|\mathbf{\Delta}_{\mathcal{A}}|^2, \; c_{\mathcal{A}} < 0 \tag{2.44}$$

The ground state may now be determined by minimizing Eq. (2.44) with respect to $\Delta_{\mathcal{A}}$ with the $c_{\mathcal{A}}(\Delta)$ obtained by numerical integration of the RG equations. The ground state energy gap will then be equal to the value of $|\Delta|$ at the minimum.

It is important to note that we expect to find this minimum when the coefficient $c(|\Delta|) \sim \frac{1}{2N}$ which is inside of range of validity for our RG equation, $g \sim 1/N$. The remaining subtlety is the inclusion of the long-range Coulomb interaction into the mean-field description. Usually, it enters in the statically screened limit $g_{00z0} \simeq 1/N$ and does not diverge at the transition. Furthermore, according to Eq. (2.38), this constant can produce only finite $1/N^2$ correction (positive to all supercoducting states and negative for all normal states). Therefore, we will neglect g_{00z0} in the further manipulations.

2.5 The phase diagram

The result of minimizing Eq. (2.44) is presented in Fig. 2.9. We find by extensive numerical investigation only five out of the possible sixty-four phases enumerated in Appendix A (10 in

the charge channel, 22 in the spin and 32 in the Cooper channels). They are the nematic phase, the antiferromagnetic phase, the spin flux phase, and in the corners of the parameter space of bare interaction, ferroelectric phase, and singlet and triplet superconductor phases.

Note that it is also possible that the resulting gaps are smaller than the energy of the Lifshitz transition[13], $\mathcal{E}_{LiTr} \approx 1meV$. In this case the renormalization of coupling constants is stopped at $\mathcal{E}_{LiTr}$, spontaneous symmetry breaking does not occur and the system remains in the symmetric state with the four Dirac cone spectrum.

Figure 2.9 shows the results of the RG analysis in terms of the resulting symmetry broken phases. We find that there is significant variation in the scale $\mathcal{E}$, $\log(\mathcal{E}_0/\mathcal{E}) \sim 1 \div 20$, as expected from the wide range of couplings analyzed. If we consider small initial couplings the $g_{\mathcal{A}} \ll 1/N$ then the RG is driven by the constant term and $\log(\mathcal{E}_0/\mathcal{E}) \sim 10$ irrespective of the initial conditions, resulting in a symmetry breaking only at extremely small energy scale $\mathcal{E} \sim 10^{-2}meV$.

There is a variety of phases that have been proposed as the ground state of BLG that we do not find. An anomalous quantum Hall state (QAH) state was suggested in Ref. [9], corresponding to the representation g_{A_2} with order parameter $\langle\psi^\dagger\tau_z^{AB}\psi\rangle$. This is not found as a ground state in our analysis. In the same paper, and in Refs. [6, 11], a large manifold of quantum hall ferromagnetic states were suggested containing the representations E_2'', A_2 and B_2 in both spin singlet and spin triplet representation. All of these states were considered as degenerate appealing to the $SU(4)$ symmetry of the single particle Hamiltonian, Eq. (2.7). In both cases the artificial $SU(4)$ symmetry was assumed to be exact, which is contradicted by the importance of the short range interactions we find here in solving the complete set of RG equations. The loop current state of Ref [12] corresponding to representation A_2 in the singlet channel also does not appear. In Ref. [38] they suggest a "CDW_3 state",which is in the singlet G representation. We do not find it here.

In subsections below, we discuss the details of each phase. We will present a comparative flows of the couplings defined in Eq. (2.38) to illustrate the competition between phases, see Figs. 2.10 – 2.15.

2.5.1 Nematic Phase (N)

In the nematic phase, there is a finite expectation value for the order parameter $\langle\psi^\dagger\tau_z^{KK'}\tau_{x,y}^{AB}\psi\rangle$, breaking the rotational symmetry of the system from six-fold to two-fold while maintaining translational symmetry. The order parameter is characterized by enhanced electron hopping in one direction. The interaction energy for this phase depends on the combination of parameters

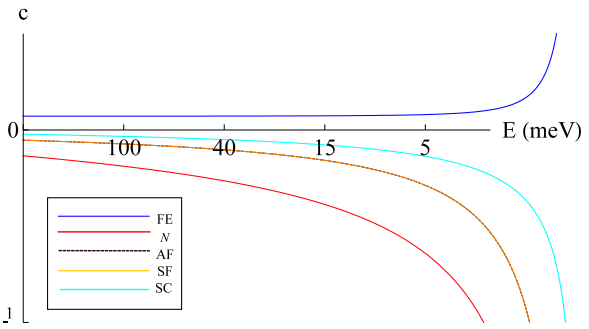

FIGURE 2.10: Interaction energy as a function of energy scale for selected phase with initial conditions $g_G = -.0$, $g_{B_2} = .06$, $g_{E_2''} = 0$, $g_{E_2} = -.03$ and all others zero. For these initial conditions the nematic phase is the ground state

obtained from Eq. (2.38):

$$c_N = \frac{1}{8}g_{B_2} - \frac{1}{4}g_{E_2''} + g_{E_2} + \frac{1}{8}g_{B_1} - \frac{1}{8}g_{E_1''} - \frac{1}{8}g_{A_2}. \tag{2.45}$$

It is the preferred ground state in the absence of intervalley scattering, and it is also generally the ground state when the bare g_{E_2} coupling is negative. Note that a negative contribution towards bare g_{E_2} comes from the electron-electron interaction via the polarization of the lattice, ie. via virtual excitation/absorption of in plane phonons near the Γ point. The nematic phase is also the ground state over other large parts of the parameter space as can be seen in Fig. 2.9. This reflects the fact that the coupling g_{E_2} almost always becomes negative rapidly (see Fig. 2.8).

We previously proposed the nematic phase as a possible ground state in based on a more limited analysis of the RG equations [13]. Using a similar renormalization group analysis Vafek and Yang[8, 14] also find the nematic phase as a possible ground state, supporting the analysis in this paper.

The most notable characteristic of the nematic phase is that it remains gapless, but with the parabolic bands reconstructed into two Dirac mini-cones at energies less than $|\mathbf{\Delta}|$. The nematic phase would show metallic behavior in conductance measurements, but decreasing density of states at low densities. The nematic state preserves time reversal symmetry and so it should not show asymmetry between positive and negative magnetic fields in magneto-transport. The nematic order parameter transforms in the same representation of $\mathcal{D}_{3d''}$ as uniaxial strain so that

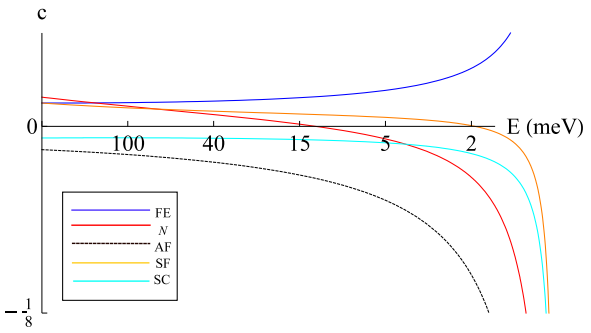

FIGURE 2.11: The interaction energy as a function of energy scale for some choice of initial parameters with initial conditions $g_G = -.075$, $g_{B_2} = .06$, $g_{E_2''} = 0$, $g_{E_2} = .015$ and all others zero. In this case the ground state is the AF phase.

strain will couple directly to this state. It is possible that strain could induce a transition into the nematic phase[40], even if unperturbed BLG chooses another phase as the ground state.

2.5.2 Anti-ferromagnetic Phase (AF)

The anti-ferromagnetic phase is defined by a nonzero expectation value of $\langle \psi^\dagger \tau_z^{AB} \tau_z^{KK'} \vec{\sigma} \psi \rangle$. This state corresponds to opposing magnetic moments on the A and B sublattices. The orbital part breaks the reflection symmetry between the two sublattices but otherwise preserves the $\mathcal{D}_{3d}''$ symmetry of the BLG in its entirety.

The exchange energy depends on the following combination of coupling constants obtained from Eq. (2.38):

$$\begin{aligned} c_{AF} = &-\frac{1}{2} g_G - \frac{1}{8} g_{B_2} \\ &+ \frac{1}{4} \left(g_{E_2''} + 2 g_{E_2} + g_{E_1} + g_{E_1''} \right) - \frac{1}{8} g_{B_1} - \frac{1}{8} g_{A_2} \end{aligned} . \tag{2.46}$$

The AF promoted strongly by the coupling g_G, with the factor of four coming from the dimension of the representation G. This effect is amplified by the sensitivity of the RG equations to the coupling g_G. As a result even small values of g_G near the free field point make the AF state the ground state. The AF state is also promoted by negative $g_{E_2''}$ and is generally the ground state when we start with negative $g_{E_2''}$. Again we emphasize that these conclusions come from the combination of RG equations and interaction energy, not just from the interaction energy alone. Other authors have proposed this AF state as a possible ground state. Kharitonov [5] suggested the AF state based on experimental evidence and simple mean field theory arguments applied

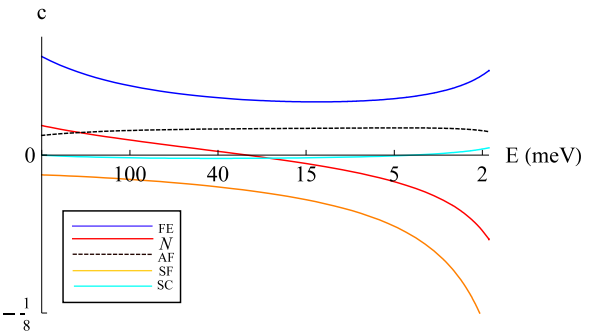

FIGURE 2.12: Interaction energy for selected phases a function of energy scale with initial conditions $g_G = 0$, $g_{B_2} = .06$, $g_{E_2''} = .06$, $g_{E_2} = .03$ and all others zero. In this case the ground state is the spin flux state shown in orange

at the high-energy scale directly. The structure of our RG equations indicate that such a simple mean field theory is not applicable to BLG, although it does suggest the same state.

The AF phase is expected to be an insulating state with activated gap behavior in transport measurements. Although the magnetic field does not couple directly to the AF state since it is antiferromagnetic, the Zeeman energy splitting does break the $SU(2)$ spin symmetry of the system (spin-orbit is negligible). The LAF state is adiabatically connected to a quantum Hall ferromagnetic state at higher magnetic field. A lack of features between the zero and high magnetic field state might be the evidence that the zero magnetic field state is AF[5].

2.5.3 Spin flux (spin Hall) Phase (SF)

The spin flux (SF) phase (elsewhere called a quantum spin Hall state) is defined by the finite expectation value of $\langle \psi^\dagger \tau_z^{AB} \vec{\sigma} \psi \rangle$. The effect of this on the electrons is equivalent to the development of a finite spin orbit coupling, and gaps the electronic spectrum. It may be viewed as a state where spin currents circle the honeycomb rings, or as a quantum anomalous Hall effect state, but with opposite signs for opposite spins, producing no net charge current, so that this state preserves time reversal invariance.

The interaction energy of the SF depends on the combination of coupling constants obtained from Eq. (2.38):

$$c_{SF} = \frac{1}{4}\left(g_{E_2''} - g_{E_2} + g_{E_1} - g_{E_1''}\right) - \frac{1}{8}\left(g_{B_2} + g_{B_1} + g_{A_2}\right). \tag{2.47}$$

The SF state has a similar matrix structure as the AF state and therefore a similar interaction

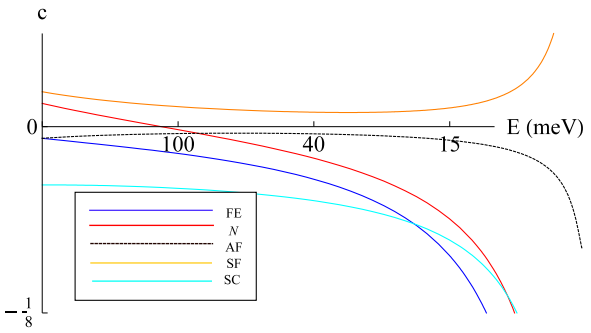

FIGURE 2.13: The evolution of the interaction energy of the selected phases as a function of the energy scale with initial conditions $g_G = .06$, $g_{B_2} = 0$, $g_{E_2''} = .06$, $g_{E_2} = .075$ and all others zero. In this case the ground state is a ferroelectric phase. The difference in energy between the F phase and nearby phases is quite small.

energy. However it is not promoted by large g_G, unlike the AF phase. Therefore, generically, large g_G generally suppresses the SF in favor of other states as can be seen in Fig. 2.9.

Analogously to the case of spin-orbit coupling in monolayer graphene[41], the finite value of the spin flux OP may create a "spin Hall effect" with quantized spin Hall conducivity. The edge states and insulating bulk imply a quantized conductance of $4e^2/h$, unless they are localized by magnetic and intervalley-scattering disorder. The state is time reversal invariant, so no transverse conductance at zero magnetic field is possible.

2.5.4 Limits of applicability: Ferroelectric Phase

The ferroelectric (FE) phase is characterized by a non-zero expectation value of $\langle \psi^\dagger \tau_z^{AB} \tau_z^{KK'} \psi \rangle$. It is a spontaneous charging of the BLG with opposite charge on the two layers.

The interaction energy for this phase depends on the combination of couplings obtained from Eq. (2.38):

$$c_F = \frac{7}{8} g_{B_2} + \frac{1}{4}\left(g_{E_2''} - g_{E_2} + g_{E_1} - g_{E_1''}\right) - \frac{1}{8} g_{B_1} - \frac{1}{8} g_{A_2}. \tag{2.48}$$

We find that the ferroelectric phase is strongly suppressed by positive bare g_{B_2} and the development of the FE phase requires the g_{B_2} coupling to diverge to negative infinity, which can only happen in a small sliver of the phase space where the combination of the higher order diagrams conspire to drive g_{B_2} negative. Even in this section the energy difference between the ferroelectric and competing phases is never large, and it may be that in a more accurate calculation it never appears as the ground state.

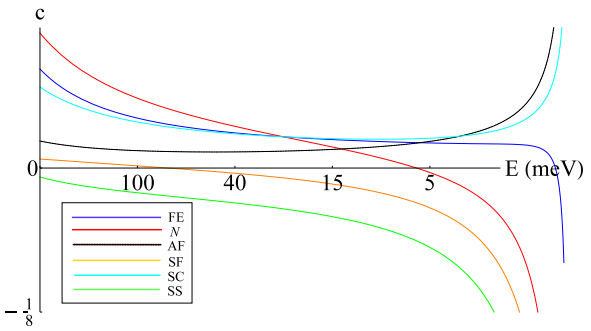

FIGURE 2.14: Interaction energy for selected phases as a function of the energy scale with initial conditions $g_G = -.045$, $g_{B_2} = .06$, $g_{E_2''} = -.06$, $g_{E_2} = .09$ and all others zero. In this case the singlet superconducting phase is the ground phase.

The FE state was also proposed in Ref. [3]. However this analysis was based on a flawed mean field theory treatment counting only the diagrams from Fig. 2.6 (c) marked (i) and (ii) as well as considering only the single parameter scaling theory with one interaction constant in the B_2 channel. These are not parametrically justified approximations.

The ferroelectric phase is a completely gapped state, with neither neutral nor charged excitations. It is also a trivial insulator in that it does not possess protected edge modes. Therefore, it should display insulating transport behavior. An external field perpendicular to the BLG flake would promote the FE phase, increasing the gap due to the interlayer symmetry breaking at the single particle level [1]. This does not seem to take place in any of the recent experiments [16, 18] on BLG, where the external transverse field destroyed the zero-field state, and introduced a distinct state determined by the interlayer asymmetry.

2.5.5 Limits of applicability: Superconducting Phases

The singlet superconducting (SS) phase is characterized by the usual order parameter $\langle \psi^\dagger \mathcal{T} \psi^\dagger \rangle$. The coupling for this phase is found from Eq. (2.38) to be:

$$\begin{aligned} c_{SS} = &\frac{1}{2} g_G + \frac{1}{8} g_{B_2} \\ &+ \frac{1}{4}\left(g_{E_2} + g_{E_2''} - g_{E_1} - g_{E_1''} \right) - \frac{1}{8} g_{A_2} - \frac{1}{8} g_{B_1}. \end{aligned} \tag{2.49}$$

The stability of this phase requires very significant negative couplings from the very beginning and the phase can not arise from the purely repulsive interaction.

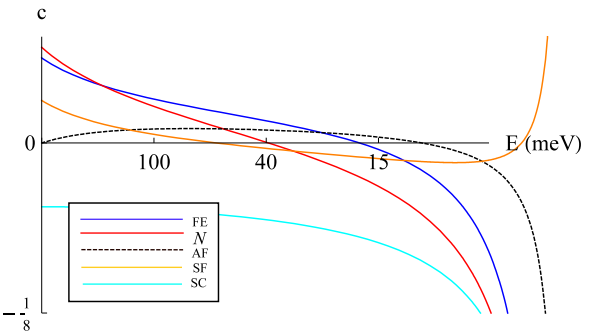

FIGURE 2.15: Interaction energy for selected phases as a function of the energy scale for initial repulsive short range interaction. In this case the triplet superconducting phase is very close to the ground phase with initial conditions $g_G = .06$, $g_{B_2} = .06$, $g_{E_2''} = -.12$, $g_{E_2} = .06$ and all others zero. Even though c_{SC} appears to be the most negative, minimization of Eq. (2.44) gives the nematic state as a preferd ground state.

The triplet superconducting (SC) phase has the order parameter $\langle \psi^\dagger \tau_z^{KK'} \vec{\sigma} \mathcal{T} \psi^\dagger \rangle$, with the pairing function of the opposite signs in the K and K' valleys.

Its interaction depends on the combination of couplings obtained from Eq. (2.38):

$$\begin{aligned} c_{SC} = &-\frac{1}{2} g_G + \frac{1}{8} g_{B_2} \\ &+ \frac{1}{4} \left(g_{E_2} - g_{E_2''} - g_{E_1} + g_{E_1''} \right) - \frac{1}{8} g_{A_2} - \frac{1}{8} g_{B_1}. \end{aligned} \tag{2.50}$$

For the repulsive interaaction, the triplet SC phase only appears as a stable phase at large couplings.

To conclude, both superconducting phases appear only on the limits of the applicablity of the theory. Moreover, finite value of the underscreened Coulomb interaction push the energies of those stated further up. It is therefore possible that the appearance of the SC phases is merely an artifact of our inability to deal properly with strong couplings, and that the superconductivity does not belong to the actual phase diagram.

2.6 Conclusion

Several results have been established in this paper. The ground state of BLG cannot be understood without considering the high energy couplings in detail, because different couplings lead to different ground states. Moreover naive expectations about the importance of certain couplings are not borne out and all plausible combinations must be considered. In particular excluding

intervalley scattering leads to misleading results. The previously reported nematic state is the ground state for a significant fraction of these couplings. Of the large number of ground states that are possible we find only five appear. They are nematic, antiferromagnetic, ferroelectric and triplet superconductor, as well as a "spin flux" phase not previously proposed. The nematic, antiferromagnetic and spin flux phases seem the most likely candidates.

The present work may be extended in a variety of ways. The accuracy of the renormalization group equations may be improved and validated by considering higher order diagrams and a more detailed mean field theory constructed. One may also try to connect the value of the couplings at the scale $\gamma_1/2 \approx 0.2eV$ with their value at the bandwidth of the π orbitals. The possible phase transitions between the proposed states and the behavior of domain walls between regions of different phases may be needed to properly account for the transport data.

Such improvements aside, the unique challenge of theoretically determining the electronic ground state of BLG has been laid out. The problem naturally involves the competition of an uncommonly large set of phases and interactions. Truncating the theory to a more tractable subset does not appear to give accurate results. Instead the problem must be attacked in its full complexity.

Chapter 3

Memory Effects in Disordered Metals

3.1 Introduction

There are several phenomena in electronic systems that occur on extremely long time scales. One well-known example is the $1/f$ noise[42], where the power spectrum of the conductivity noise shows power law scaling in a range of frequencies from 1×10^5Hz to 1×10^{-6}Hz.

Another such phenomenon is the conductivity memory effect[43–45], where after a sudden change of the electron density the conductivity will jump above its equilibrium value, as illustrated in Fig. 3.1. The conductivity will relax to its equilibrium value very slowly, without any visible time scale. Anomalies at the old Fermi level (see Fig 3.7) may remain detectable up to a day later.

In the case of $1/f$ noise in conductors, it has been proposed[47–49] that these scales come from two-level systems[50–52] (TLS) with a broad spectrum of tunneling times. The prototypical example of a TLS is an impurity tunneling between a close pair of host sites. The reaction of the electrons to this motion naturally reproduces the $1/f$ noise.

In this paper we show that this mechanism *by necessity* produces a conductivity memory effect. The effect is, in a sense, the inverse of the $1/f$ noise, as it derives from the reaction of the TLSs to the mesoscopic fluctuations of the electron density. As a mesoscopic phenomenon, it is sensitive to magnetic fields and a change in the magnetic field produces qualitatively similar behavior to a change in electron density. Moreover we derive a “memory magneto-resistance", where the magnetoresistance depends on the history of the magnetic field.

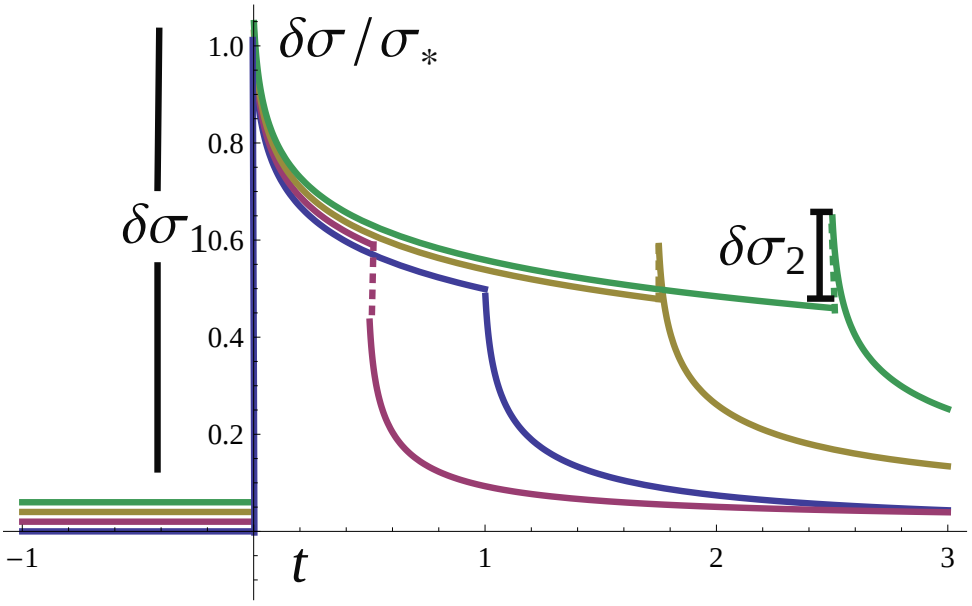

FIGURE 3.1: Figure showing the reponse of the conductivity to a change in the density n_e. The behavior is quaitatively similar for a change in magnetic field. The density is changed by δn_e at $t = 0$ and returned to its original value at $t = t_h$. The graph plots conductivity vs. time for several different choices of t_h, but the same δn_e. There is a jump in the conductivity $\delta\sigma_1$ when the chemical potential is first changed and a second jump $\delta\sigma_2$ at $t = t_h$. The time scale is in arbitrary units. Figures offset slightly for clarity. The scale σ_* is defined in Eq. (3.26). A positive σ_2 only appears when $t_h > \sqrt{t_i t_f}$ when 50% of the TLS are relaxed.

Since the $1/f$ noise and memory effect derive from the same interaction we can derive a "universal" relationship between the noise and the memory effect, independent of the microscopic details of the TLSs. This relationship depends only on the phase coherence length, as measured by the magneto-resistance.

The plan of the paper is as follows. In Section 3.2 we give a qualitative discussion of the model and the results. In Section 3.3 we give a quantitative derivation of these results using the standard quantum theory of metals. We also analyze the effect of magnetic fields and derive the memory magneto-resistance effect. A derivation of the properties of the TLS is given in Appendix B. In Appendix C we discuss an experimental protocol for detecting the memory effect and the relationship between the charging properties of thin films and the underlying energy scales.

3.2 Qualitative discussion and results

The purpose of this section is to review known facts about the $1/f$ noise and to make a connection to the proposed memory effect.

3.2.1 $1/f$ noise and mesoscopic corrections

It has been known for over 50 years that the conductivity noise in metals has strange behavior in the low-frequency limit[42]. Consider a sample of linear dimension L with a fixed voltage applied such that a mean current I is produced. If the fluctuations of the current around the mean $\delta I(t)$ are measured it is found that,

$$\overline{\delta I(t)\delta I(t')} = I^2 L^{-d} \mathcal{F}(t-t'), \tag{3.1}$$

where $\overline{\cdots}$ denotes the time average. The factor of L^{-d} takes into account the central limit theorem so that the function $\mathcal{F}$ does not depend on the sample geometry. The Fourier transform of $\mathcal{F}$ was found to behave as

$$\int dt\, \mathcal{F}(t) e^{i\omega t} \sim \frac{1}{|\omega|} \tag{3.2}$$

at low frequencies $\omega = 2\pi f$. This behavior persists in some samples from frequencies of a khZ to an inverse day. The basic problem is a mismatch of scales. The typical elastic scattering times are of the order of picoseconds. The inelastic scattering (either the dephasing or the energy relaxation time) may exceed the elastic scattering by several orders of magnitude. But even these are never larger than a microsecond. How can there be behavior on times of an inverse day? What scale can be the cutoff for the $1/f$ behavior?

A resolution of this problem has two components. The first component is the two-level system[50–52] (TLS). There are many possible microscopic mechanisms that produce appropriate TLSs. As our final results should be independent of the microscopic details we will work with a particularly simple model. This is a heavy but mobile atom with two equilibrium positions r_1 and r_2. Under the action of inelastic scattering by electrons and phonons the atom can switch its position.

The probablistic description of the TLS is the following: $P^{eq}_{1,2}$ are the probability for the TLS to be in the state 1 and 2 respectively. These are dictated by the Gibbs distribution. The motion between these states is characterized by $P(t, r|t's)$, the conditional probability to be in state r at time t provided that it was in state s at time t'. A particular TLS is governed by a single relaxation time τ_{12},

$$P(t, r|t', r) = P^{eq}_r + (1 - P^{eq}_r) e^{-|t-t'|/\tau_{12}}. \tag{3.3}$$

The TLS's transitions necessarily involve tunneling. Therefore the relaxation time τ_{12} must be of the form,

$$\frac{1}{\tau_{12}} \propto \exp\left(-\frac{|\vec{r}_1 - r_2|}{a}\right), \tag{3.4}$$

where a is a constant on the order of the lattice constant. Assuming that the positions $r_{1,2}$ are homogeneously distributed we find that the probability distribution of the relaxation times is

$$d\tau_{12}\mathcal{P}(\tau_{12}) \sim \frac{d\tau_{12}}{\tau_{12}}. \tag{3.5}$$

Averaging Eq. (3.3) over the tunneling time of the TLS with the distribution (3.5) gives

$$\int d\tau_{12}\mathcal{P}\left(\tau_{12}\right) e^{-t/\tau_{12}} \propto \frac{\ln\left(t_f/t\right)}{\ln\left(t_f/t_i\right)} = \mathcal{K}(t), \tag{3.6}$$

valid when $t_i < t < t_f$. The lower cutoff t_i is given by some microscopic scale and the upper cutoff t_f is larger than t_i by many orders of magnitude in reasonable models. The function $\mathcal{K}(t)$ therefore shows $1/f$ behavior over the extremely large range of scales that is characterstic of $\mathcal{F}(t)$. If there were a mechanism that would tranlsate the motion of a TLS into an observable transport coefficient of electrons, we could write $\mathcal{K}(t) \propto \mathcal{F}(t)$ and claim the phenomena explained.

Such a translation is in fact subtle. Naively, the conductivity is determined by the Drude formula,

$$\sigma_D = e^2 \nu v_F^2 \tau_{tr}, \tag{3.7}$$

where ν is the density of states, v_F the Fermi velocity and the transport time τ_{tr} is given by

$$\frac{1}{\tau_{tr}} = v_F N_{imp} s, \tag{3.8}$$

where N_{imp} is the density of impurities and s is the scattering cross-section. Given that shifting an impurity does not change its scattering cross-section[46], it would seem that the motion of the impurity has no effect on the conductivity at all.

It was realized in Refs. [[47, 49]] that the theory of meseoscopic conductance fluctuations[53–55] resolves this issue. To illustrate this resolution let us recall the justification for the Drude equation. The Fermi wavelength λ_F is much smaller than the mean free path between impurities ℓ_{imp}, so we may consider the electrons as wavepackets following semiclassical trajectories. Consider the probability W_{AB} for an electron to propagate from point A to point B. Because the electrons can scatter off an impurity to any direction there are many paths connecting the two points. Quantum mechanically, we assign to each path i the amplitude $\mathcal{A}_i$, sum the amplitudes,

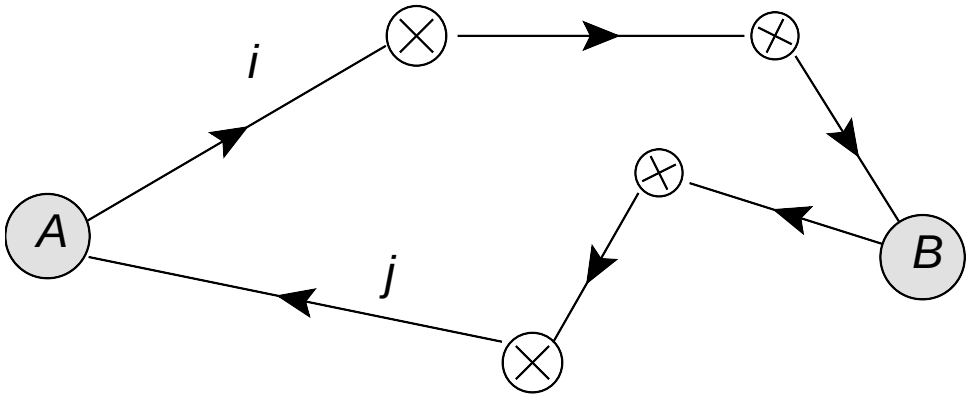

FIGURE 3.2: An illustration of semi-classical paths in the "interference" contribution to the probabiliy to propagate from point A to point B. The crossed circles represent static impurities and the reversed arrow indicates the complex conjugate of the amplitude.

and square the result. This gives,

$$W_{AB} = \sum_i |\mathcal{A}_i|^2 + \sum_{i \neq j} \mathcal{A}_i^* \mathcal{A}_j. \tag{3.9}$$

The first term is a classical sum of probabilities which leads to the diffusion equation and the Drude formula. The second "interference term", illustrated in Fig. 3.2, is neglected in the Drude equation. The usual justification is that the interference depends on the relative phase of two paths,

$$\phi_{ij} \sim (L_i - L_j) p_F / \hbar, \tag{3.10}$$

where L_i is the length of the ith trajectory and p_F is the Fermi momentum. But this phase fluctuates wildly since $p_F L_i \gg \hbar$. Thus, one may think, incorrectly, that the interference correction is a sum of terms with random signs and may be neglected. The remaining terms are purely classical and so any correction to the conductance G would take the form,

$$\delta G \overset{?}{\sim} \frac{1}{N} \sum_i \left(|\mathcal{A}_i|^2 + \delta g_i \right), \tag{3.11}$$

where N is the number of paths and δg_i is a correction to the classical probability. This leads to a variance

$$\langle \Delta G^2 \rangle \overset{?}{\sim} \langle \delta g_i^2 \rangle \frac{1}{N^2} N \propto \frac{1}{N}.$$

Thus, according to this logic, the correction to the conductivity decays with N. Since N grows with the size of the system, this leads one to think that all corrections must decay with the size of the system.

However, the neglect of the interference term above is careless, since there are pairs of paths whose phases are fixed by symmetry, such as a path and its time reverse. These will not have cancelling phases and therefore they contribute to W_{AB}. Let us estimate the correction $\delta\sigma$ to the Drude formula that the interference term produces. We may think of it as a random quantity and calculate its variance. The true conductivity $\sigma = \sigma_{dr} + \delta\sigma$ is proportional to W_{AB} so

$$\Delta G \propto \frac{1}{N^2} \sum_{ijkl} \mathcal{A}_i^* \mathcal{A}_j \mathcal{A}_k^* \mathcal{A}_l \tag{3.12}$$

There are two sets of paths that give a nonvanishing contribution to Eq. (3.12). The "diffuson" term where path $i = l$ and $j = k$ and the "cooperon" term where path k is the time reverse of path i and likewise for j and l. These are illustrated in Fig. 3.3. Substituting these paths into Eq. (3.12), gives a contribution $\sim \left(\sum_i |\mathcal{M}_i|\right)^2 \sim N^2$, not N as in the classical estimate, Eq. (3.11). This means that the correct expression for ΔG is independent of the system size. It follows that this correction is describing processess that occur on linear scales larger that all microscopic lengths and therefore must be universal and independent of material parameters. The only possible expression is,

$$\langle \Delta G^2 \rangle \sim \left(\frac{e^2}{\hbar}\right)^2 . \tag{3.13}$$

There are two mechanisms that violate the universality of Eq. (3.13): dephasing by inelastic processes characterized by the the inelastic time τ_ϕ (see Refs. [[56–58]] for a detailed discussion of τ_ϕ in mesoscopic fluctuations) and temperature averaging due the dependence of the phases $\mathcal{A}_i$ on the electron energy ϵ_i,

$$\mathcal{A}_i(\epsilon_1)\mathcal{A}_j(\epsilon_2) \propto \exp\left[i\left(\epsilon_1 - \epsilon_2\right) L_i/v_F\right] . \tag{3.14}$$

The dephasing restores the central limit theorem in the sense that the system can now be separated into uncorrelated subsystems of size $\ell_\phi \equiv \sqrt{\mathcal{D}\tau_\phi}$. Here $\mathcal{D} = v_F^2 \tau_{tr}$ is the electron diffusion constant. The temperature averaging similarly means that contributions from energy differences larger than $\epsilon_1 - \epsilon_2 \sim \hbar/\tau_\phi$ are independent. This results in

$$\langle \Delta G^2 \rangle \sim \left(\frac{e^2}{\hbar}\right)^2 \left(\frac{\ell_\phi}{L}\right)^{4-d} \left(\frac{\hbar}{T\tau_\phi}\right) , \tag{3.15}$$

where d is the dimensionality of the sample.

While δG is not directly observable, this correction manifests as the universal conductance fluctuations. If an adjustment is made to the system - a change in chemical potential, thermal cycling, magnetic field etc... - the phases in the interference term will be changed and so the

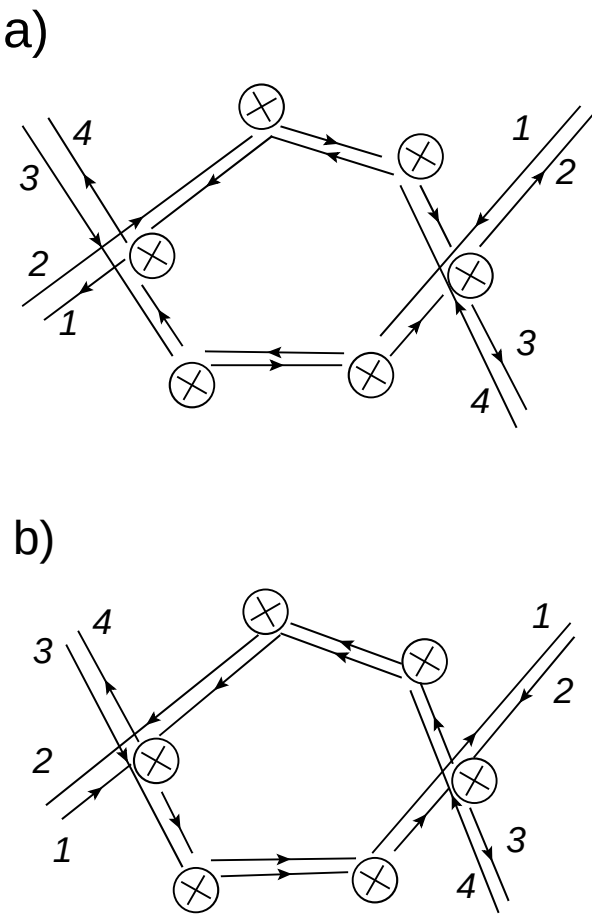

FIGURE 3.3: Examples of an interference contribution to the variance of the conductivity. The crossed circles represent static impurities. (a) The pair of paths 1 and 2 contribute to the classical probability probability to propagate. Because the two paths are different they have a random phase, which means the sum over all paths is self canceling. But combined with the paths 3 and 4, the diagram makes a non-vanishing contribution to the variance of the conductivity. (b) A cooperon contribution, where the path 3 is the time reverse of path 1 and likewise for 4 and 2.

interference will be randomized, leading to fluctuations in the conductivity. These fluctuations are universal in the sense that they do not depend on physics at the scale ℓ_{imp} or λ_F , but on much longer scales such as the system size or phase coherence length.

Returning to the TLS, we now understand how the motions of the impurities may affect the conductivity. Consider a path involving the scattering on a mobile impurity (TLS) as in Fig. 3.4. The geometric length of the paths differ depending on the location of the impurity. Therefore, the accumulated phase ϕ_i of the trajectory depends on the state of the TLS. We write $\phi_i = p_F L_i + \alpha_r$ where $r = 1, 2$ is the state of the TLS. The numbers $\alpha_{1,2}$ are effectively random since they depend

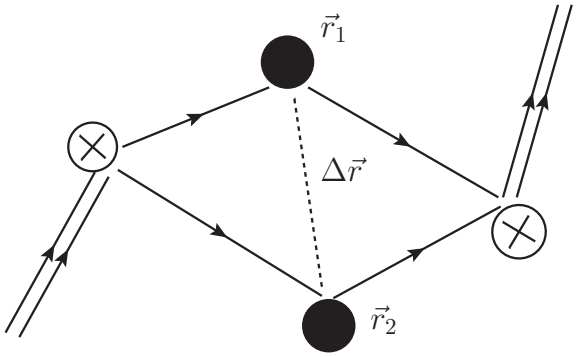

FIGURE 3.4: Figure showing the change in the geometric length of a path because of a shift a mobile impurity from position $\vec{r}_1$ to $\vec{r}_2$. The crossed circles represent static impurities and the solid dot shows two possible positions of a TLS.

on the orientation of the electron path and the displacement $\vec{r}_{12}$ between the two sites of the mobile impurity. Thus the contribution of the path i to the fluctuation of the conductance becomes dependent on the state of the TLS,

$$\Delta G_{i,r} \sim \cos\left(k_F L_i + \alpha_r\right). \tag{3.16}$$

Substituting such paths into Eq. (3.12), we can calculate the contribution to the conductance fluctuation for paths passing through the TLS. In the limit that $\alpha_1 - \alpha_2 \gg 1$ the sign of $\Delta G_{i,r}$ is random and the terms where $r \neq s$ do not contribute. Therefore, [see Eq. (3.3)],

$$\begin{aligned} \Delta G_i(t)\Delta G_i(t') &\propto \sum_r P_r^{eq} P(r,t|r,t') \\ &\propto P_1^{eq} P_2^{eq} e^{-t/\tau_{12}}. \end{aligned} \tag{3.17}$$

The correlation function of the conductances is determined by the impurity dynamics. The summation over different TLSs lead to the correction of Eq. (3.15)

$$\begin{aligned} &\ll \overline{\Delta G(t)\Delta G(t')} \gg \\ \sim\ &\left(\frac{e^2}{\hbar}\right)^2 \left(\frac{\ell_\phi}{L}\right)^{4-d} \left(\frac{\hbar}{T\tau_\phi}\right) \left(\frac{\tau_\phi}{\tau_*}\right) \mathcal{K}(t-t'), \end{aligned} \tag{3.18}$$

where $\ll \cdot \gg$ indicates an average over the positions and tunneling rates of the TLS.

The time τ_* is the elastic scattering time of an electron from a mobile impurity and the factor $\tau_\phi/\tau_* \ll 1$ is the fraction of paths that encounter a mobile impurity before the phase coherence is destroyed. This factor can also be understood as follows. The scattering time τ_* is approximately

the density of states ν over the density of the TLSs, ρ_*. This gives us

$$\left(\frac{\tau_\phi}{\tau_*}\right) = \left(\frac{\rho_* \ell_\phi^d}{g\left(\ell_\phi\right)}\right), \tag{3.19}$$

where $g\left(\ell_\phi\right) = \nu \mathcal{D} \ell_\phi^{d-2}$ is the conductance at the scale ℓ_ϕ in units of $e^2/\hbar$. The phase coherence splits the system into cells of volume ℓ_ϕ^d each with $\rho_* \ell_\phi^d$ impurities. Therefore to produce a change in the conductance of order $e^2/\hbar$ in a sample of linear size ℓ_ϕ, one must move a number of impurities equal to $g\left(\ell_\phi\right)$.

We can compare Eqs. (3.1) and (3.18) by using the facts that on applying a voltage V, the current $I = G(L)V$ and the fluctuations $\delta I = \delta G V$. Further, the conductances at scales L and ℓ_ϕ are related by $G(L) = \frac{e^2}{\hbar} g(\ell_\phi) \left(\frac{\ell_\phi}{L}\right)^{2-d}$. We thus obtain a relationship between the functions $\mathcal{F}(t)$ and $\mathcal{K}(t)$:

$$\frac{\mathcal{F}(t)}{\mathcal{K}(t)} \propto \frac{\ell_\phi^d}{g\left(\ell_\phi\right)^2} \left(\frac{\hbar}{T \tau_*}\right). \tag{3.20}$$

Equation (3.20) describes the mechanism of quantum interferance that translates the microscopic motion of the TLSs into an observable noise. We will show now that this interference inevitably leads to the memory effect, not previously studied in the literature.

3.2.2 Memory effect

Memory effects are the slow responses of, say, the conductivity $\sigma\left(n_e, B\right)$ to sudden changes of the electron density n_e or the applied magnetic field B, as illustrated in Fig. 3.1. After the change, the conductivity $\delta\sigma(t)$ is usually larger than its equilibrium value $\sigma_f(n_e + \delta n, B + \delta B)$ and approaches this equilibrium value very slowly, without any visible time scale. Moreover, if after some time t_h, n_e and B are returned to their starting value, σ will jump again (the value and even the sign of the jump depending on t_h) and then return to the starting value $\sigma(n_e, B)$ during a time of the order of t_h.

We give here a qualitative explanation of this behavior using the concepts introduced in Sec. 3.2A. The rigorous derivation of these results is relegated to Sec. 3.3.5.

As before consider the interference contribution to the conductivity from two trajectories shown in Fig. 3.5(a). The contribution to the conductivity $\Delta\sigma_i$ from this path corresponds to an enhancement of the scattering rate $1/\tau_{tr}$, and so the effect can be estimated as,

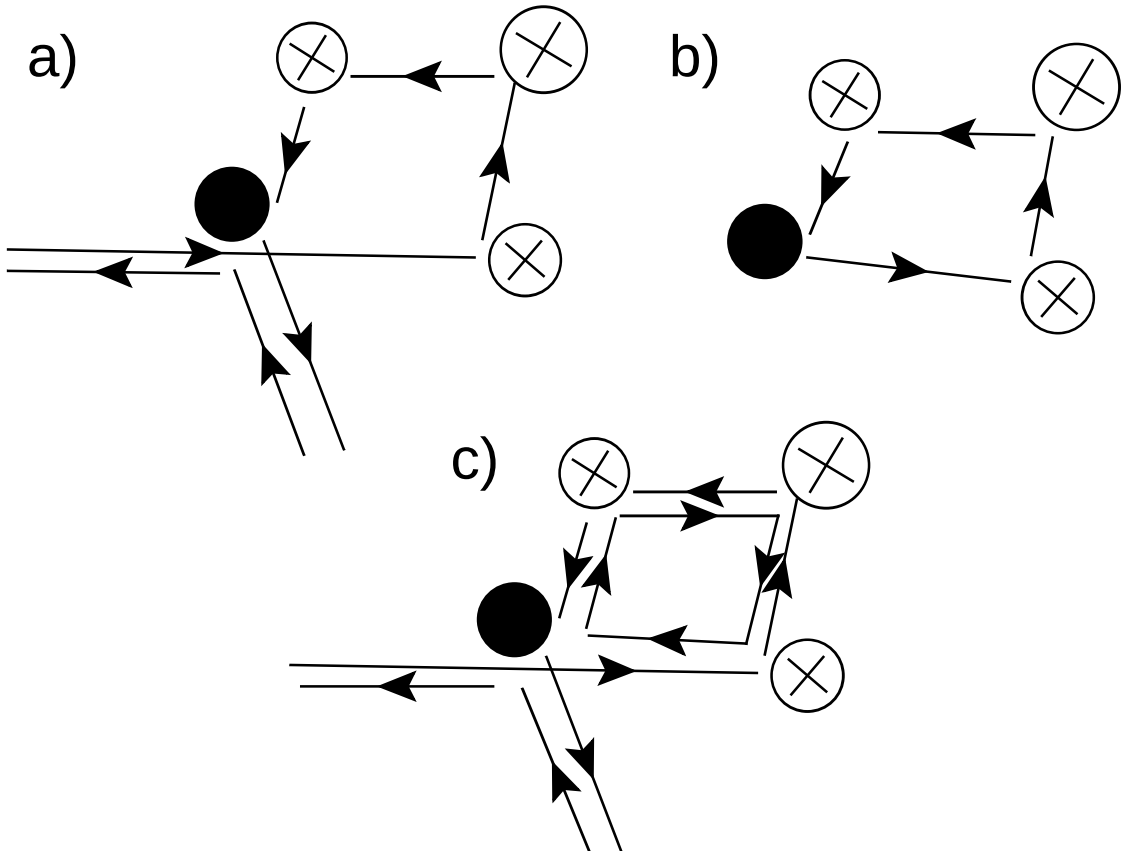

FIGURE 3.5: Semi-classical paths demonstrating the memory effect. The impurity in the TLS is represented by a solid dot and the crossed circles represent static impurities. (a) A multiple scattering contribution to the scattering rate of the TLS with a random phase. (b) A contribution to the energy in the semi-classical picture. (c) An interference contribution to the covariance of the scattering rate and the energy.

$$\frac{\Delta\sigma_i}{\sigma} \sim -V_{imp}\sum_{r=1,2}\cos(k_F L_i + \alpha_r)P_r, \tag{3.21}$$

where P_r is the probability for the TLS to be in state r and the coefficient V_{imp} is the average of the impurity-electron potential, which gives the scattering amplitude in the first Born approximation. Because the phase of the cosine is random one might expect Eq. (3.21) to vanish on averaging. However this neglects the possibility that the phase is correlated with P_r and is therefore incorrect. Let us see how this correlation arises.

The equilibrium probability P_r^{eq} for a TLS is given by the Gibbs distribution $P_r^{eq} \propto \exp(-E_r/T)$, where T is the temperature and E_r is the energy of the r state. Because the mobile impurity interacts with the electrons, this energy will depend on the density of electrons $\rho(r)$ near the mobile impurity. The density of electrons itself fluctuates throughout the metal because of the

Friedel oscillations[59] of the randomly placed impurities. The role of Friedel oscillations in the interaction correction to the conductivity is discussed in Refs. [[60, 61]]. Such a fluctuation of the energy δE_r will produce a fluctuation in the occupation probability δP_r,

$$\delta P_1 - \delta P_2 = -\frac{\delta E_1 - \delta E_2}{T} P_1^{eq} P_2^{eq}. \tag{3.22}$$

Assuming that these density fluctuations are small, we may write that the fluctuation of the energy δE_r is proportional to the fluctuation of the density $\delta\rho_r$. In the semiclassical picture, the density of electrons at the site r is given by all loops that pass through the site as in Fig 3.5(b), so the path i gives a contribution

$$\delta E_r^{(i)} \sim V_{imp}\delta\rho_r^{(i)} \sim V_{imp}\int d\epsilon\, n_F(\epsilon)\, C_{i,r}\,(\epsilon)\,, \tag{3.23}$$

where,

$$C_{i,r}\,(\epsilon) \equiv \cos\left[(k_F + \epsilon/v_F)\, L_i + \alpha_r\right], \tag{3.24}$$

and $n_F(\epsilon) \equiv [1+\exp(\epsilon/T)]^{-1}$ is the Fermi distribution function. Crucially the energy shift is determined by the same potential V_{imp} that defines the scattering amplitude in Eq. (3.21). Substituting Eqs. (3.22) and (3.23) into Eq. (3.21) and keeping only the non-oscillating terms we obtain,

$$\frac{\Delta\sigma_i}{\sigma_D} \sim -\frac{V_{imp}^2}{T}\int d\epsilon\, n_F(\epsilon)\cos\left(\frac{\epsilon}{v_F}L_i\right) P_1^{eq} P_2^{eq}. \tag{3.25}$$

It is important to note that only the quantity V_{imp}^2 appears in Eq. (3.25) and this is of definite sign. Therefore the sign of Eq. (3.25) is fixed regardless of whether the interaction is repulsive or attractive.

The next step is the summation of Eq. (3.25) over all the diffusive paths that involve the scattering off of the mobile impurities. This is precisely the sum [Eq. (3.12)] we have discussed in Sec. 2A, where we found that the change in the conductance is given by the inverse conductance on the scale ℓ_ϕ. The only difference is that, because of the integral over ϵ in Eq. (3.25), the phase coherence will already be destroyed for paths longer than $\hbar v_F/T$. This corresponds to a diffusive length $L_T = \sqrt{\hbar\mathcal{D}/T} \ll \ell_\phi$ [seeRef. [[58]]]. Calling the total correction to the conductivity σ_*, we obtain that

$$\frac{\sigma_*}{\sigma_D} \approx -\frac{1}{g\,(L_T)}\frac{1}{T\tau^*}. \tag{3.26}$$

Equation (3.26) is a quantum correction to the conductivity with a singular dependence on temperature. Similar effects were discussed inRef. [[62]] in relation to zero bias anomalies in point contacts.

Due to the small factor $1/(T\tau_*)$ this correction is not observable in bulk systems in comparison with the interaction correction[63]. It is only the memory effect that makes the correction (3.26) observable.

Let us at time $t=0$ suddenly change the electron density so that $k_F \to k'_F$, or apply a magnetic field B. The electrons equilibriate instantly compared to the time scales we are interested in, so we should change in Eqs. (3.21) and (3.24)

$$C_{i,r}(\epsilon) \to \tilde{C}_{i,r}(\epsilon) \equiv \cos\left(2\pi\frac{\Phi_i}{\Phi_0}\right)\cos\left[\left(k'_F+\frac{\epsilon}{v_F}\right)L_i+\alpha_r\right], \tag{3.27}$$

where Φ_i is the flux enclosed by the diffusive path and $\Phi_0 = hc/e$ is the flux quantum. However, the occupation probability of a TLS does not immediately follow the change in density, because it relaxes only on the long time scale τ_{12}. Therefore, we should write for the occupation probability,

$$\begin{aligned}\Delta P_r(t) = &-\frac{e^{-t/\tau_{12}}}{T}\int d\epsilon n_F(\epsilon)\, C_{i,r}(\epsilon)\\ &-\frac{1-e^{-t/\tau_{12}}}{T}\int d\epsilon\, n_F(\epsilon)\,\tilde{C}_{i,r}(\epsilon)\,.\end{aligned} \tag{3.28}$$

Then, Eq. (3.21) yields

$$\begin{aligned}\frac{\Delta\sigma_i(t)}{\sigma} \sim -\sum_{r=1,2}P_1P_2\int d\epsilon\, n_F(\epsilon)\Big[&\frac{e^{-t/\tau_{12}}}{T}C_{i,r}(\epsilon)\,\tilde{C}_{i,r}(0)\\ &-\frac{1-e^{-t/\tau_{12}}}{T}\tilde{C}_{i,r}(\epsilon)\,\tilde{C}_{i,r}(0)\Big].\end{aligned} \tag{3.29}$$

Once again, keeping only the terms which do not oscillate on the scale of $1/k_F$ we obtain instead of Eq. (3.26)

$$\begin{aligned}\frac{\Delta\sigma_i(t)}{\sigma} &= -\frac{P_1P_2}{T}\\ \times\int d\epsilon\Bigg\{&e^{-t/\tau_{12}}\cos\left[\left(k'_F-k_F+\frac{\epsilon}{v_F}\right)L_i\right]\cos\frac{2\pi\Phi_i}{\Phi_0}\\ &+\left(1-e^{-t/\tau_{12}}\right)\cos\frac{\epsilon}{v_F}\cos^2\frac{2\pi\Phi_i}{\Phi_0}\Bigg\}.\end{aligned} \tag{3.30}$$

Equation (3.30) is the key for the qualitative understanding of the memory effect. The first term characterizes the slow decay of the system's memory of the initial interference pattern. The second term characterizes the slow approach of the conductivity to the new equilibrium. The term $\cos^2(2\pi\Phi_i/\Phi_0)$ describes the suppression of the constructive interference between time-reversed paths by the magnetic field. The same suppression by magnetic field appears in the $1/f$ noise[64, 65] and is evidence of the importance of mesoscopic physics in the system.

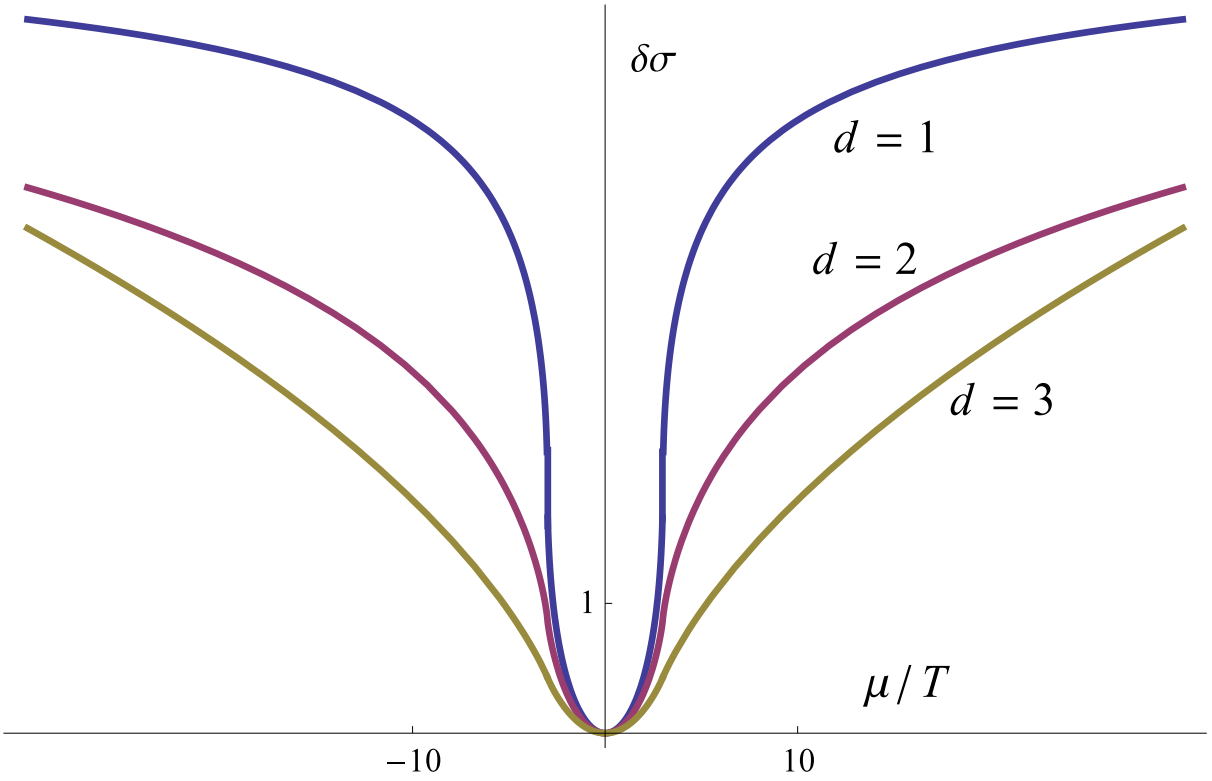

FIGURE 3.6: Graph of the zero-bias anomaly in the conductivity. The conductivity and chemical potential are measured from the resting values. The curves are obtained by numerical integration of Eq. (3.73)

Equation (3.30) has several immediate applications. Let us consider the change in conductivity immediately after a change in the density. [1] Summing over all the trajectories and all the TLSs in Eq. (3.30) we obtain the total correction to the conductivity,

$$\frac{\delta\sigma(B,k_F',t=0)}{\sigma_D}=-\frac{1}{g\left(L_T\right)}\frac{1}{T\tau_*}S\left(\frac{v_F|k_F-k_F'|}{T},\frac{L_T}{L_B}\right), \tag{3.31}$$

where $L_B\equiv\sqrt{\hbar c/\left(eB\right)}$ is the magnetic length and the function $S(x,y)$ counts the fraction of diffusive paths whose interference is not destroyed due to changes in k_F or B. It has the asymptotic limits

$$S\left(0,0\right)=1;\ S\left(x\to\infty,y\right)=S\left(x,y\to\infty\right)=0. \tag{3.32}$$

The explicit form of S is given in Eq. (3.67). The dependence of the conductivity on the density is shown in Fig. 3.6. It can be seen as a fingerprint of the electron density that is stored in the TLSs.

[1] Note the interaction correction does not produce any singular density dependence, because the self consistent potential created by the electron-electron interactions equilibriates almost instantaneously.

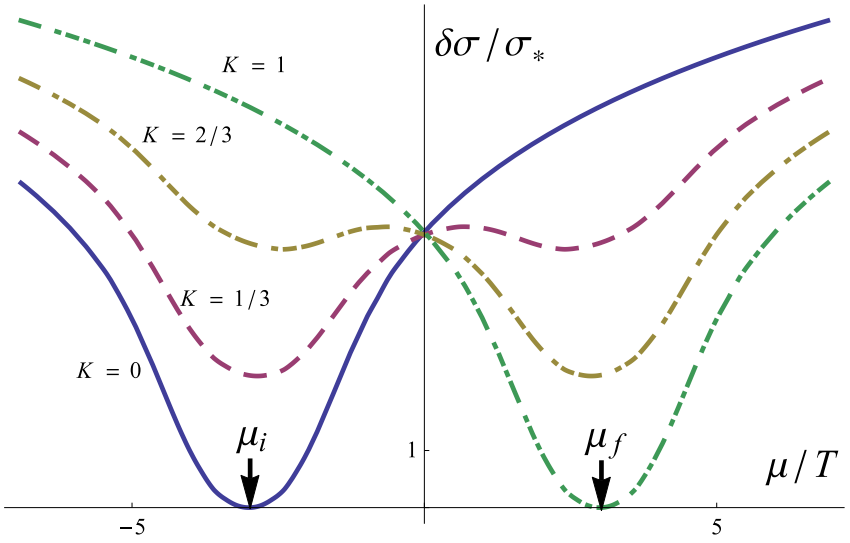

FIGURE 3.7: Graph showing the relaxation in a thin film of the conductivity singularity from the old Fermi level μ_i to the new Fermi level μ_f. The curves are labeled by the fraction K of TLS that have relaxed to the new equilibrium.

The time dependence of the conductivity is even more dramatic. Taking Eq. (3.30) and summing over all the diffusive paths and all the TLSs with the distribution function from Eq. (3.6) we obtain,

$$\frac{\delta\sigma(B,k_F';t)}{\sigma_D} = -\frac{1}{g\left(L_T\right)}\frac{\hbar}{T\tau_*}\left\{\mathcal{K}(t)S\left(\frac{v_F|k_F-k_F'|}{T};\frac{L_T}{L_B}\right)\right.$$
$$\left.+\frac{1}{2}\left(\mathcal{K}(0)-\mathcal{K}(t)\right)\left[1+S\left(0,\sqrt{2}\frac{L_T}{L_B}\right)\right]\right\}. \tag{3.33}$$

This dependence has two anomalies, one at the old Fermi level and the second at the new Fermi level. The ratio between the amplitude of these anomalies characterizes the fraction of the TLS that have adjusted to the new electron density. The form of the density dependence is shown on Fig. 3.7.

The function $\mathcal{K}$ is precisely the function given in Eq. (3.6) which determines the correlations of the $1/f$ noise [see Eqs. (3.1) and (3.20)]. Moreover, the unknown factor $\hbar/\left(T\tau_*\right)$ is removed if the memory effect is expressed in terms of the measurable correlation function of the $1/f$ noise from Eq. (3.6),

$$\frac{\delta\sigma\left(B,k_F';t\right)}{\sigma_D} = -\frac{1}{V_q}\left\{\mathcal{F}(t)S\left(\frac{v_F|k_F-k_F'|}{T};\frac{L_T}{L_B}\right)\right.$$
$$\left.+\frac{1}{2}\left(\mathcal{F}(0)-\mathcal{F}(t)\right)\left[1+S\left(0,\sqrt{2}\frac{L_T}{L_B}\right)\right]\right\}, \tag{3.34}$$

where V_q is the effective volume of the subsystem which contribute to the memory effect and is defined by,

$$\frac{1}{V_q} \equiv \frac{g\left(\ell_\phi\right)^2}{\ell_\phi^d g\left(L_T\right)} \approx \nu T \left(\tau_\phi T\right)^{2-d}. \tag{3.35}$$

The time τ_ϕ can be extracted from the usual weak localization magneto-resistance measurement.

The closest relative of the density memory effect discussed above is the magnetic field memory effect. Let us keep the density fixed and switch the magnetic field at $t = 0$ from $B = 0$ to B_0. Then, at some later time t we briefly shift the magnetic field to a third value B and measure the resistance. Repeating the arguments starting from Eq. (3.30) we find the that the time-dependent part[2] of the resistance is,

$$\begin{aligned}\frac{\delta\sigma\left(B, k_F'; t\right)}{\sigma_D} &= -\frac{1}{V_q}\Bigg\{\mathcal{F}(t) S\left(0; \frac{L_T}{L_B}\right) \\ &+ \frac{1}{2}\left(\mathcal{F}(0) - \mathcal{F}(t)\right)\left[S\left(0, \frac{L_T}{L_{B_+}}\right) + S\left(0, \frac{L_T}{L_{B_-}}\right)\right]\Bigg\}, \\ L_{B_\pm} &\equiv \sqrt{\frac{\hbar c}{e\left|B_0 \pm B\right|}}.\end{aligned} \tag{3.36}$$

At large value of the magnetic field ($2L_T \gtrsim L_B$) the magneto-resistance shows a distinct two dip structure, shown in Fig. 3.8. Note that the magneto-resistance is always symmetric. This is because the electrons are always in quasi-equilibrium and so Onsager's relation applies.

There is a different way to probe the same memory physics, by performing a cyclic perturbation of the system. We can at $t = 0$ turn on a magnetic field or change the density and wait for a time t_h. We then switch off the magnetic field or return the density to its previous value. We may then measure the conductivity $\sigma(t)$ at time $t > t_h$, when the system has the parameters as at $t < 0$ but still retains a memory of the period $0 < t < t_h$. This protocol corresponds to the correction of the energy levels of the TLS only during the finite time t_h. We obtain instead of Eq. (3.21) at $t > t_h$,

$$\begin{aligned}\delta P_r(t) = &\int d\epsilon\, n_F\left(\epsilon\right)\left[\tilde{C}_{i,r}\left(\epsilon\right) - C_{i,r}\left(\epsilon\right)\right] \\ &\times\left(e^{-t/\tau_{12}} - e^{-(t-t_h)/\tau_{12}}\right).\end{aligned} \tag{3.37}$$

Repeating the previous derivation we obtain a correction to the conductivity,

$$\frac{\delta\sigma(t)}{\sigma_D} = \frac{\mathcal{F}\left(t\right) - \mathcal{F}\left(t - t_h\right)}{V_q}\left[1 - S\left(\frac{v_F|k_F - k_F'|}{T}, \frac{L_T}{L_B}\right)\right]. \tag{3.38}$$

[2] There is also a contribution from the anomalous magneto-resistance, but this does not depend on time.

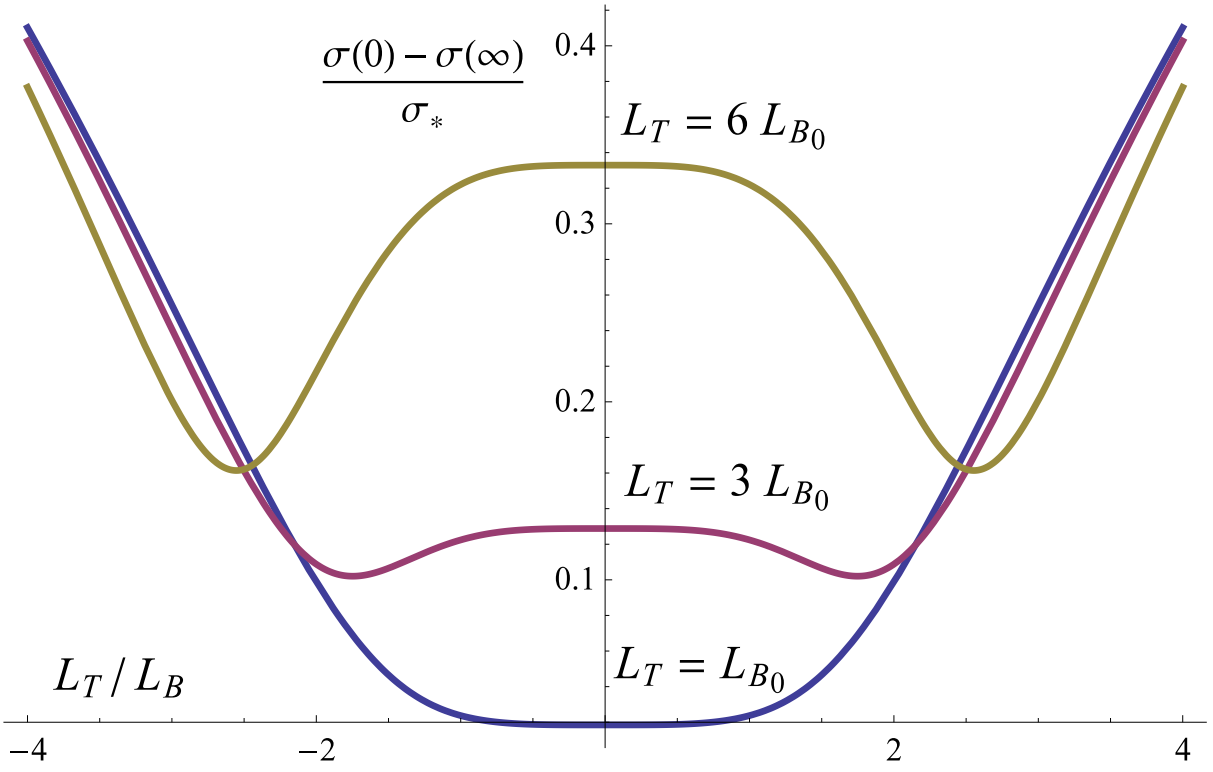

FIGURE 3.8: Plot of the magnetic memory effect. The curves plot the difference between $\sigma(0)$, the conductivity of a sample equilibriated in zero-field, and $\sigma(\infty)$, the conductivty after the sample has equilibriated in a transverse field with magnetic length L_{B_0}. The curves are shown for different choices of the resting magnetic length L_{B_0} and plotted in term of the L_B, the magnetic field length when the conductivity is measured. They are obtained by numerical evaluation of Eq. (3.70).

Equation (3.38) describes the relaxation dynamics of the conductivity. This protocol has the advantage of being insensitive to the fastest time of scale of the TLS dynamics [it does not contain $\mathcal{F}(0)$]. It is also non-invasive in that it does not require sweeps of the parameters which may affect the evolution of the system. However the measurement of $\Delta\sigma(t)$ and the jumps in conductivity can still be used to extract the function S. Therefore the consistency of the different protocols would be an important test of this framework.

We conclude this section by noting that the theory developed here can predict the change in conductivity from any history of the density or magnetic field, by application of Eq. (3.67). It therefore constitutes a complete description of the memory phenomenon.

3.3 Diagrammatics for electrons and TLS

In this section we will introduce the diagrammatic technique for disordered metals with TLSs and perform a rigorous derivation of the results discussed in Sec. 3.2. The model is defined in Secs. 3.3.1 and 3.3.2. Secs. 3.3.3 and 3.3.4 rederive the known results for the mesoscopic fluctuations and the $1/f$ noise in order to harmonize the notation and allow an easy comparison with the memory effect. The quantitative derivation of the memory effect is performed in Sec. 3.3.5.

We make several simplifying assumptions, but they do not appear crucial to the results: (i) all dependence on the electron-electron and electron-phonon interactions appears only through the phase coherence length ℓ_ϕ, (ii) we work to leading order in $g\left(\ell_\phi\right)^{-1}$, (iii) we work to leading order in $T\tau_\phi/\hbar \ll 1$, (iv) the calculation is perturbative in the density of the TLS, (v) we neglect spin-orbit coupling and magnetic impurities. We revisit the last assumption in the conclusion. We set $\hbar = c = 1$ in all intermediate formulae.

3.3.1 Model

The total Hamiltonian for our system is

$$\hat{H} = \hat{H}_{metal} + \hat{H}_{TLS} + \hat{H}_{el-TLS}. \tag{3.39}$$

The metallic system is described by the Hamiltonian,

$$\hat{H}_{metal} = \int d^d\vec{r}\, \psi^\dagger\left(\vec{r}\right)\left[\epsilon\left(-i\vec{\nabla} - e\vec{A}\right) + U\left(\vec{r}\right)\right]\psi\left(\vec{r}\right). \tag{3.40}$$

Here $\psi^\dagger$ is the electron creation operator, $\epsilon(p)$ is the electron spectrum, $\vec{A}$ is the vector gauge potential, $U(r)$ is a random scalar field representing static disorder and we suppress throughout spin indices. We take the simplest model of a local Gaussian disorder with correlation function

$$\ll U(\vec{r})U(\vec{r}')\gg = \frac{1}{2\pi\nu\tau}\delta^{(d)}(\vec{r}-\vec{r}'). \tag{3.41}$$

Here ν is the electron density of states per spin at the Fermi level and τ is the scattering rate. The double brackets $\ll \cdot \gg$ throughout this text mean average over both the static impurities and all others kinds of disorder.

The Hamiltonian for the TLSs,

$$\hat{H}_{TLS} = \sum_{i=1}^{N_{TLS}} \hat{h}_i, \tag{3.42}$$

is a sum of Hamiltonians for each of the $N_{TLS} \gg 1$ two level systems,

$$\hat{h}_i = \Delta_m \left[x_i \hat{\sigma}_z^i + e^{-r_i} \hat{\sigma}_x^i \right]. \tag{3.43}$$

The $\hat{\sigma}_{x,y,z}^i$ are the usual Pauli matrices, commuting for different TLSs. The parameters x_i are independent random variables uniformly distributed $0 \leq x_i \leq 1$, and r_i are independent random variables uniformly distributed $0 \leq r_i \leq R$, where the large distance cutoff $R \gg 1$ characterizes the lowest frequency at which the $1/f$ noise is observed. The energy Δ_m is the maximal level splitting of a TLS.

The motion of the TLSs produces an additional potential for the electrons $V\left(\vec{r}; \{\hat{\sigma}_i\}_{i=1}^{N_{TLS}}\right)$, which depends on the state of the TLSs, σ_i,

$$\hat{H}_{el-TLS} = \int d^d\vec{r}\, V\left(\vec{r}; \{\hat{\sigma}_i\}_{i=1}^{N_{TLS}}\right) \psi^\dagger(\vec{r})\, \psi(\vec{r}). \tag{3.44}$$

As the static potential is already disordered, the potential of the TLSs can be modeled as a random function with zero mean, no correlation with the static potential U and that has variance given by,

$$\begin{aligned} &\ll V\left(\vec{r}; \{\hat{\sigma}_i\}_{i=1}^{N_{TLS}}\right) \otimes V\left(\vec{r}'; \{\hat{\sigma}_i\}_{i=1}^{N_{TLS}}\right) \gg \\ &\qquad = \frac{\gamma}{2\pi\nu\tau} \delta^{(d)}\left(\vec{r} - \vec{r}'\right) \sum_{i=1}^{N_{TLS}} \hat{\sigma}_z^i \otimes \hat{\sigma}_z^i, \end{aligned} \tag{3.45}$$

where $\gamma \ll 1$ describes the ratio of scattering off of the mobile impurities to the elastic scattering. Equation (3.45) states that the random potential becomes decorrelated when a TLS changes, i. e. when σ_z changes sign. Any residual self correlation may be included in the static potential U. Otherwise, no restrictions are placed on the potential V. It is important to emphasize that averaging here is performed only over the spatial locations of the TLS and that the average over the parameters of the TLS (x_i and r_i) should be performed in the final answer. The resulting diagrammatics are summarized in Fig 3.9.

3.3.2 Fluctuation-dissipation theorem for dilute TLS

By using the fluctuation-dissipation theorem we may relate the noise and the quantum memory effects without any appeal to the microscopic details of the TLS. For dilute TLS (meaning that

the average number of TLS per coherent volume ℓ_ϕ^d is much less than one) the dynamics of the different TLS are independent. The fluctuations are expressed in the exact Keldysh Green's function,

$$F^K(t_1 - t_2) = \frac{1}{2N_{TLS}} \sum_{i=0}^{N_{TLS}} \left\langle \hat{\sigma}_z^i(t_1)\hat{\sigma}_z^i(t_2) + \hat{\sigma}_z^i(t_2)\hat{\sigma}_z^i(t_1) \right\rangle , \tag{3.46}$$

Here $\hat{\sigma}_z^i(t)$ is the operator defined in Eq. (3.43) in the Heisenberg representation and the quantum mechanical expectation $\langle\cdot\rangle$ is performed over the equilibrium density matrix of the electron system. The response of the TLS to the change in it's environment, such as perturbations of the electrons, is encoded in the retarded Green's function,

$$F^R(t_1 - t_2) = \frac{i}{2N_{TLS}} \sum_{i=0}^{N_{TLS}} \left\langle \left[\hat{\sigma}_z^i(t_1), \hat{\sigma}_z^i(t_2)\right] \right\rangle \theta\left(t_1 - t_2\right) , \tag{3.47}$$

where $\theta(t)$ is the step function. Note that we remove a factor of i from Eq. (3.46) so that both F^K and F^R are real functions.

Further microscopic calculation is relegated to Appendix B. For our purposes it is sufficient to use the fluctuation dissipation theorem. From the fact that all time scales are much longer than $\hbar/T$ we may write,

$$F^R(t) = \frac{\theta(t)}{T} \frac{\partial F^K(t)}{\partial t}. \tag{3.48}$$

Therefore everything may be expressed in terms of $F^K(t)$.

3.3.3 Mesoscopic conductance fluctuations

The properties of the conductance fluctuations are well studied. We reproduce the results in this section in order to establish the notation and the building blocks of the diagrammatic technique. The diagrams for the impurity averaged Green's functions $\ll G^{R,A} \gg$ and the average of their product $\ll G^R G^A \gg$ are shown in Fig. 3.9. Because we are averaging measurements made at well-separated times we can attach a definite time to each electron line. The most interesting part of the long-range dynamics is encoded in the diffuson and cooperon propagators $\mathbf{D}$ and $\mathbf{C}$ [see Figs. 3.9(d) and 3.9(e). These are the solutions of the "classical" equations,

$$\begin{aligned} \left\{ i\eta + \left[i\nabla_{r_1} + \left(\vec{A}(t_1, r_1) + \vec{A}(t_2, r_1)\right) \right]^2 + \tau_\phi^{-1} \right\} \\ \times \mathbf{C}\left(\eta, r_1, r_2; t_1, t_2\right) = \delta^{(d)}\left(r_1 - r_2\right) , \end{aligned} \tag{3.49a}$$

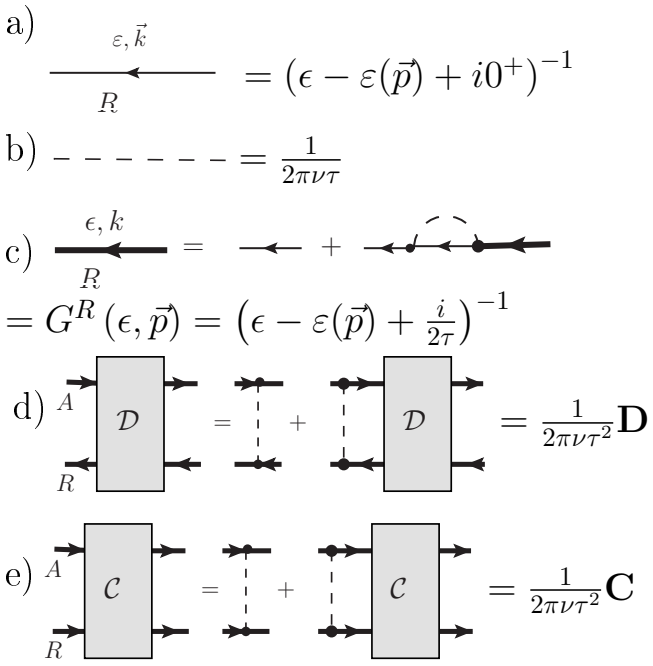

FIGURE 3.9: The definition of the diagrammatic elements: (a) bare electron Green's function, (b) static impurity, (c) dressed electron Green's function, (d) and (e) the resummation for the cooperon and diffuson pole. The external fermion lines are amputated and the functions $\mathbf{D}$ and $\mathbf{C}$ are defined in Eq. (3.49b) and Eq. (3.49a) respectively.

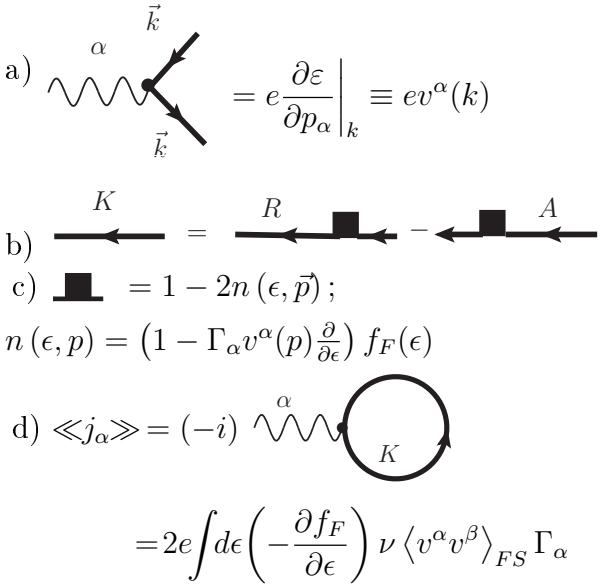

FIGURE 3.10: The definition of the diagrammatic elements: (a) current operator, (b) Keldysh Green's function, (c) electron distribution function, (d) expectation of the current operator. The factor of 2 comes from the spin summation. The Fermi function $f_F(\epsilon) \equiv [1 + \exp(\epsilon/T)]^{-1}$. Note the factor of $-i$ in the definition (c) of the average current

and

$$\left\{ i\eta + \left[i\nabla_{r_1} + \left(\vec{A}(t_1, r_1) - \vec{A}(t_2, r_1) \right) \right]^2 + \tau_\phi^{-1} \right\} \times \mathbf{D}\left(\eta, r_1, r_2; t_1, t_2\right) = \delta^{(d)}\left(r_1 - r_2\right), \tag{3.49b}$$

where $\eta \equiv \epsilon_1 - \epsilon_2$ is the difference of the energy of the two electron lines. The constant τ_ϕ is the phase coherence time, which captures the effect of the interacting processes not explicitly included in our model, such as phonons. The gauge is fixed with $A^0 = 0$ so that $\mathbf{C}\left(r, r; t_1, t_2\right)$ is invariant under the residual, time-independent gauge transformations.

In the absence of a magnetic field, there is no dependence on the times t_1 and t_2 and the Fourier transform of the propogators is given by,

$$\mathbf{C}\left(\eta, \vec{Q}\right) = \mathbf{D}\left(\eta, \vec{Q}\right) = \left(-i\eta + \mathcal{D}Q^2 + \tau_\phi^{-1} \right)^{-1}. \tag{3.50}$$

The non-equilibrium distribution of the electronic system due to a finite current is expressed by the Keldysh Green's function G^K shown in Fig. 3.10(b) or equivalently by the electron distribution function $n\left(\epsilon, \vec{p}\right)$. The average current, shown in Fig. 3.10(d) reproduces the usual Drude formula.

In addition to affecting the long-range correlations as encoded in the diffuson and cooperon, the disorder also affects the short range correlations of operators. This is encoded in the Hikami box subdiagrams shown in Fig. 3.11.

The mesoscopic fluctuations originate in the dependence of G^K on the disorder. The variance is calculated diagrammatically in Fig. 3.12. In the limit $T\tau_\phi \gg 1$, calculation yields,

$$\ll \delta j^\alpha(r, t_1) \delta j^\beta(r', t_2) \gg = (\pi\nu)^{-2} \int d\epsilon_1 d\epsilon_2 \left(\frac{\partial f_F}{\partial \epsilon_1} \right) \left(\frac{\partial f_F}{\partial \epsilon_2} \right) \left\{ |\mathbf{C}(\epsilon_1 - \epsilon_2, r, r')|^2 j^\alpha(r, t_2) j^\beta(r', t_1) + \delta^{(d)}(r - r') \delta^{\alpha\beta} \sum_\gamma \int dr'' \left[|\mathbf{D}(\epsilon_1 - \epsilon_2, r, r'')|^2 j^\gamma(r'', t_1) j^\gamma(r'', t_2) \right] \right\} \tag{3.51}$$

We now simplify Eq. (3.51), working in $d < 2$ and analytically continuing to higher dimensions. Using the fact $\eta \equiv \epsilon_1 - \epsilon_2$ is of the order of τ_ϕ whereas $\epsilon_{1,2} \sim T$, we may take one of the integrals over ϵ. Further, the function $\mathbf{C}(r, r')$ falls off exponentially for $|r - r'| \gg \ell_\phi$. Assuming that $j(r)$ is smooth on the scale ℓ_ϕ, we can remove $j(r)$ from any integral over position. Lastly, using the fact that,

$$\int dr dr' \int_{-\infty}^{\infty} d\eta \, |\mathbf{C}\left(\eta, r, r'\right)|^2 = \pi \int dr \, \mathbf{C}\left(0; r, r\right) \tag{3.52}$$

a)

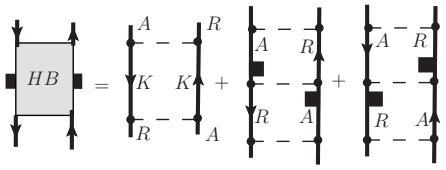

$$= -\frac{4\pi\tau^2}{\nu\mathcal{D}} \ll\vec{j}\gg \cdot \ll\vec{j}\gg f'_F(\epsilon_1) f'_F(\epsilon_2)$$

b)

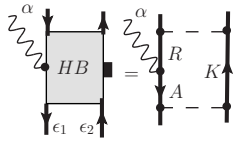

$$= 4\pi i\tau^2 \ll j_\alpha \gg f'_F(\epsilon_2)$$

c)

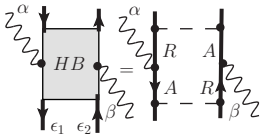

$$= 4\pi\tau^2 \nu\mathcal{D}\delta_{\alpha\beta}$$

d)

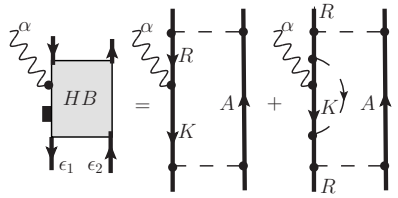

$$= 2\pi i\tau^2 \ll j_\alpha \gg f'_F(\epsilon_2)$$

e)

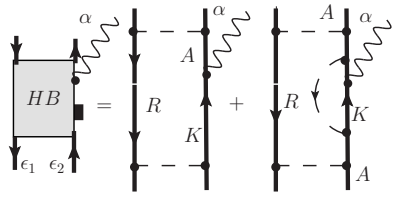

$$= 2\pi i\tau^2 \ll j_\alpha \gg f'_F(\epsilon_2)$$

FIGURE 3.11: The Hikami box subdiagrams. The external lines are amputated.

we obtain

$$\begin{aligned} \ll\delta j^\alpha(r,t_1)\delta j^\beta(r',t_2)\gg &= \delta^{(d)}(r-r')\sum_{\rho\sigma} j^\rho(r,t_1) j^\sigma(r',t_2) \\ &\times \frac{1}{3\pi T\nu^2}\Big[\delta^{\alpha\beta}\delta^{\rho\sigma}\mathbf{D}\,(0,r,r) + \delta^{\alpha\rho}\delta^{\sigma\beta}\mathbf{C}\,(0,r,r)\Big]. \end{aligned} \tag{3.53}$$

We now apply Eq. (3.51) to the experimental setup of interest. Consider a cubical system of linear dimension L, with leads welded on to the faces normal to the $\hat{x}$ direction. Apply a voltage V and measure the current I. To relate I to the local fluctuation δj we should recall that the

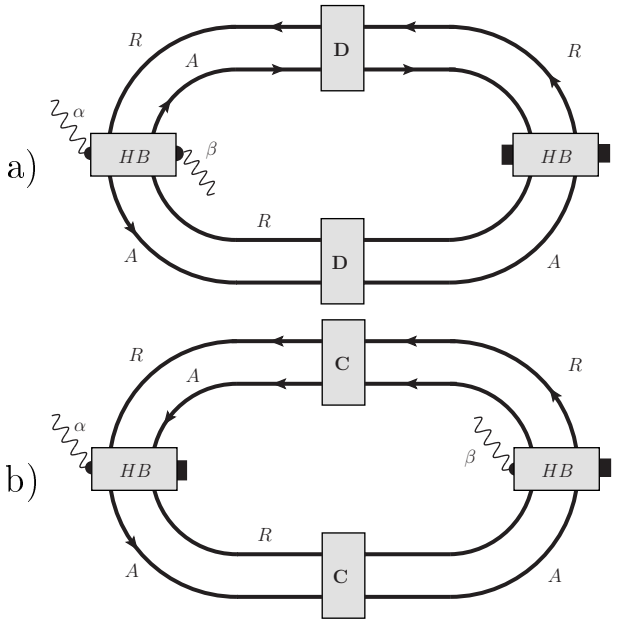

FIGURE 3.12: The diagrams contributing to the universal conductance fluctuations. They must be multiplied by the factor $(-i)^2$. Compare with Fig. 3.10(d)

correct interpretation of the term $\delta j(r,t)$ is as a Langevin source for the current density $j(r)$,

$$j^\alpha(r,t) = \sigma E^\alpha + \delta j^\alpha(r,t), \tag{3.54}$$

where E is the electric field and $\delta j(r)$ is to be treated as a random term with statistics given by Eq. (3.51). However, since we are dealing with a good conductor there is no local charge accumulation on the time scales of interest, as the electric field E compensates instantly. The only effect of the Langevin force $\delta j(r)$ is to affect the charge transport across the system, so the correction to the current $\delta I(t)$,

$$\delta I(t) = \frac{1}{L}\int d^d r\ \delta\vec{j}(r,t)\cdot\hat{x}. \tag{3.55}$$

To first order, the current density that appears on the right hand side of Eq. (3.53) can be taken to be the Drude result $j = V\sigma L^{2-d} = IL^{1-d}$ giving [compare with Eq. (3.15)],

$$\begin{aligned} \ll \delta I(t)\delta I(0) \gg = &\frac{I^2}{L^d}\frac{\ell_\phi^d}{T\tau_\phi g(\ell_\phi)^2}\left[Y\left(\frac{\ell_\phi}{\ell_{B_-}}\right) + Y\left(\frac{\ell_\phi}{\ell_{B_+}}\right)\right] \\ &+ \frac{I^2}{L^d}\frac{L_T^d}{g\,(L_T)^2} f_d, \end{aligned} \tag{3.56}$$

where $L_{B_\pm} \equiv (e\,|B(0) \pm B(t)|)^{-1/2}$ and Y is the scaling function defined by

$$Y\left(\frac{\ell_\phi}{\ell_B}\right) \equiv \frac{1}{3\pi}\frac{\ell_\phi^d}{\tau_\phi}\left[\mathbf{C}\,(0,r,r;B) - \mathbf{C}\,(0,r,r;0)\right]. \tag{3.57}$$

This function is well known from the study of weak localization[66, 67]. The magnetic-field-indepedent term f_d appears on analytic continuation to $d = 2, 3$. In $d = 2$ it is given by,

$$f_2 = \frac{1}{6\pi^2}\log\left(\frac{1}{T\tau}\right), \tag{3.58}$$

and is a nonuniversal constant in $d = 3$.

3.3.4 1/f noise

The mesoscopic fluctuations can be made observable by varying an external parameter, such as magnetic field. The shifting of the TLS is another mechanism by which the mesoscopic fluctuations are manifested, in this case as the $1/f$ noise. The appropriate diagrams are collected in Fig. 3.13. In fact, no new calculation is needed since we may use the result for the mesoscopic fluctuation (3.51), make the substitution $\tau_\phi^{-1} \to \tau_\phi^{-1} + \tau_*^{-1}\left(\bar{F}^K(t) - \bar{F}^K(0)\right)$ and then expand to first order. The resulting correlations of the current are

$$\begin{aligned}\ll\delta j^\alpha(r,t_1)\delta j^\beta(r',t_2)\gg &= \delta^{(d)}(r-r')\sum_{\rho\sigma} j^\rho(r,t_1)j^\sigma(r',t_2)\\ \times\frac{1}{3\pi\nu^2 T\tau_*}&\frac{\partial}{\partial\tau_\phi^{-1}}\left[\delta^{\alpha\beta}\delta^{\rho\sigma}\mathbf{D}\,(0,r,r) + \delta^{\alpha\rho}\delta^{\sigma\beta}\mathbf{C}\,(0,r,r)\right].\end{aligned} \tag{3.59}$$

We may follow the same arguments as above to translate this expression into an expression for the fluctuations of the current. In terms of the function $\mathcal{F}$ (see Eq. (3.1)),

$$\mathcal{F}(t) = L^d(\ll \delta I(0)\delta I(t) \gg)/I^2, \tag{3.60}$$

the result is

$$\begin{aligned}\mathcal{F}(t) = &\frac{\ell_\phi^d}{T\tau_* g(\ell_\phi)^2}\left[Z\left(\frac{\ell_\phi}{\ell_{B_-}}\right) + Z\left(\frac{\ell_\phi}{\ell_{B_+}}\right)\right]\\ &\times\left[F^K(t) - F^K(0)\right],\end{aligned} \tag{3.61}$$

where,

$$Z(x) = (d/2-1)\,Y(x) - 2xY'(x) + \frac{1}{12\pi^2}\delta_{2,d}. \tag{3.62}$$

a) 

$$= \frac{1}{2\pi\nu\tau_*} F^K(t_1 - t_2)$$

b) 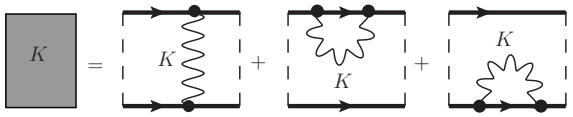

$$= \frac{2\pi\nu\tau^2}{\tau_*} \left[F^K(t_1 - t_2) - F^K(0)\right]$$

c) 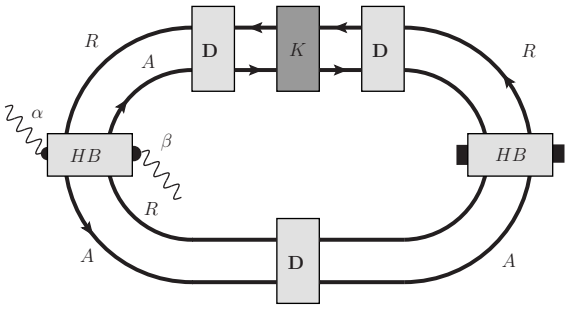

d) 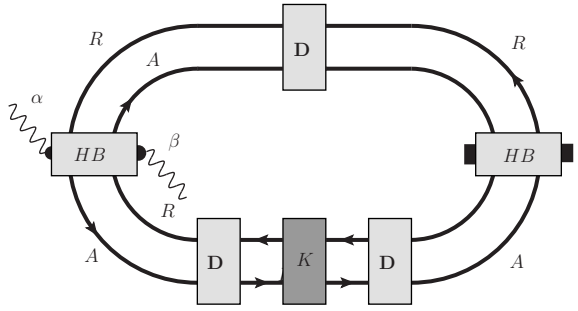

e) 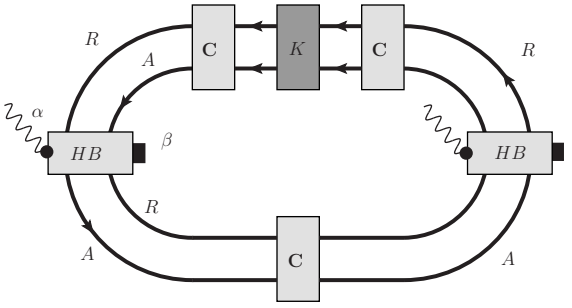

f) 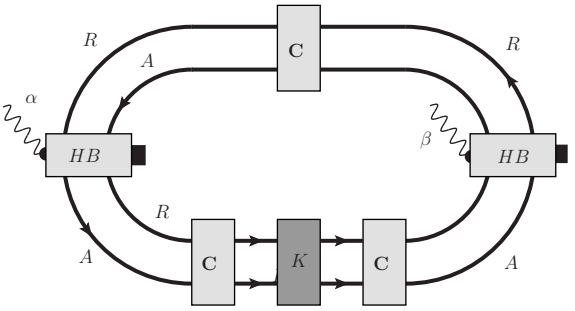

FIGURE 3.13: The diagrams contributing to the noise. The TLS enter through subdiagram (b).

The final term of Eq. (3.61), in square brackets, carries all of the details of the microscopic model. The noise can therefore be used to calculate τ_* and the correlations of the impurities.

On insertion of the result for the TLS (see Appendix B) becomes

$$\mathcal{F}(t) \propto -\frac{\log(t/t_0)}{\log(t_m/t_0)}, \tag{3.63}$$

for times t with $t_0 < t < t_m$. For frequencies f with $t_0 < f^{-1} < t_m$ the Fourier transform of the autocorrelation has the expected $1/f$ scaling. Given that t_0 is microscopic while t_m may be on the order of a day, this reproduces the experimental fact of $1/f$ scaling over many orders magnitude.

3.3.5 Memory effect

We now calculate the memory effect, which is the correction to the conductivity arising from the past history of the chemical potential $\mu(t)$ and magnetic field $B(t)$. By quickly sweeping the chemical potential at well-separated times, the entire time history of the conductivity at all energies may be reconstructed. Throughout this section, we will suppress the dependence of $\mathbf{C}$ and $\mathbf{D}$ on magnetic field.

The corrections to the measured current are shown in Fig. 3.14. The history of the system parameters $\mu(t)$ and $B(t)$ enter through the history of the electron occupation function, $n_\epsilon(t) = \tanh\left(\frac{\epsilon-\mu(t)}{2T}\right)$. The correction to the measured conductivity is,

$$\begin{aligned}\frac{\delta\sigma(t)}{\sigma_D} = &\int dt' \frac{F^R(t-t')}{\nu\tau^*} \\ &\times \int \frac{d\epsilon}{2\pi}\frac{d\epsilon'}{2\pi} X(\epsilon'-\epsilon)\frac{\partial n_\epsilon(t)}{\partial\epsilon} n_{\epsilon'}(t').\end{aligned} \tag{3.64}$$

It is important to note that the energies in the distribution function are defined relative to the chemical potential at the time t. The kernel X is defined by

$$X(\eta) = 2\mathrm{Re}\left\{ i\int \frac{d^d\vec{Q}}{(2\pi)^d}\left[\mathbf{C}(\vec{Q},\eta)^2 + \mathbf{D}(\vec{Q},\eta)^2\right]\right\}. \tag{3.65}$$

The integral over η and Q is not convergent in $d = 2$ and 3, so there are logarithmic terms in $d = 2$ and non-universal constant terms in $d = 3$. Using the fact that $\mathcal{C}(\eta)^2 = -i\partial_\eta \mathcal{C}(\eta)$ and

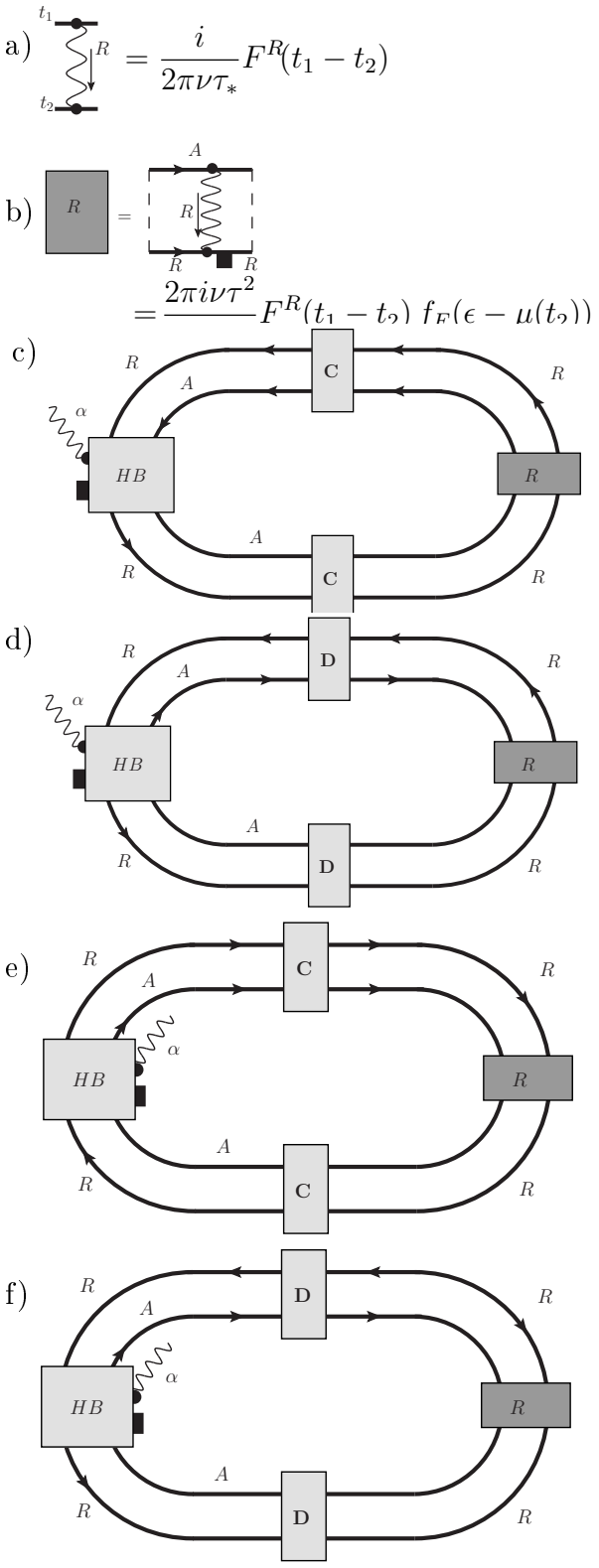

FIGURE 3.14: The diagrams contributing to the memory effect. The TLS enter through subdiagram (a). Note there is an overall factor of i from the definition of j in Fig. 3.10(c)

likewise for the diffuson, we can integrate by parts, obtaining:

$$\begin{aligned}&\int_{-\infty}^{\infty}\frac{d\epsilon'}{2\pi}X(\epsilon'-\epsilon)n_{\epsilon'}(t')\\&=\mathrm{Re}\Big\{\int_{-\infty}^{\infty}\frac{d\epsilon'}{2\pi}\frac{\partial n_{\epsilon'}(t')}{\partial\epsilon'}\left[\mathbf{C}(r,r,\epsilon'-\epsilon)\ +\mathbf{D}(r,r,\epsilon'-\epsilon)\right]\Big\}.\end{aligned}\tag{3.66}$$

Finally, using the fluctuation dissipation relationship between F^K and F^R [see Eq. (3.48)], we obtain the main result of this section:

$$\begin{aligned}\frac{\delta\sigma(t)}{\sigma_D}=\frac{1}{T\tau_*}\frac{1}{g\left(L_T\right)}\int_{-\infty}^{t}dt'\ \frac{d\bar{F}^K(t-t')}{dt}\Bigg[\\S\left(\frac{\mu(t)-\mu(t')}{T},\frac{L_T}{L_{B_+}}\right)+S\left(\frac{\mu(t)-\mu(t')}{T},\frac{L_T}{L_{B_-}}\right)\Bigg],\end{aligned}\tag{3.67}$$

compare with Eq. (3.31). The conducance at scale T is determined by the scaling

$$\frac{g\left(L_T\right)}{g\left(\ell_\phi\right)}\equiv\left(\frac{L_T}{\ell_\phi}\right)^{2-d},\tag{3.68}$$

and the magnetic length $L_{B_\pm}$ is defined by

$$L_{B_\pm}\equiv\sqrt{\frac{\hbar c}{e\left|B(t)\pm B(t')\right|}}.\tag{3.69}$$

The scaling [3] function S is defined by,

$$S\left(u,v\right)\equiv 8\int_{-\infty}^{\infty}dx\ \frac{x\mathrm{coth}x-1}{\sinh^2 x}\mathfrak{Re}\Big\{\bar{\mathbf{C}}\left(0,(2x+u),v\right)\Big\}.\tag{3.70}$$

Here $\bar{\mathbf{C}}$ is the cooperon expressed in dimensionless units, given by the equation,

$$\left[iu+\left(i\vec{\nabla}+v\bar{A}(r)\right)^2\right]\bar{\mathbf{C}}\left(r,u,v\right)=\delta^{(d)}(r),\tag{3.71}$$

where $\tilde{A}$ is a dimensionless gauge potential obeying,

$$\vec{\nabla}\times\tilde{A}=\hat{z},\tag{3.72}$$

and $\hat{z}$ is the unit vector in the direction of the magnetic field. Although Eq. (3.70) only contains the symbol $\bar{\mathbf{C}}$, it includes the diffuson contribution through the second term of Eq. (3.67). The

[3] There also may be an effect of the magnetic through the Zeeman coupling, but this should be a secondary effect.

correction is similar to the usual quantum correction to conductance, but around the old chemical potential.

The integral over $x \equiv 2(\epsilon_1 - \epsilon_2)/T$ serves to smooth the result over the scale of the temperature. At zero magnetic field we may evaluate S explicitly and we obtain

$$S\left(u,0\right) = \int_{-\infty}^{\infty} dx \; \frac{x \coth x - 1}{\sinh^2 x} P_d\left(2x+u\right). \tag{3.73}$$

The function P_d depends on the dimension and is given by

$$\begin{aligned} P_1(z) &\equiv \frac{2}{\sqrt{2}} \left|z\right|^{-1/2} \\ P_2(z) &\equiv -\frac{2}{\pi} \log\left|\frac{1}{z(T\tau)}\right| \\ P_3(z) &\equiv a - \frac{\sqrt{2}}{\pi} \left|z\right|^{1/2}, \end{aligned} \tag{3.74}$$

where a is a non-universal constant. When $u \gg 1$, S has the limiting form

$$S(u,0) = P_d(u). \tag{3.75}$$

We now calculate the effect of a transverse magnetic field in $d = 2$. In a magnetic field the Cooperon must be expanded in Landau levels,

$$\bar{\mathbf{C}}\left(0,u,v\right) = \frac{4v^2}{4\pi} \sum_{n=0}^{\infty} \left[i\eta + \left(n + \frac{1}{2}\right) 4v^2 \right]^{-1}. \tag{3.76}$$

Introducing an integral over the auxialiary variable s this may be rewritten as

$$\begin{aligned} &\bar{\mathbf{C}}\left(0,u,v\right) - \mathbf{C}\left(0,u,0\right) = \\ &\frac{1}{4\pi} \int_0^{\infty} \frac{ds}{s} \exp\left(-i\frac{\eta}{T}s\right) \left(\frac{2v^2 s}{\sinh\left(2v^2 s\right)} - 1\right). \end{aligned} \tag{3.77}$$

The change in the line shape $S(u,v)$ can now be evaluated with the result that

$$\begin{aligned} S(u,v) - S(u,0) = \frac{2}{\pi} \int_0^{\infty} \frac{ds}{s} &\left(\frac{2v^2 s}{\sinh\left(2v^2 s\right)} - 1\right) \\ \times &\left(\frac{2\pi s}{\sinh(2\pi s)}\right)^2 \cos(us). \end{aligned} \tag{3.78}$$

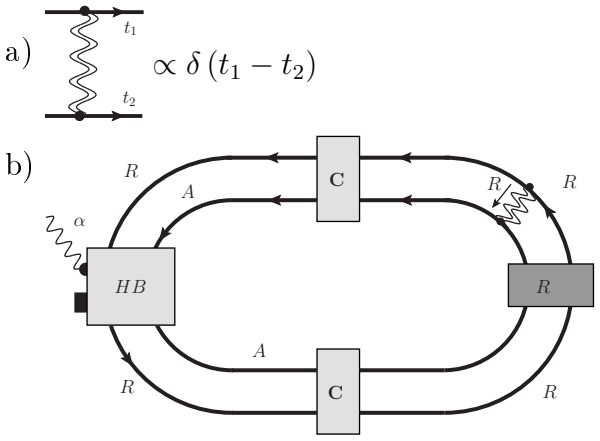

FIGURE 3.15: A normal electron-electron interaction, indicated by the double wavy line in figure (a), is effectively a delta function in time on the scales of interest. Therefore diagrams of the form (b) do not contribute to the memory effect and there is no Fermi-liquid type resummation.

Proceeding in the regime where $v \ll 1$, the bulk of the integral comes from the region near zero where the first term may be perturbatively expanded,

$$S(u, v) \approx S(u, 0) + v^4 H(u), \tag{3.79}$$

where

$$H(u) = \frac{4}{3\pi} \int_0^\infty dx \, \frac{(2\pi x)^2 x}{\sinh^2(2\pi x)} \cos(ux). \tag{3.80}$$

Finally, although there is a superficial resemblance between the retarded line F^R and the usual electron-electron interactions, the term F^R does not get simply resummed in the usual Fermi-liquid fashion, see Fig. 3.15. This is because any interaction between an electron at time t_1 and t_2 will produce make the diagram proportional to $\delta(t_1 - t_2)$ and therefore not contribute to the memory effect. It has been shown[68]]that in $d = 2$ electron-electron interactions can produce $1/f$ noise, but this is only true for frequencies $fL^2/\mathcal{D} \gg 1$ and thus has no relevance for the longest time behavior in mesoscopic systems.

3.4 Conclusion

The essential conclusions of this paper are as follows: The existence of the two level systems that have been suggested to cause the $1/f$ noise in metals, *necessarily* leads to a memory effect. The strength of the memory effect is universally related to the strength of the $1/f$ noise. The

lineshape of the memory effect is also a universal function. Since the effects are related to the mesoscopic fluctuations they are sensitive to the magnetic field in a universal fashion. The sensitivity to the Aharonov-Bohm effect, which leads to the magnetic field dependence, is a universal feature of quantum coherent systems.

We emphasize that the conclusions here do not depend on the microscopic model of the TLS. The TLS do not have to be structural defects or mobile impurities. Any set of localized systems that produce low-frequency noise will, by the fluctuation-dissipation theorem, lead to a long-time memory effect following the universal relationship. There is no necessity for the spectrum to be exactly of the form $1/f$ - any slowly decaying spectrum will lead to a memory effect. Even a mechanism such as atoms diffusing through a network of tunnelling sites - while not in some sense a "localized system" - will still lead to the same relationship between noise and memory[4].

We have neglected spin orbit coupling in our calculation. In the limit of strong spin orbit coupling the strength of both the memory effect and $1/f$ noise is reduced by $1/4$. Therefore the ratio of the two effects is the same as at zero spin orbit coupling. There is an small intermediate regime where the spin-orbit scattering length is between the phase coherence length and the temperature length. In this case the 1/f noise will be suppressed by up to $1/4$ but the memory effect will be unchanged. Therefore for this regime the ratio of the two will be changed by a numerical factor ≤ 4. In any case, the time dependence and lineshape of the memory effect will be qualitatively unchanged.

To close our discussion we discuss relevant theoretical and experimental works.

Other theoretical work on memory effects has been conducted in the insulating phase. In particular, the role of TLS of in memory effects was suggested in Ref. [[69]], where it was shown that TLS may cause slow relaxation of the local density of states in insulators. The possibility that memory effects can be a manifestation of Anderson Glass[70–72] physics has also been investigated[73, 74].

Since the memory effect we have calculated is a necessary consequence of the TLS, it may be used to test whether the TLS are indeed the source of the $1/f$ in a system. Although in systems with a large conductance samples the memory effect will be suppressed, there are several systems that have anomolously high $1/f$ noise[75, 76]. A search for memory effects in these materials may help elucidate the source of this noise.

Experimentally, memory effects have been found in a variety of systems, including indium oxide films[77, 78], thin films of Pb or Bi[44], and granular metals[43, 79–81]. However these systems

[4]We are grateful to A. Andreev for drawing our attention to this point

are understood to be in the insulating regime. We are not aware that any comparable effects have been found in diffusive systems.

We note that in the metallic regime the separation of the screening length and the phase coherence length leads to some dependence of the anomalous capacitance on the thickness of the sample. We discuss this in Appendix C.

Chapter 4

Tuning the BEC-BCS crossover into a non-equilibrium phase transition

4.1 Introduction

The Bose-Einstein condensation (BEC) [85] and Bardeen-Cooper-Schriffer state (BCS) [86] are two extreme scenarios for the formation of the superfluid state in fermionic systems. By superfluid phase we mean a system with spontaneously broken $U(1)$ symmetry where the only allowed gapless mode is the acoustic bosonic branch. In the BEC scenario, the fermions are first paired into compact two-particle complexes (molecules). These molecules experience Bose-Einstein condensation with the acoustic low energy spectrum due to the weak repulsion between molecules. In the BCS scenario, weakly coupled Cooper pairs are formed from states near the Fermi level so that the characteristic size for the pair correlation significantly exceeds the inter-particle distance. Nevertheless, this weak coupling is sufficient to gap the fermionic excitation and leads to bosonic acoustic excitations as the oscillations of the order parameter. The physical effects occuring in between those two scenarios are referred to as BCS-BEC *crossover*.

The BCS-BES crossover is captured by the simplest Hamiltonian density [91]

$$H = \psi^*_\sigma h^{(1)} \psi_\sigma + b^* h^{(2)} b + \left[\lambda b^* \psi_{\sigma_1} \tau^y_{\sigma_1\sigma_2} \psi_{\sigma_2} + \text{h.}c.\right], \tag{4.1a}$$

where σ labels two (spin or pseudospin) states for the fermions described by Grassman fields $\psi_\sigma(\mathbf{r}), \psi^*_\sigma(\mathbf{r})$ (summation over repeated indices is implied, and τ^y is the standard Pauli matrix), and the bosonic fields $b(\mathbf{r}), b^*(\mathbf{r})$ describe the bound states of two fermions. Therefore the kinetic

energy part is described by ($\hbar = 1$)

$$h^{(q)} \equiv (-i\nabla - q\mathbf{a})^2/(2qm) + q\varphi - \delta_{2,q}\varepsilon_b, \tag{4.1b}$$

where the background vector $\mathbf{a}(\mathbf{r}, t)$ and scalar potentials $\varphi(\mathbf{r}, t)$ are introduced to highlight the continuity equation for the total particle density $n(\mathbf{r}) = \psi_\sigma^*\psi_\sigma + 2b^*b$.

The parameter ε_b describes the energy of the bound state when $\varepsilon_b > 0$ or the position of the resonance when $\varepsilon_b < 0$. In models of pre-formed pairs in superconductors[90], ε_b is a material dependent parameter. In experiments with cold atoms ε_b is the directly tunable position of the Feshbach resonance [87, 88]. Thus, cold atom system provide a versatile platform for a detailed study of the BEC-BCS crossover.

In Eq. (4.1b), the constant λ controls the coupling of the bound state (molecules) with fermionic continuum. If λ is sufficiently small $n^{2/d}/m \gg |\lambda| n^{1/2}$ (the so-called narrow resonce regime), an analytic treatment of the problem is possible for any ϵ_b. This is done in the Appendix D. For large λ the crossover can be investigated only numerically [89].The arguments below are independent of the width of the resonance.

All numerical and analytical study of the ground state energy of the Hamiltonian (4.1a) at $\varphi, \mathbf{a} = 0$ indicates that the ground state energy density $E_{GS}(n, \varepsilon_b)$ is an analytic function of its arguments, (hence the term *crossover* rather than *transition*). The usual argument is that regardless of the values of the paramters, the last term in Eq. (4.1a) leads to an anomalous average $\langle \psi_{\sigma_1} \tau^y_{\sigma_1\sigma_2} \psi_{\sigma_2} \rangle \propto \langle b \rangle \propto e^{i2\theta}$. Given that apparently no other symmetry breakings occur, there is apparently no sharply defined critical field $\varepsilon_b^c(n)$ that separates the BEC and BCS regimes. Moreover, for all parameters the low energy excitations are described by superfluid hydrodynamics given by the Lagrangian

$$\mathcal{L} = n\left[\phi - \frac{\mathbf{v}^2}{2m}\right] - E_{GS}(n) + \gamma_\sigma^*\left[i\tilde{\partial}_t - \epsilon(-i\nabla; n)\right]\gamma_\sigma, \tag{4.2}$$

where $\tilde{\partial}_t \equiv \partial_t + \mathbf{v}\cdot\nabla$ is the convective derivative, $\phi \equiv \partial_t\theta + \varphi$ and $\mathbf{v} \equiv \nabla\theta - \mathbf{a}$ are the gauge invariant potential and velocities respectively, , the fields n and θ are real, and $\gamma_\sigma, \gamma_\sigma^*$ are the Grassman fields describing the fermionic excitations (which for the problem of interest can be viewed as neutral BCS quasiparticles). This Lagrangian is an analytic function of variables, which apparently does not allows a definition of a critical field separating the two regimes. The first term in Lagrangian (4.2) is protected by the gauge and Galilean invariances and the second term, $E_{GS}(n; \epsilon_b)$, is an analytic function of ϵ_b. This implies that the spectrum of the bosonic

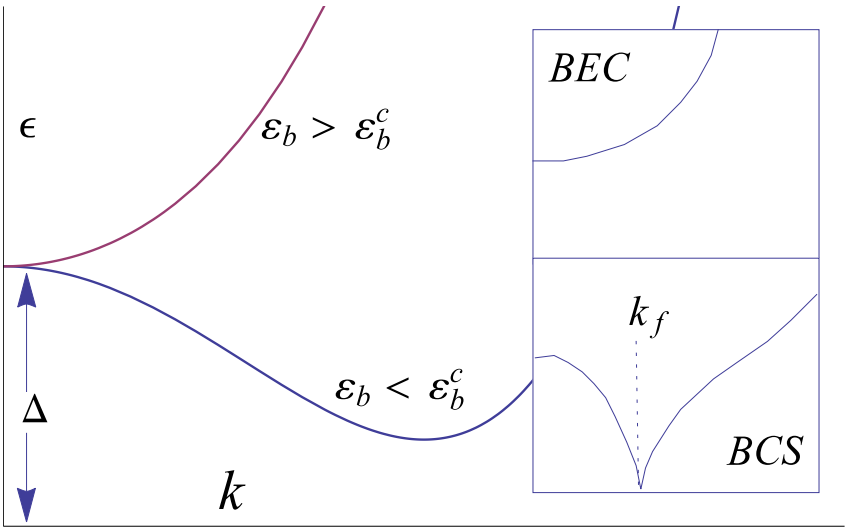

FIGURE 4.1: The fermionic quasiparticle spectrum $\epsilon(k)$ from Eq. (4.2) for ε_b close to its critical value (4.3a). Insets are the fermionic spectra deep in the BEC and BCS regimes.

excitations (phonons) also must be analytic. However, the spectrum of the fermionic excitations $\epsilon(k)$ does experience a reconstruction that allows for the definition of the critical field $\varepsilon_b^c(n)$.

In the deep BEC regime the fermions are entirely decoupled from bosons so that the spectrum has a minimum at $k = 0$. In the opposite limit, in the deep *BCS* regime, the spectrum of the quasiparticles has minima on the Fermi surface $k = k_F$, see inset to Fig. 4.1. As the transition from point to sphere can not be analytic, there must exist a point $\varepsilon_b^c(n)$ such that

$$d^2\epsilon(k;\varepsilon_b,n)/dk^2\big|_{k=0,\ \varepsilon_b=\varepsilon_b^c(n)} = 0. \tag{4.3a}$$

We will call $\varepsilon_b^c(n)$ from Eq. (4.3a) the *critical field* of the BEC-BCS *transition*. The fermionic spectrum for small momenta can be written as

$$\epsilon(k,n) = \Delta(n,\varepsilon_b) + \alpha\,(\varepsilon_b - \varepsilon_b^c)\,k^2/2 + \beta k^4/4 \tag{4.3b}$$

where $\alpha, \beta > 0$. At fields below the transition $\varepsilon_b < \varepsilon_b^c$, the spectrum is mexican hat shaped with the position of the minimum $|k| = k_F$, and its energy $\Delta - \Lambda$:

$$k_F = \sqrt{(\alpha/\beta)\,(\varepsilon_b^c - \varepsilon_b)}, \quad \Lambda = \beta k_F^4/4 \tag{4.3c}$$

At first glance, the definition (4.3) appears to be of no physical consequence. Indeed, at $\varepsilon_b = \varepsilon_b^c$ the fermionic spectrum remains gapped so that there is neither a reconstruction of the ground state nor a thermodynamic singularity at finite temperature. However we now show that by an

arbitrarily weak time-dependent perturbation it is possible to induce a spontaneous symmetry breaking of the ground state of the two-dimensional system precisely at the critical point (4.3a). For a finite perturbation, the theory outlined below predicts the formation of the incommensurate *supersolid* state via a weak quantum first order phase transition. The periodicity of this phase will be determined by the "order parameter" (4.3c).

4.2 Coupling to radiation

The controlled radiative coupling to the "external" fermions has been experimentally demonstrated, for example in Ref. [92]. It involves a third species of fermions described by the Grassmann fields f^*, f which originally do not interact with any of the particles of the original problem (4.1). In the context of cold atom systems this would be given by a third hyperfine state. The radiation induces transitions between the third species and one of the fermions from Eq. (4.1), so that in terms of the low energy theory (4.2) it creates or annihilates two fermionic excitations,

$$H_{RF} = f^* \left(h^{(1)} + \Delta_f \right) f + \left[F_\sigma(t) e^{-i\theta} f \gamma_\sigma + h.c. \right], \tag{4.4}$$

where $F(t)$ is proportional to the strength of the radiation field , and $\Delta_f > 0$ is the boundary of the spectrum. The functional form of the second term in Eq. (4.4) is protected by gauge invariance. Let us concentrate on the case of the monochromatic radiation $F(t) \propto e^{i\omega t}$,

$$d \equiv \Delta(n, \varepsilon_b) + \Delta_f - \omega. \tag{4.5}$$

If $d < 0$ the Hamiltonian (4.4) creates *real* fermion pairs and phonons and therefore leads to entropy growth (heating). For $d < 0$ real processes are not allowed (in fact, multi-photon real processes are also forbidden), and the coupling (4.4) introduces a correction to the ground state energy density

$$\delta E^{(0)}_{GS} = \int \frac{d^2k}{(2\pi)^2} \mathcal{E}(k); \quad \mathcal{E}(k) = -\frac{F_\sigma F^*_\sigma}{\xi(k)}, \tag{4.6}$$

where $\xi(k) \equiv k^2/(2m) + \epsilon(k) - \Delta + d$ is the energy of the virtual state consisting of two excited fermions, and the meaning of the superscript (0) will become clear shortly.

The correction $\delta E^{(0)}_{GS}$ is logarithmically divergent as $d \to 0$. This corresponds to a photon with energy just sufficient for the excitation of f and γ fermions with zero momentum. Above the BCS-BEC *transition* field, $\varepsilon_b > \varepsilon^c_b$ This is the lowest energy of *any* excitaiton of a f and a γ fermion and (4.6) is the final answer. As this energy correction by itself is not observable,

radiation below the threshold, $d < 0$, does not lead to any changes in the properties of the ground states of the system.

The situation changes qualitatively below the BCS-BEC *transition*, $\varepsilon_b < \varepsilon_b^c$. Indeed the minimal energy of the pair excitations is given by a fermion f with $k = 0$ and one of the γ femions at $|k| = k_F$ from Eq. (4.3c), i.e. the lowest boundary of the two particle continuum is given by $\Delta(n)+\Delta_f-\Lambda$. If this were to appear in the denominator in Eq. (4.6) this would give a divergence already at $d = \Lambda$, and a singular correction to the ground state. For the homogeneous state this is impossible as the translational invariance of the ground state and of the Hamiltonian (4.4) prohibits the exctitation of two-quasiparticle with the total momentum $|k| = k_F$ from a zero momentum photon. The main idea to propose a spontaneous breaking of translational symmetry to enable this process, that is the formation.

The resulting state has no currents and the variation of density $\delta n(\mathbf{r}) \ll \langle n \rangle$ is periodic in space $\delta n(\mathbf{r} + j_1\mathbf{t}_1 + j_2 t_2) = \delta n(\mathbf{r})$ (here $\mathbf{t}_{1,2}$ are the primitive translation vectors) It can therefore be classifed as a *supersolid* state. If the primitive vectors of the reciprocal lattice $\mathbf{b}_{1,2}$ have the length of k_F the excitation of the lowest state becomes allowed and the logartihmacally divergent negative correction to the ground state is present. We will see that this correction can overcome the positive contribution to the ground state energy from the compressibility $(1/2)(\delta n)^2(\partial^2 E_{GS}/\partial n^2)_{F=0}$ thus making the supersolid state energetically favorable.

4.3 Supersolid state and the phase diagram

In the presence of the peridic density variation, the fermionic gap in Eq. (4.3b) also acquires a spatial variation, $\tilde{\Delta} \equiv (\partial\Delta/\partial n)_{n=\langle n\rangle}\delta n$. The correction (4.6) changes due to the effect of the periodic potential produced by the supersolid:

$$\delta^{(n)} E_{GS} = -\sum_{\mathbf{b},\alpha} \int_{\mathbf{k}\in BZ} \frac{d^2k}{(2\pi)^2} \mathcal{E}_{\mathbf{b},\alpha}(\mathbf{k});\ \mathcal{E} = -\frac{|F_\sigma^{\mathbf{b},\alpha}(\mathbf{k})|^2}{\xi_{\mathbf{b},\alpha}(k)}, \tag{4.7a}$$

where the quasimomentum integration is performed within the first Brillouin zone, $\mathbf{b}$ is a vector of the reciprocal lattice, α labels the band for the γ fermion in the periodic potential, described by Schrödinger equation for the Bloch functions, $u_{j,\mathbf{k}}(\mathbf{r}+\mathbf{t}) = u_{j,\mathbf{k}}(\mathbf{r})e^{i\mathbf{kt}}$,

$$\left[\beta\left(k_F^2 + \nabla^2\right)^2/4 + \tilde{\Delta}(\mathbf{r})\right] u_{\alpha,\mathbf{k}}(\mathbf{r}) = \tilde{\xi}_\alpha(\mathbf{k}) u_{\alpha,\mathbf{k}}(\mathbf{r}). \tag{4.7b}$$

The energy of the two particle virtual state is $\xi_{\mathbf{b},\alpha}(\mathbf{k}) \equiv d - \Lambda + (\mathbf{k}+\mathbf{b})^2/(2m) + \tilde{\xi}_\alpha(\mathbf{k})$, and the matrix elements connecting excited states to the ground state are

$$F_\sigma^{\mathbf{b},\alpha}(\mathbf{k}) \equiv F_\sigma / S_{uc} \int_{uc} d^2 r e^{-i(\mathbf{k}+\mathbf{b})\cdot\mathbf{r}} u_{\alpha,\mathbf{k}}(\mathbf{r}). \tag{4.7c}$$

The integration is within the lattice unit cell of area S_{uc}, and Bloch functions are normalized as

$$\int_{uc} d^2 r |u_{\alpha,\mathbf{k}}(\mathbf{r})|^2 = S_{uc}. \tag{4.7d}$$

For $\tilde{\Delta} = 0$, equations (4.7) are nothing but the expression (4.6) folded into the first Brillouin zone, as all the other couplings (4.7c) vanish.

For small $\tilde{\Delta}$ the relevant part of the spectrum can be described in the weak coupling approximation. Consider triangular lattice

$$\tilde{\Delta}(r) = -\tilde{\Delta} \sum_{l=1}^{6} \exp(i\mathbf{b}_l \cdot \mathbf{r}), \tag{4.8}$$

where the vectors b_l are shown on Fig. 4.2 a).

On symmetry grounds only A_1 state, invariant under the symmetry group (see Fig. 4.2 b), can contribute to the matrix elements (4.7c) and

$$F_\sigma^{0,A_1}(\mathbf{k}=0) = -\sqrt{6} F_\sigma \tilde{\Delta}/\Lambda, \quad \tilde{\xi}_{A_1}(0) = -2\tilde{\Delta}. \tag{4.9}$$

The linear in Δ shift of the lowest energy level $\tilde{\xi}_{A_1}$ is the signature of the triangular symmetry, $\mathcal{D}_6$; the shift makes this lattice the most energetically profitable in comparison with, *e.g.*, square one.

The main contribution to the energy differences because the symmetry broken and the symmetric states comes from the lowest energy part of the spectrum. For the calculation with logarithmic accuracy, the partial contribution $\mathcal{E}$ can be approximately written as $\mathcal{E} \approx d - \Lambda - 2\tilde{\Delta} + k^2/(2m)$. It yields

$$\left[\delta^{(n)} - \delta^{(0)}\right] E_{GS} = \frac{3\tilde{\Delta}^2 m}{\pi} \left[-\frac{|F_\sigma^2|}{\Lambda^2} Y(\tilde{d} - 2\tilde{\Delta}) + g \right], \tag{4.10}$$

where the detuning from the lowest excitatation energy is given by $\tilde{d} \equiv d - \Lambda$, and function Y is defined as

$$Y(X) = \ln\left[k_F^2/(mX)\right]. \tag{4.11}$$

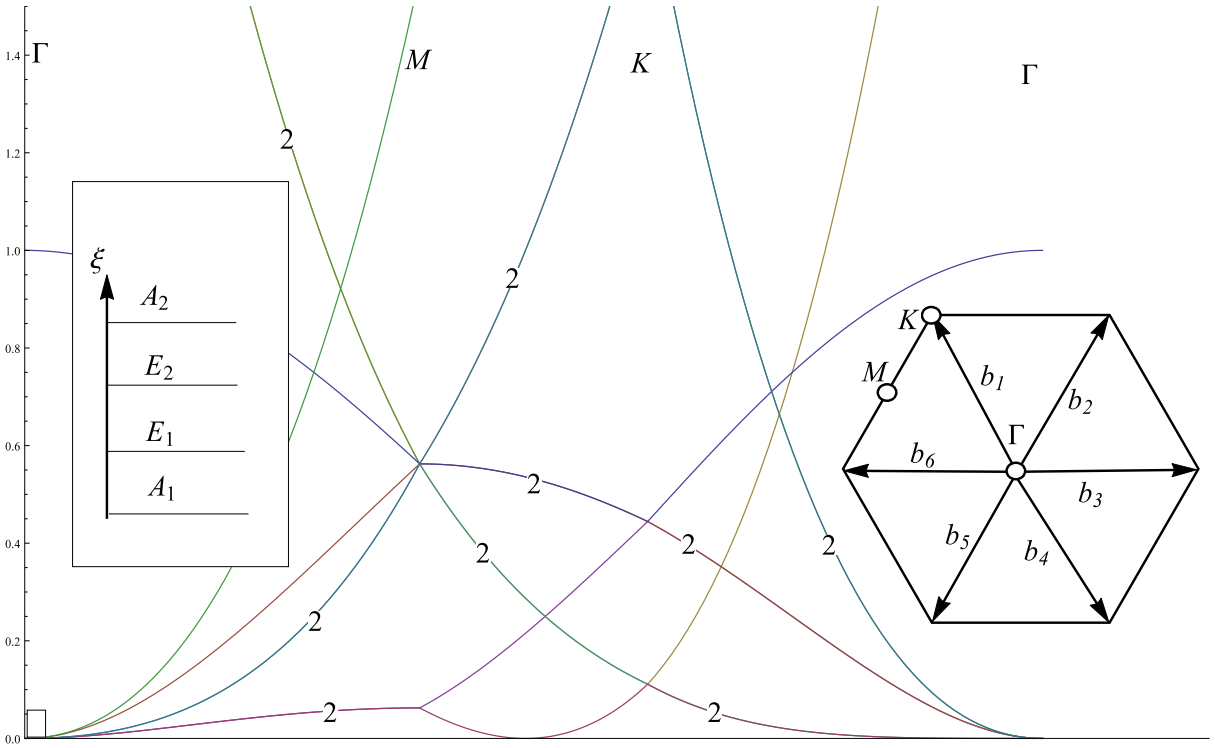

FIGURE 4.2: The weak coupling spectrum of the γ-fermions in the periodic potential. The zoom shows the band structure near Γ point. The labeling corresponds to the irreducible representations of the point symmetry group $\mathcal{D}_6$. Right inset: The basis vectors for the reciprocal lattice $\mathbf{b}_{1,\ldots,6}$ and the first Brillouin zone.

The last term is the compressibility contribution and the positive constant

$$g \equiv (\pi/m)\left(\partial^2 E_{GS}/\partial n^2\right)_{F=0}\left(\partial\Delta/\partial n\right)^{-2} \tag{4.12}$$

is of the order of unity.

The correction given in Eq. (4.10) is the main result for the ground state energy at the lowest order in $|F|^2$. It shows that the broken symmetry *supersolid* state is always energetically profitable for any finite F. However the potential is apparently pathological, as $Y(X)$ diverges as $X \to 0$. This infinite growth is an artifact of the lowest in F approximation, as the presence of the external field leads to level. This level repulsion cuts the logarithm, and we turn to study of such a repulsion.

For $|F_\sigma| \ll \lambda$ it is sufficient to take into account only the lowest states shown by bullets on the Fig. 4.2 b) and their interaction with the reference state without fermions. Then, the partial energy $\mathcal{E}$ from Eq. (4.7a), with account of Eq. (4.9), becomes the lowest eigenvalues of the three

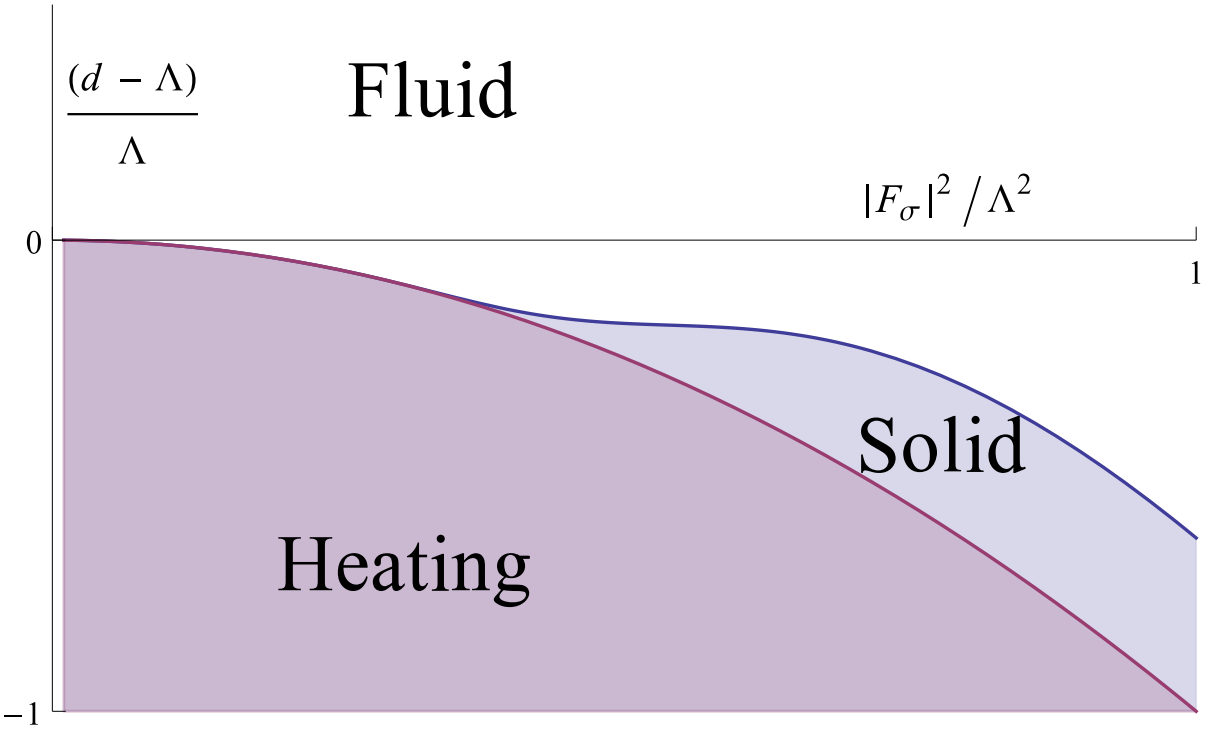

FIGURE 4.3: The proposed phase diagram as a function of the detuning d_c and the amplitude $|F|$ of the RF field. Note the line separating the two phases is a first order phase transition. Inset: the correction to the ground state energy as a function of the order parameter, shown for several values of compressibility.

state effective Hamiltonian

$$\hat{H}_{eff} \simeq \begin{pmatrix} d+\frac{k^2}{2m} & 0 & F_\sigma \\ 0 & d-\Lambda-2\tilde{\Delta}+\frac{k^2}{2m} & -\frac{\sqrt{6}F_\sigma\tilde{\Delta}}{\Lambda} \\ F_\sigma^* & -\frac{\sqrt{6}F_\sigma^*\tilde{\Delta}}{\Lambda} & 0 \end{pmatrix}. \tag{4.13}$$

Straightforward calculation leads to the replacement

$$Y(\tilde{d}-2\tilde{\Delta}) \to Y\left[\sqrt{\left(\tilde{d}(F_\sigma)-2\tilde{\Delta}\right)^2+\frac{6\tilde{\Delta}^2|F_\sigma|^2}{\Lambda^2}}\right] \tag{4.10′}$$

in Eq. (4.10), where $\tilde{d}(F_\sigma) \equiv d-\Lambda+|F_\sigma|^2/\Lambda$ has the meaning of the lowest energy of the two-fermionic excitations shifted by the RF field. The resulting form of the energy profile (4.10), (4.10′) is shown on Fig. 4.3. It shows two locally stable state characteristic of the *first order* phase transition. Direct inspection shows that the supersolid state becomes more energetically

profitable when $|\tilde{d}(F_\sigma)| \leq \tilde{d}_c(F_\sigma)$ where the critical detuning is given by

$$Y\left(\frac{\sqrt{3}\tilde{d}_c(F_\sigma)|F_\sigma|^2}{2\Lambda^2}\right) = \frac{\Lambda^2 g}{|F_\sigma|^2}, \tag{4.14}$$

The resulting phase diagram is shown on Fig. 3 b).

4.4 Conclusion

We have noted the BCS-BES crossover is necessarily followed by the reconstruction of topology of the spectrum of the fermionic excitations and the critical field can be rigorously defined as the point of such change. We suggested an experimental scheme which transmutes this reconstruction of the *excitation* spectrum into a changein the symmetry of the *ground state*. For this scenario the *supersolid* state is predicted to form.

The actual process by which the supersolid state forms is apparently quite complex. The process is an inherently non-equilibrium, zero temperature and first order phase transition. Each of these features alone bring interesting facets to the issue of the phase transition kinetics. Therefore this transition could be an interesting arena for testing theories of phase transition kinetics.

Bibliography

[1] E. McCann and V. I. Fal'ko, Phys. Rev. Lett. 96, 086805 (2006).

[2] K. S. Novoselov, E. McCann, S.V. Morozov, V.I. Falko, M.I. Katsnelson, U. Zeitler, D. Jiang, F. Schedin and A.K. Geim, Nature Phys. 2, 177 (2006).

[3] R. Nandkishore and L. Levitov, Phys. Rev. Lett., 104, 156803 (2010).

[4] J. Jung, F. Zhang and A. H. MacDonald, Phys. Rev. B 83, 115408 (2011).

[5] M. Kharitonov arXiv:1109.1553v1

[6] H. Min, G. Borghi, M. Polini, A. H. MacDonald, Phys Rev. B 77, 041407(R) (2008).

[7] F. Zhang, J. Jung, G.A. Fiete, Q. Niu, and A.H. MacDonald, Phys. Rev. Lett. 106, 156801 (2011).

[8] O. Vafek, Phys.Rev. B 82 205106 (2010).

[9] R. Nandkishore and L. Levitov, Phys. Rev. B 82, 115124 (2010).

[10] H. Dahal, T. Wehling, K. Bedell, J. Zhu, and A.V. Balatsky, Physica B. 405, 2241 (2010).

[11] F. Zhang, H. Min, M. Polini, A. H. MacDonald, Phys. Rev. B 81, 041402(R) (2010).

[12] L. Zhu, V. Aji, C. Varma arXiv:1202.0821.

[13] Y. Lemonik, I. Aleiner, C. Toke, and V. Fal'ko, Phys. Rev. B 82, 201408 (2010).

[14] O. Vafek and K. Yang, Phys. Rev. B 81, 041401(R) (2010).

[15] B. Feldman, J. Martin and A. Yacoby, Nature Physics 5, 889 (2009).

[16] R. T. Weitz, M.T. Allen, B.E. Feldman, J. Martin, and A. Yacoby, Science 330, 812 (2010).

[17] A.S. Mayorov, D.C. Elias, M. Mucha-Kruczynski, R.V. Gorbachev, T. Tudorovskiy, A. Zhukov, S.V. Morozov, M.I. Katsnelson, V.I. Fal'ko, A.K. Geim, and K.S. Novoselov, Science 333, 860 (2011).

[18] J. Velasco Jr., L. Jing, W. Bao, Y. Lee, P. Kratz, V. Aji, M. Bockrath, C.N. Lau, C. Varma, R. Stillwell, D. Smirnov, Fan Zhang, J. Jung, and A.H. MacDonald, arXiv:1108.1609.

[19] F. Freitag et al., Phys. Rev. Lett. 108, 076602 (2012)

[20] W. Bao et al., arXiv:1202.3212 (2012)

[21] A. Veligura et al., arXiv:1202.1753 (2012).

[22] T. Ohta, A. Bostwick, T. Seyller, K. Horn, and E. Rotenberg, Science 313, 5789 (2006).

[23] E. A. Henriksen, Z. Jiang, L.-C. Tung, M. E. Schwartz, M. Takita, Y.-J. Wang, P. Kim, and H. L. Stormer, Phys. Rev. Lett. 100, 087403 (2008).

[24] L. M. Zhang, Z. Q. Li, D. N. Basov, M. M. Fogler, Z. Hao, and M. C. Martin, Phys. Rev. B 78, 235408 (2008).

[25] Z. Q. Li, E. A. Henriksen, Z. Jiang, Z. Hao, M. C. Martin, P. Kim, H. L. Stormer, and D. N. Basov, Phys. Rev. Lett. 102, 037403 (2009).

[26] A. B. Kuzmenko, I. Crassee, D. van der Marel, P. Blake, and K. S. Novoselov, Phys. Rev. B 80, 165406 (2009).

[27] A. B. Kuzmenko, E. van Heumen, D. van der Marel, P. Lerch, P. Blake, K. S. Novoselov, and A. K. Geim, Phys. Rev. B 79, 115441 (2009).

[28] M. Mucha-Kruczynski, I. Aleiner, V. Falko, Phys. Rev. B 84, 041404 (2011).

[29] D.T. Son, Phys. Rev. B 75, 2355423 (2007).

[30] I. L. Aleiner, D. E. Kharzeev, and A. M. Tsvelik, Phys. Rev. B 76, 195415 (2007).

[31] J. E. Drut ad D. T. Son, Phys. Rev. B 77, 075115 (2008).

[32] D.M. Basko, Phys. Rev. B 78, 125418 (2008).

[33] Y. Lemonik and I. Aleiner (in preparation).

[34] For generic choices of the coupling constants these interactions reduce the symmetry of the model from the artificial $SU(4) \otimes U(1) \otimes U(1)$ down to $SU(2) \otimes U(1) \otimes U(1) \otimes \mathcal{D}_{3d}$ This is still larger than the original symmetry group as $\tau_z^{KK'}$ does not generate continuous

rotations in the original space group. The continuous $\tau_z^{KK'}$ rotation is broken by Umklapp terms down to Z_3. However, the lowest order Umklapp term is of the form $H_{umklapp} \sim (\psi^\dagger \tau_+^{KK'} \tau_z^{AB} \psi)^3 + h.c.$ Since this contains six fermion creation and annihilation operators it will be strongly RG irrelevant and we will not consider it.

[35] Equations (2.25) and (2.26) appeared in Ref. [13] with several typos. Furthermore, a misdefinition of ℓ led to incorrect statements on the critical temperature of nematic state. The errors have been corrected in the present paper.

[36] Coleman, S, *Aspects of Symmetry*, (Cambridge University Press 1985).

[37] In the body of this paper the case of BLG with $N = 1$ fermion flavors is discussed. This is not a case of physical interest. In an unpublished appendix to arXiv:0907.2448 they list RG equations for ten independent couplings. This contradicts the symmetry analysis of this paper which demonstrates there can be only nine independent couplings. Further, the set of interactions chosen violates SU(2) spin rotational invariance, a fact which is not noted. Note that only requiring invariance under spin rotations in the BLG plane requires 13 independent parameters, so this does not explain the claims of Ref. [11].

[38] Scherer, Uebelacker and Honerkamp, arXiv:1112.5038 (2011);

[39] MacDonald, Jung and Zhang, Phys. Scr. 014012, (2012)

[40] Y. Lemonik, I. Aleiner, and V. Falko (in preparation).

[41] C. L. Kane and E. J. Mele, Phys. Rev. Lett. 95, 226801 (2005).

[42] P. Dutta and P. M. Horn, Rev. Mod. Phys. **53**, 497 (1981).

[43] T. Grenet, Eur. Phys. J. B, **32**, 275 (2003).

[44] G. Martinez-Arizala, D. E. Grupp, C. Christiansen, A. M. Mack, N. Markovic, Y. Seguchi and A. M. Goldman, Phys. Rev. Lett., **78** 1130 (1997).

[45] T. Grenet and J. Delahaye, Phys. Rev. B **85**, 235114 (2012).

[46] Models where the scattering cross section does change with defect motion have also been considered, see J. Pelz and J. Clarke, Phys. Rev. B **36**, 4479 (1987). These are not believed to be relevant at low temperatures. We thank N. Birge for the reference.

[47] S. Feng, P. A. Lee, A. Stone, Phys. Rev. Lett. **56**, 1960 (1986); *ibid.* **56**, 2772 (E) (1986).

[48] Y. Imry, *Introduction to Mesoscopic Physics* (Oxford University Press, Oxford, 1997).

[49] B. Altshuler and B. Spivak, JETP Lett. **42**, 447 (1985). B. Altshuler and B. Spivak, Pis'ma Zh. Eksp. Teor. Fiz. **42**, No. 9, 363 (1985)].

[50] W. A. Phillips, Rep. Prog. Phys. **50**, 1657 (1987) .

[51] P.W. Anderson, B.I. Halperin and C.M. Varma, Philos. Mag. **25**, 1 (1972).

[52] J.L. Black, in *Glassy Metals 1*, edited by H.J. Gunterodt and H. Beck (Springer, Berlin, 1981).

[53] P. A. Lee, A. D. Stone and H. Fukuyama, Phys. Rev. B **35**, 1039 (1987).

[54] B. Altshuler, JETP Lett. **41**. 648 (1985). B. Altshuler, Pis'ma Zh. Eksp. Teor. Fiz. **41**, No. 12, 530 (1985)

[55] P. A. Lee and A. D. Stone, Phys. Rev. Lett. **55**, 1622 (1985).

[56] I.L. Aleiner and Y. M. Blanter, Phys. Rev. B. **65**, 115317 (2002).

[57] I. Aleiner, B. Altshuler and M. Gershenson, Waves in Random Media **9**, 201 (1999).

[58] B. Altshuler, A. Aronov and D. Khmelnitsky, Jour. Phys. C **15**,7367 (1982).

[59] J. Friedel, Phil. Mag. **43**, 153 (1952).

[60] A. M. Rudin, I. L. Aleiner, and L. I. Glazman, Phys. Rev. B **55**, 9322 (1997).

[61] G. Zala, B. N. Narozhny, and I. L. Aleiner, Phys. Rev. B **64**, 214204 (2001).

[62] V. I. Kozub and A. M. Rudin, Phys. Rev. B **55**, 259 (1997).

[63] B. Altshuler and A. Aronov, in *Electron-Electron Interactions in Disordered Systems*, edited by A. Efros and M. Pollack (North-Holland, Amsterdam, 1985).

[64] N. O. Birge, B. Golding and W. H. Haemmerle, Phys. Rev. B **42**, 2735 (1990).

[65] A. Trionfi, S. Lee and D. Natelson, Phys. Rev. B **70**, 041304(R) (2004); *ibid.* **72**, 035407 (2005).

[66] B.L. Altshuler, D. Khmel'nitzkii, A.I. Larkin and P.A. Lee, Phys. Rev. B **22**, 5142 (1980).

[67] S. Hikami, A. I. Larkin and Y. Nagaoka Prog. Theor. Phys. **63** 707 (1980).

[68] F. von Oppen and A. Stern, Phys. Rev. Lett. **79**, 1114 (1997).

[69] A L Burin, V. Kozub, Y. Gaplerin and V. Vinokur J. Phys.: Condens. Matter **20**, 244125 (2008)

[70] J. H. Davies, P. A. Lee and T. M. Rice, Phys. Rev. Lett. **49**, 758 (1982).

[71] M. Grunewald, B. Pohlmann, L. Schweitzer and D. Wurtz, Jour. Phys. C **15**, L1153 (1982).

[72] D. Thouless, P. Anderson and R. Palmer, Philos. Mag. **35**, 593 (1977).

[73] Y. Meroz, Y. Oreg and Y. Imry, Europhys. Lett. **105** 37010 (2014).

[74] E. Lebanon and M. Muller, Phys. Rev. B **72**, 174202 (2005).

[75] O. Cohen, Z. Ovadyahu, and M. Rokni, Phys. Rev. Lett., **69**, 3555 (1992).

[76] D. McCammon *et al* Phys. Stat. Sol. (b) **230**, 197 (2002).

[77] M. Ben-Chorin, D. Kowal and Z. Ovadyahu, Phys. Rev. B **44**, 3420 (1991).

[78] M. Ben-Chorin, Z. Ovadyahu and M. Pollak, Phys. Rev. B, **48**, 15025 (1993).

[79] T. Grenet and J. Delahaye, The European Physical Journal B **76**, 229 (2010).

[80] T. Grenet, J. Delahaye, M. Sabra and F. Gay, The European Physical B **56**, 183 (2007).

[81] J. Delahayea, T. Grenet and F. Gay, Eur. Phys. J. B **65**, 5 (2008).

[82] A. Vaknin, Z. Ovadyahu, and M. Pollak, Phys. Rev. B **65**, 134208 (2002).

[83] Z. Ovadyahu, Phys. Rev. B **88**, 085106 (2013).

[84] J. Korringa, Physica **16**, 601 (1950).

[85] F. Dalfovo, S. Giorgini, L. P. Pitaevskii, and S. Stringari, Rev. Mod. Phys. 71, 463 (1999)

[86] J. Bardeen, L. N. Cooper, and J. R. Schriefer, Phys. Rev. 108, 1175 (1957).

[87] I. Bloch, J. Dalibard, and W. Zwerger, Rev. Mod. Phys. 80, 885 (2008).

[88] C. Chin, R. Grimm, P. Julienne, and E. Tiesinga, Rev. Mod. Phys. 82, 1225 (2010).

[89] G. Bertaina and S. Giorgini, Phys. Rev. Lett. 106, 110403 (2011).

[90] Q. Chen, J. Stajic, S. Tan, and K. Levin, Physics Reports 412, 1 (2005).

[91] M. Holland, S. Kokkelmans, M. L. Chiofalo and R. Walser, Phys. Rev. Lett. 87, 120406 (2001)

[92] M. W. Zwierlein, C. A. Stan, C. H. Schunck, S. Raupach, S. Gupta, Z. Hadzibabic and W. Ketterle, Phys. Rev. Lett. 91, 250401 (2003)

Appendix A

Group theory of BLG

In this appendix we classify the possible phases of BLG. We will use the matrix notation defined in Sec. 2.2.

Phases are defined by all possible expectations $\Delta \equiv \langle \Psi \otimes \Psi^\dagger \rangle$ that belong to an irreducible representations (irrep) of the symmetry group $\mathcal{G}$ of BLG. Every phase defines a subgroup $\mathcal{H}$ of $\mathcal{G}$ consisting of all operations that leave Δ invariant. Two phases within an irrep are distinct if their invariant subgroups are not conjugate. (Recall two subgroups $\mathcal{H}$ and $\mathcal{H}'$ of a group $\mathcal{G}$ are conjugate if they is an element of $g \in \mathcal{G}$ such that $g\mathcal{H}g^{-1} = \mathcal{H}'$). This definition is correct is in the sense that it gives all physically distinct states that may be reached via a second order phase transition at the highest critical temperature, per the usual Landau theory.

Let us notice, however, that the anomalous averages belonging to the same irrep of the original group $\mathcal{G}$ may correspond to the different phases. For example, $\Delta_I = \tau_y^{AB}\tau_y^{KK'}$ and $\Delta_{II} = \tau_x^{AB}\tau_x^{KK'} + \tau_y^{AB}\tau_y^{KK'}$ are both charge density waves with a tripled unit cell transforming in the G representation. However, these two phases are distinct since Δ_{II} is invariant under rotations by $2\pi/3$ around a lattice site, whereas Δ_I is not invariant under any conjugate operation, see Fig. A.1. As a further example, a canted anti-ferromagnetic phase would be given by $\Delta = \tau_x^{AB}\tau_z^{KK'}\sigma_x + \sigma_z$. This is not considered in the present classification since it does not belong to an irrep of $\mathcal{G}$ (it is a linear combination elements of the B_2 and A_1 representations). Of course all such mixed states may be constructed from linear combinations of phases in our classification.

We classify the phases according to the symmetry group $\mathcal{G}$ of BLG which is effective at intermediate energies, see Sec. 2.2. In this regime the effect of RG irrelevant perturbations such as Umklapp scattering may be ignored, and RG relevant but weak perturbations, such as trigonal warping and spin-orbit coupling, may be neglected. This approximation should be effective at

energies between $\gamma_1/2 = 0.2eV$ and $\mathcal{E}_{LiTr} = 1meV$, which contains any energy scale associated with spontaneous symmetry breaking. In this regime the symmetry group is

$$\mathcal{G} = \mathcal{D}_{\text{inf}}^{(rot)} \times \mathcal{D}_{\text{inf}}^{(tran)} \times SU(2)^{(spin)} \times U(1)^{(gauge)}) \times T. \tag{A.1}$$

The first subgroup, $\mathcal{D}_{\text{inf}}^{(rot)}$, is generated by infinitesimal spatial rotations C and inversion R_C of the BLG plane. The second subgroup, $\mathcal{D}_{\text{inf}}^{(tran)}$, is generated by an infinitesimal translation t and reflection R_t. The action of these operators on the low-energy electrons is given in terms of the Pauli matrices:

$$\begin{aligned} C \equiv& i\tau_z^{AB} \\ t \equiv& i\tau_z^{KK'} \\ R_C \equiv& \tau_x^{AB}\tau_z^{KK'} \\ R_t \equiv& \tau_z^{AB}\tau_x^{KK'} \\ R_t \cdot R_v =& \tau_y^{AB}\tau_y^{KK'} \end{aligned} \tag{A.2}$$

Note that these two groups commute with each other, unlike true translation and reflection. In the presence of the appropriate symmetry breaking these are reduced down to the $D_{3d''}$ group discussed in the text. In this case the continuous translations and rotations $\exp(\theta_t t + \theta_c C)$ become discrete with $\theta_{t,c} = 0, \pm 2\pi/3$ and the inversions R_t and R_C become $R_h \cdot R_v$ and R_v of Sec. 2.2 respectively.

The $SU(2)^{(spin)}$ is the group of spin rotations, which is decoupled from the physical rotations because there are no spin-orbit interactions. It is generated by rotations $\vec{S} = (S_x, S_y, S_z)$. The high symmetry axis of any phase will always chosen to be z. Infinitesimal rotations around the z axis are represented by S_z. There are also reflections and inversion of the spin space, but these do not distinguish any phases, so we will suppress them.

The gauge groups acts by multiplication. We label the infinitesimal generator g, which acts on the wavefunctions ψ simply by $g\psi = i\psi$.

The time reversal operator T commutes with all of the above except the gauge generator $TgT = -g$. It is given in terms of Pauli matrices by

$$T \equiv i\sigma_y\tau_y^{KK'}\tau_y^{AB}K, \tag{A.3}$$

where K is complex conjugation.

This defines the symmetry group $\mathcal{G}$ fully. A further enlarged symmetry group isomorphic to $U(1) \times U(4)$ is considered at points in the body of the text [see Eq. (2.9)] and other works, but

there is no reason to expect that this will ever be an accurate approximation. We will proceed to categorize the phases according to the symmetry group $\mathcal{G}$. One may always collapse classification to obtain the distinct phases under the artificially enlarged symmetry groups.

In the following subsections we present the tables enumerating the possible symmetry breaking for the singlet, triplet, and superconducting phases each. Each table is split into subsections corresponding to the IrReps of $\mathcal{D}_{3d''}$. These are listed in the first column. At the beginning of each subsection the second column gives the order parameter (OP) for the IrRep in terms of the notation $\hat{\Delta} \equiv \Delta_{abc}\tau_a^{AB}\tau_b^{KK'}\sigma_c$ and arranges these into a vector. Next to this are the generators of symmetries under which the order parameter is invariant (generators and Δ commute). This completely characterizes one dimensional represntations.

In the case of the multi-component representations, particular values of the order parameter may have higher symmetries than the generic values - these are the distinct phases. The values of the order parameter that produce the phase are given according to the vector representation in the second column. Next to these in the third column are the additional residual symmetries under which the phase is invariant, and the phase is labeled with the additional subscript.

For example, let us take in section G in the first table. The second column of first line defines a vector for the representation. The third column states that all vectors in that representation are invariant under the time T time reversal operation. The next line says that when the vector is proportional to $(1,0,0,1)$, i.e. $\Delta \propto \tau_x^{AB}\tau_x^{KK'} + \tau_y^{AB}\tau_y^{KK'}$, the symmetry is higher. The higher symmetries are in the third column; in particular, this vector is invariant under the combined $C+t$ rotation and the $R_C \cdot R_t$ reflection in addition to the T rotation. The next line of the table says that when the vector takes the value $(0,0,0,1)$ the state is invariant under the reflections R_t, R_C. Note that each phase is generally defined by a coset of values of the order parameter, which are all invariant under conjugate groups. We only list one representative from each coset. For example, in the case of G, the $(1,0,0,1)$ vector is part of the coset of vectors $(\cos\theta, \sin\theta, -\sin\theta, \pm\cos\theta)$, $\theta \in [0, 2\pi]$. These are all invariant under subgroups conjugate to the one listed in the third column.

We use α, β as arbitrary real parameters when there is a continuous manifold of cosets. When listed under symmetries the symbols t, C, g and S_z mean the phase is invariant under the entire $U(1)$ group generated. The symbol $\vec{S}$ means the phase is invariant under all spin rotations. There are several symmetry operations involving rotations by π or $\pi/2$ in one the $U(1)$ groups. Like the spin reflections, these do not distinguish any of the phases so we do not list them. Five of the phases belonging to the G representation are illustrated in Fig. A.1. Notice that,

according to the Landau theory, the transition to the G -type phase can not occur directly but rather through the pattern with incommensurate periodicity.

A.0.1 Normal Phases

The normal phases are by definition invariant under spin and gauge transformation so we will suppress them. A product of Pauli matrices acting in different sub-spaces should be understood as a direct product.

Irr.	OP	M^α	Symmetry
A_2	Δ_{0z0}	$\tau_z^{AB}\hat{1}^{KK'}\hat{1}^N\hat{1}^s$	C, t, R_C
B_1	Δ_{z00}	$\hat{1}^{AB}\tau_z^{KK'}\hat{1}^N\hat{1}^s$	C, t, R_t
B_2	Δ_{zz0}	$\tau_z^{AB}\tau_z^{KK'}\tau_z^N\hat{1}^s$	$C, t, R_C \cdot R_t, T$
E_2	$(\Delta_{xz0}, \Delta_{yz0})$	$\tau_{x,y}^{AB}\tau_z^{KK'}\tau_z^N\hat{1}^s$	t, R_C, R_t, T
E_2''	$(\Delta_{zx0}, \Delta_{zx0})$	$\tau_z^{AB}\tau_{x,y}^{KK'}\tau_z^N\hat{1}^s$	C, R_C, R_t, T
E_1	$(\Delta_{x00}, \Delta_{y00})$	$\tau_{x,y}^{AB}\hat{1}_z^{KK'}\hat{1}^N\hat{1}^s$	$t, R_C, R_t \cdot T$
E_1''	$(\Delta_{0x0}, \Delta_{0y0})$	$\hat{1}^{AB}\tau_{x,y}^{KK'}\hat{1}^N\hat{1}^s$	$C, R_C, R_t \cdot T$
G	$(\Delta_{xx0}, \Delta_{xy0}, \Delta_{yx0}, \Delta_{yy0})$	$\tau_{x,y}^{AB}\tau_{x,y}^{KK'}\tau_z^N\hat{1}^s$	T
G_1	$(1, 0, 0, 1)$		$C{+}t, R_C \cdot R_t$
G_2	$(0, 0, 0, 1)$		R_t, R_C

TABLE A.1: Classification of the order parameters corresponding to distinct normal phases of BLG according to the underlying symmetry group. The structure of the table is described in the text of the appendix.

A.0.2 Magnetic phases

We restore the spin symmetries but continue to suppress the gauge symmetry. The high symmetry axis is arbitrarily chosen to be the z direction.

Irr.	OP	M^α	Symmetry
A_1	$(\Delta_{00x}, \Delta_{00y}, \Delta_{00z})$	$\hat{1}^{AB}\hat{1}^{KK'}\hat{1}_z^N\sigma_{x,y,z}$	C, t, S_z, R_t, R_C
A_2	$(\Delta_{0zx}, \Delta_{0zy}, \Delta_{0zz})$	$\hat{1}^{AB}\tau_z^{KK'}\tau_z^N\sigma_{x,y,z}$	C, t, S_z, R_C, T
B_1	$(\Delta_{z0x}, \Delta_{z0y}, \Delta_{z0z})$	$\tau_z^{AB}\hat{1}^{KK'}\tau_z^N\sigma_{x,y,z}$	C, t, S_z, R_t, T

B_2	$(\Delta_{zzx}, \Delta_{zzy}, \Delta_{zzz})$	$\tau_z^{AB}\tau_z^{KK'}\hat{1}^N\sigma_{x,y,z}$	$C, t, S_z,$ $R_C \cdot T, R_t \cdot T$
E_2	$(\Delta_{xzx}, \Delta_{xzy}, \Delta_{xzz};$ $\Delta_{yzx}, \Delta_{yzy}, \Delta_{yzz})$	$\tau_{x,y}^{AB}\tau_z^{KK'}\hat{1}^N\sigma_{x,y,z}$	t, R_C, R_t
$E_{2,1}$	$(0,0,1;0,0,0)$		S_z
$E_{2,2}$	$(1,0,0;0,1,0)$		$S_z + C$
E_2''	$(\Delta_{zxx}, \Delta_{zxy}, \Delta_{zxz};$ $\Delta_{zyx}, \Delta_{zyy}, \Delta_{zyz})$	$\tau_z^{AB}\tau_{x,y}^{KK'}\hat{1}^N\sigma_{x,y,z}$	C, R_C, R_t
$E_{2,1}''$	$(0,0,1;0,0,0)$		S_z
$E_{2,2}''$	$(1,0,0;0,1,0)$		$S_z + t$
E_1	$(\Delta_{x0x}, \Delta_{x0y}, \Delta_{x0z};$ $\Delta_{y0x}, \Delta_{y0y}, \Delta_{y0z})$	$\tau_{x,y}^{AB}\hat{1}^{KK'}\tau_z^N\sigma_{x,y,z}$	t, R_t, T
$E_{1,1}$	$(0,0,1;0,0,0)$		S_z
$E_{1,2}$	$(1,0,0;0,1,0)$		$S_z + C$
E_1''	$(\Delta_{0xx}, \Delta_{0xy}, \Delta_{0xz};$ $\Delta_{0yx}, \Delta_{0yy}, \Delta_{0yz})$	$\hat{1}^{AB}\tau_{x,y}^{KK'}\tau_z^N\sigma_{x,y,z}$	C, R_C, T
$E_{1,1}''$	$(0,0,1;0,0,0)$		S_z
$E_{1,2}''$	$(1,0,0;0,1,0)$		$S_z + t$
G	$(\Delta_{xxx}, \Delta_{xxy}, \Delta_{xxz};$ $\Delta_{xyx}, \Delta_{xyy}, \Delta_{xyz};$ $\Delta_{yxx}, \Delta_{yxy}, \Delta_{yxz};$ $\Delta_{yyx}, \Delta_{yyy}, \Delta_{yyz})$	$\tau_{x,y}^{AB}\tau_{x,y}^{KK'}\hat{1}^N\sigma_{x,y,z}$	None
G_1	$(0,0,1;0,0,0;$ $0,0,0;0,0,1)$		$S_z, C+t, R_C \cdot R_t$
G_2	$(0,0,0;0,0,0;$ $0,0,0;0,0,1)$		S_z, R_C, R_t
G_3	$(0,0,0;1,0,0;$ $0,0,0;0,1,0)$		$S_z + t, R_C$
G_4	$(0,0,0;0,0,0;$ $1,0,0;0,1,0)$		$S_z + C, R_t$
G_5	$(1,0,0;0,1,0;$ $0,-1,0;1,0,0)$		$S_z + C, S_z + t$

TABLE A.2: Classification of the order parameters corresponding to distinct magnetic phases of BLG according to the underlying symmetry group. The structure of the table is described in the text of the appendix.

A.0.3 Superconducting Phases

The order parameter M is defined by the non-zero expectation values $\langle\psi^\dagger M T\psi^\dagger\rangle$. This M is listed under OP. M must contain an even number of Pauli matrices because of fermion anticommutivity but may take complex values.

Irr.	OP	M^α	Symmetry
A_1	Δ_{000}	$\hat{1}^{AB}\hat{1}^{KK'}\tau^N_{x,y}\hat{1}^s$	$\vec{S}, C, t, R_C,$ R_t, T
A_2	$(\Delta_{0zx}, \Delta_{0zy}, \Delta_{0zz})$	$\hat{1}^{AB}\tau^{KK'}_z\tau^N_{x,y}\sigma_{x,y,z}$	C, t, R_C
$A_{2,1}$	$(0,0,1)$		S_z, T
$A_{2,2}$	$(1,i,0)$		$S_z + g$
B_1	$(\Delta_{z0x}, \Delta_{z0y}, \Delta_{z0z})$	$\tau^{AB}_z\hat{1}^{KK'}\tau^N_{x,y}\sigma_{x,y,z}$	C, t, R_t
$B_{1,1}$	$(0,0,1)$		S_z, T
$B_{1,2}$	$(1,i,0)$		$S_z + g$
B_2	Δ_{zz0}	$\tau^{AB}_z\tau^{KK'}_z\tau^N_{x,y}\hat{1}^s$	$\vec{S}, C, t,$ $R_C \cdot R_t, T$
E_2	$(\Delta_{xz0}, \Delta_{yz0})$	$\tau^{AB}_{x,y}\tau^{KK'}_z\tau^N_{x,y}\hat{1}^s$	$\vec{S}, t, R_C, R_t$
$E_{2,1}$	$(1,0)$		T
$E_{2,2}$	$(1,i)$		$C + g$
E''_2	$(\Delta_{zx0}, \Delta_{zy0})$	$\tau^{AB}_z\tau^{KK'}_{x,y}\tau^N_{x,y}\hat{1}^s$	$\vec{S}, C, R_C, R_t$
$E''_{2,1}$	$(1,0)$		T
$E''_{2,2}$	$(1,i)$		$t + g$
E_1	$(\Delta_{x0x}, \Delta_{x0y}, \Delta_{x0z};$ $\Delta_{y0x}, \Delta_{y0y}, \Delta_{y0z})$	$\tau^{AB}_{x,y}\hat{1}^{KK'}\tau^N_{x,y}\sigma_{x,y,z}$	t
$E_{1,1}$	$(0,0,1;0,0,0)$		S_z, R_C, T
$E_{1,2}$	$(1,i,0;0,0,0)$		$S + g, R_C$

$E_{1,3}$	$(0,0,1;0,0,i)$		$S_z, C+g, R_C \cdot T$
$E_{1,4}$	$(\alpha, i\alpha, i\beta; i\alpha, -\alpha, \beta)$		$C+S+2g$
$E_{1,5}$	$(1,i,0;i,-1,0)$		$C+g, S+g$
E_1''	$(\Delta_{0xx}, \Delta_{0xy}, \Delta_{0xz}; \Delta_{0yx}, \Delta_{0yy}, \Delta_{0yz})$	$\hat{1}^{AB}\tau_{x,y}^{KK'}\tau_{x,y}^{N}\sigma_{x,y,z}$	C
$E_{1,1}''$	$(0,0,1;0,0,0)$		S_z, R_t, T
$E_{1,2}''$	$(1,i,0;0,0,0)$		$S+g, R_t$
$E_{1,3}''$	$(0,0,1;0,0,i)$		$S_z, t+g, R_C \cdot T$
$E_{1,4}''$	$(\alpha, i\alpha, i\beta; i\alpha, -\alpha, \beta)$		$t+S+2g$
$E_{1,5}''$	$(1,i,0;i,-1,0)$		$t+g, S+g$
G	$(\Delta_{xx0}, \Delta_{xy0}, \Delta_{yx0}, \Delta_{yy0})$	$\tau_{x,y}^{AB}\tau_{x,y}^{KK'}\tau_{x,y}^{N}\hat{1}^{s}$	$None$
G_1	$(1,0,0,1)$		$C+t, R_C \cdot R_t, T$
G_2	$(0,0,0,1)$		R_C, R_t, T
G_3	$(0,0,-i,1)$		$C+g, R_C, R_t \cdot T$
G_4	$(0,-i,0,1)$		$t+g, R_t, R_C \cdot T$
G_5	$(1,i,i,-1)$		$C+g, t+g, R_C \cdot R_t \cdot T$

TABLE A.3: Classification of the order parameters corresponding to distinct superconducting phases of BLG according to the underlying symmetry group. The structure of the table is described in the text of the appendix.

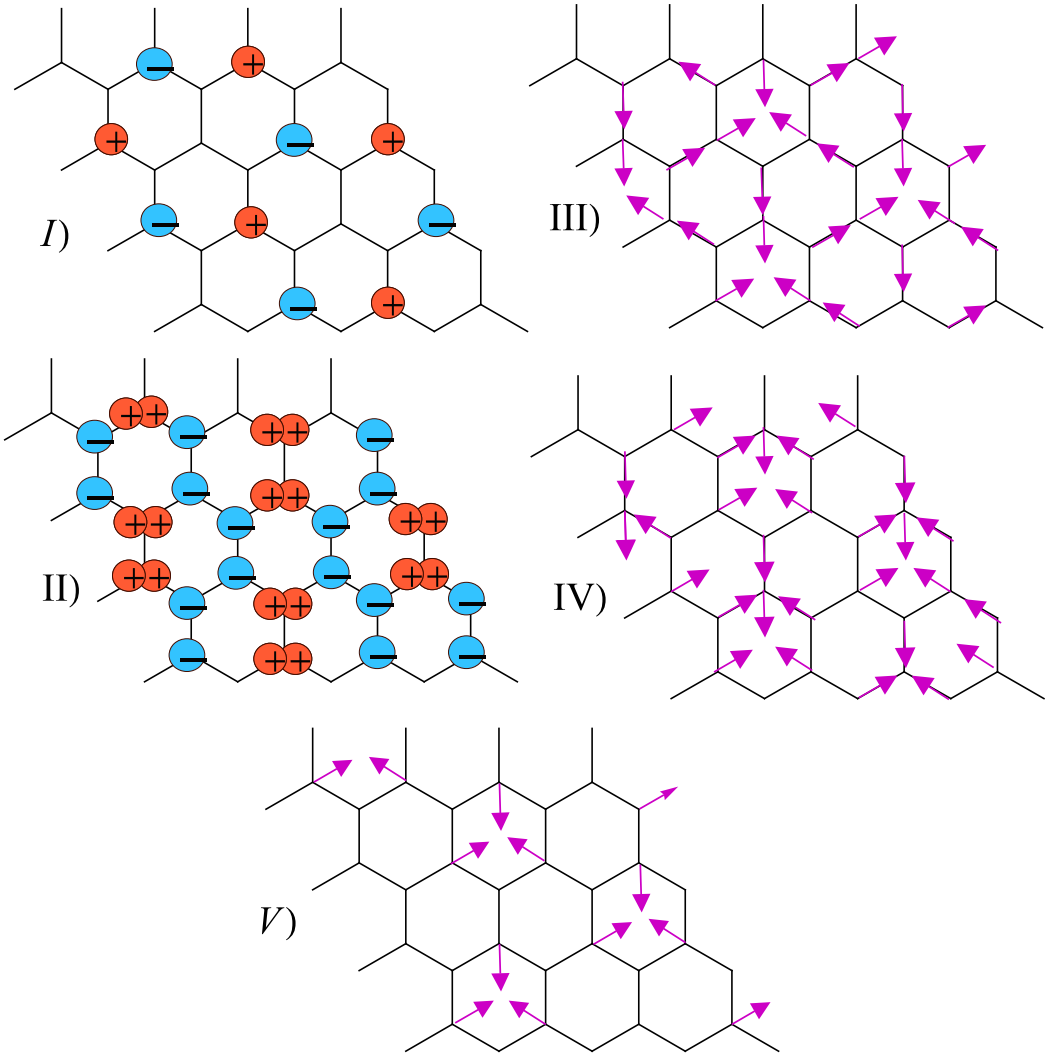

FIGURE A.1: Sketch of the symmetric magnetic and normal phases transforming according the G representation. (I) G_1 normal state; (II) G_2 normal state; (III) G_3 spin state; (IV) G_4 spin state; (V) G_5 spin state. Because of the absence of spin-orbit coupling the overall direction of the spins is arbitrary.

Appendix B

A model for two-level systems

In this section we give a model for the two level systems. In a disordered system one expects to find a large number of mobile impurities. The mobile impurity may be treated as a massive particle which sees a potential $V(r)$ depending on the static impurities and defects in the lattice, as renormalized by electron-phonon excitations. We are interested in the case where $V(r)$ is generally larger than all relevant energy scales, except for localized valleys located an average r_m apart. If r_m is large compared to the time scales of our measurement, in a sense to be made precise below, then we expect most of the "mobile" impurities to not have moved from their valley. These are indistinguishable from static impurities. However, since the valleys are randomly located we expect to find situations when one impurity sits in a valley, with an unoccupied valley a distance $r \ll r_m$ away. These are the "close pairs", which are effectively two state systems. We may write down the Hamiltonian for the TLS,

$$H_{TLS} = \tilde{\Delta}\sigma_z + \mathcal{I}\sigma_x, \tag{B.1}$$

where $\sigma_{x,y,z}$ are the usual Pauli matrices, and the "up" states has the impurity localized in one valley, and the "down" state is the opposite. The level splitting energy $\tilde{\Delta}$ is the difference in the binding energies of the two sites, and $\mathcal{I}$ is the overlap integral. We take $\mathcal{I} = \Lambda_0 e^{-\frac{r}{a}}$ where Λ_0 is some coupling energy.

As Δ and r are properties of the impurities, we take them to be random variables. Since we are looking for exponentially small terms we may take the random variables to be uniformly distributed without incuring significant error. We take them to be distributed in the region $\Delta \in [0, \Delta_m]$, $r \in [0, \ell_{imp}]$. Note we only consider close pairs where $r < \ell_{imp}$ and take this as the upper cutoff on the model. This is taken for convenience so that we may treat all impurities

as point scatterers. As longer distances correspond to exponentially longer timescales, there is a well defined regime in which we are insensitive to the details of the cutoff. Since we are only interested in the exponential dependence on r it is sufficient to our accuracy to set $r = \ell_{imp}$ everywhere except in the dependence of $\mathcal{I}$, and we do so in the remainder of this section.

The close pairs interact with the electrons by altering the local potential. Since this depends on which site the electron occupies, the impurity state and the electronic fluid become coupled. This corresponds to a term in the Hamiltonian

$$H_{TLS-el} = \frac{\gamma}{2\nu}\left((1+\sigma_z)\psi_1^\dagger\psi_1 + (1-\sigma_z)\psi_2^\dagger\psi_2\right). \tag{B.2}$$

Here γ is the dimensionless interaction strength, $\psi_{1,2}$ is the operator the annihilates a conduction electron at the position $r_{1,2}$, and $r_{1,2}$ are random positions located a distance r apart. We now calculate the time evolution of the density matrix of the close pair, averaging over the metallic system. This is done most clearly by rotating the sigma matrices so that H_{TLS} is proportional to σ_z. Working to lowest order in $\mathcal{I}$ this gives:

$$H_{TLS} = \tilde{\Delta}\tilde{\sigma}_z, \tag{B.3}$$

and,

$$H_{TLS-el} = \left(\tilde{\sigma}_z + \frac{\mathcal{I}}{\tilde{\Delta}}\tilde{\sigma}_x\right)\frac{\gamma}{\nu}\left[\psi_1^\dagger\psi_1 - \psi_2^\dagger\psi_2\right]. \tag{B.4}$$

(plus a sigma independent term). Viewing the electronic fluctuations as a random magnetic field, we see that there is a decohering field and a depolarizing field, where the depolarizing field is smaller by the factor $\mathcal{I}/\tilde{\Delta}$ - exponentially smaller. Working to second order in the electronic fluctuations we obtain the evolution equation for the density matrix, $\hat{\rho}$. If we parameterize the density matrix by,

$$\hat{\rho} = \frac{1}{2} + \vec{a}\cdot\vec{\sigma}, \tag{B.5}$$

we may give the time evolution by,

$$\frac{\partial\vec{a}}{\partial t} = \Delta\hat{z}\times\vec{a} - \frac{1}{T_2}\vec{a} - \hat{z}\frac{1}{T_1}\left(1-\tanh(\beta\Delta)\right), \tag{B.6}$$

where the energy Δ is the renormalized level splitting. This depends implicitly on the chemical potential, since the compressibilities at r_1 and r_2 are not equal because of the mesoscopic fluctuations. The decoherence times T_1 and T_2 are given by,

$$T_1^{-1} = \frac{\gamma^2\mathcal{I}^2}{\Delta^2}\frac{\Delta}{1-\exp(-\Delta/T)}f(\Delta), \tag{B.7}$$

$$T_2^{-1} = \gamma^2 T f(0), \tag{B.8}$$

where the function $f(\epsilon)$ is ν^{-2} times the local density-density correlator evaluated at frequency ϵ. This is a function of order unity, with subexponential dependence on r. We will therefore treat it as a constant absorbed into γ. The dependence on temperature comes from the phase space restricitons on emiting an electron-hole pair, analogous to Korringa[84] relaxation.

The behavior of interest happens at time scales much larger then T_2, and so the system is effectively classical. Then Eq. (B.6) reduces to a master equation for the diagonal elements of the density matrix $f_\uparrow = (1+a_z)/2$ and $f_\downarrow = (1-a_z)/2$. The properties of the system will depend on the linear respose functions. Recalling tht the Keldysh function is the autcorrelation and the retarded function is the linear response to change in Δ, we obtain

$$F^K(t) - F^K(0) = \left(\frac{\gamma}{\cosh(\frac{\Delta}{T})}\right)^2 (1 - \exp(-|t|/T_1)), \tag{B.9}$$

and

$$F^R(t) = \left(\frac{\gamma}{\cosh(\frac{\Delta}{T})}\right)^2 \frac{1}{T_1 T} \exp(-t/T_1)\Theta(t). \tag{B.10}$$

Again, some smoothly varying function of r has been absorbed into the various constants. Equation (B.10) is in accordance with the classical fluctuation dissipation theorem.

We will need the ensemble average of the F, which we call $\bar{F} = \ll F \gg$. Let us take the ensemble average over r first, since that contains all of the relevant behavior. For the Keldysh component,

$$\begin{aligned} \bar{F}^K(t;\Delta) - \bar{F}^K(0;\Delta) \equiv & \left(\frac{\gamma}{\nu \cosh(\frac{\Delta}{T})}\right)^2 \\ & \times \frac{1}{\ell_{imp}} \int_0^{\ell_{imp}} dr\, 1 - \exp\left[t/t_0 \exp(-2r/a)\right], \end{aligned} \tag{B.11}$$

where t_0 is a short time scale that depends on T and Δ from the defintion of T_1 in Eq. (B.7). This scale t_0 functions as the small time cutoff for the calculations. Changing variables to

$\lambda = \exp(-2r/a)$ we obtain,

$$\begin{aligned}
\frac{1}{\ell_{imp}} \int_a^{\ell_{imp}} dr \, \{1 - \exp\left[/t_0 \exp(-2r/a)\right]\} \\
&= \frac{a}{2\ell_{imp}} \int_{e^{-\frac{2\ell_{imp}}{a}}}^{1} d\lambda \frac{1 - e^{-\lambda t/t_0}}{\lambda} \\
&= \frac{1}{|\log t_m/t_0|} \int_{t_0/t_m}^{1} d\lambda \frac{1 - e^{-\lambda t/t_0}}{\lambda} \\
&\approx \frac{1}{|\log t_m/t_0|} \int_0^1 d\lambda \frac{1 - e^{-\lambda t/t_0}}{\lambda} \\
&\approx \frac{\log t/t_0}{\log t_m/t_0},
\end{aligned} \tag{B.12}$$

where $t_m \equiv t_0 \exp(2\ell_{imp}/a)$. The manipulations are valid for times between t_0 and t_m, which are exponentially seperated. The correlator has a "scale-free" dependence on t, which will produce long time correlations. The average of Δ only smears out the $\log t_m/t_0$ which is insignificant in our regime. The final result is therefore:

$$\bar{F}^K(t) - \bar{F}^K(0) = \frac{\log\left(t/t_0\right)}{\log(t_m/t_0)}, \tag{B.13}$$

where we have defined the average scattering time depending on the density of close pairs ρ^*,

$$\frac{1}{\tau^*} \equiv \frac{\gamma^2 \rho^*}{\nu} \frac{T}{\Delta_m} \tanh(\Delta_m/T). \tag{B.14}$$

The average of $F^R(t)$ can be found simply by taking a time derivative of $\bar{F}^K$

$$\bar{F}^R(t) = \frac{1}{Tt \log(t_m/t_0)}. \tag{B.15}$$

The time τ^* depends linearly on T when $T \ll \Delta_m$. This follows from the fact that only impurities with gaps of order T will be thermally activiated with any probability. This produces the Korringa-like result that $T\tau_*$ is approximately constant at low temperature.

Appendix C

Experimental protocol and energy scales for memory effect

In this appendix we briefly discuss some issuesr elating to the experimental measurement of the memory effect. First we outline a procedure for detecting the proposed memory effect, in the case of a weak effect in a two dimensional system. Second, we discuss how to relate the measure quantities to the underlying energy scales. We will ignore logarithmic factors throughout this appendix.

Take a mesoscopic sample of a material with pronounced $1/f$ noise. Measure the scale of the universal conductance fluctuations (UCF), S_{UCF}, with magnetic field or gate voltage,

$$S_{UCF} = \langle \left(\frac{\delta I}{I} \right)^2 \rangle. \tag{C.1}$$

Measure as well the normalized $1/f$ noise, $S_{1/f}$.

$$S_{1/f}(\omega) = \frac{1}{I^2} \int dt e^{i\omega(t-t'))} \delta I(t) \delta I(t'). \tag{C.2}$$

The strength of the $1/f$ spectrum defines a dimensionless parameter α

$$S_{1/f}(\omega) \sim \alpha |\omega|^{-1}. \tag{C.3}$$

The ratio of α and the UCF gives the small parameter of our theory,

$$\beta = \alpha / S_{UCF}. \tag{C.4}$$

The parameter β is approximately the parameter $\left(\frac{1}{T\tau_*}\right)$ that defines the strength of both $1/f$ noise (Eq. 2.18) and the memory effect (Eq. 2.26).

The memory effect would be obscured by the $1/f$ noise in a mesoscopic sample. To get around this, we use the fact that the predicted memory does not depend on system size, while the $1/f$ noise decreases like $1/L^2$. So using a large sample of the same material, one could measure the memory dip without the $1/f$ noise. The predicted depth of the peak in the conductance δG is

$$\delta G/G \sim \beta \left(e^2 R_\square/\hbar\right), \tag{C.5}$$

where G is the conductance and $R_\square$ is the sheet resistance of the sample.

There is no upper limit on the size of the sample used to detect the memory dip from the perspective of our mechanism, so the $1/f$ noise may be reduced to arbitrarily low levels, and time averaging can be used to reduce noise on shorter time scales.

The quantity that is directly measured in experiments is the applied gate voltage. We would like to relate this to scaling of the memory effect in the metallic regime. The scaling of the memory effect is determined by the ratio of the chemical potential $\delta\mu$ and the temperature T. Therefore we must appropriately relate the voltage and change of the chemical potential.

Consider a sample of thickness W, geometric capacitance per unit area C and three-dimensional density of states ν_{3d} (see Fig. C.1). We wil show that, according to our model, the width of the memory peak ΔV should scale as

$$\Delta V = \frac{eWT\nu_{3d}}{C}. \tag{C.6}$$

Importantly this does not depend on the screening length, independent of the relationship between W and the screening radius r_s.

In the limit where $W \ll r_s$ the answer is obvious and we consider the limit $W \gg r_s$. From electrostatic considerations the two dimensional screening charge density that must accumulate on the surface of the sample is $V \cdot C$. The charge distribution is determinined, in a self consistent Thomas-Fermi approximation, by the local chemical potential $\delta\phi(x)$. This obeys,

$$\nu_{3d} \int dx\, \delta\phi(x) = V \cdot C, \tag{C.7}$$

However the sample we are considering is two dimensional in the diffusive sense, $W \ll \ell_\phi$. Therefore, an electron will wander over the thickness of the material in a single measurement.

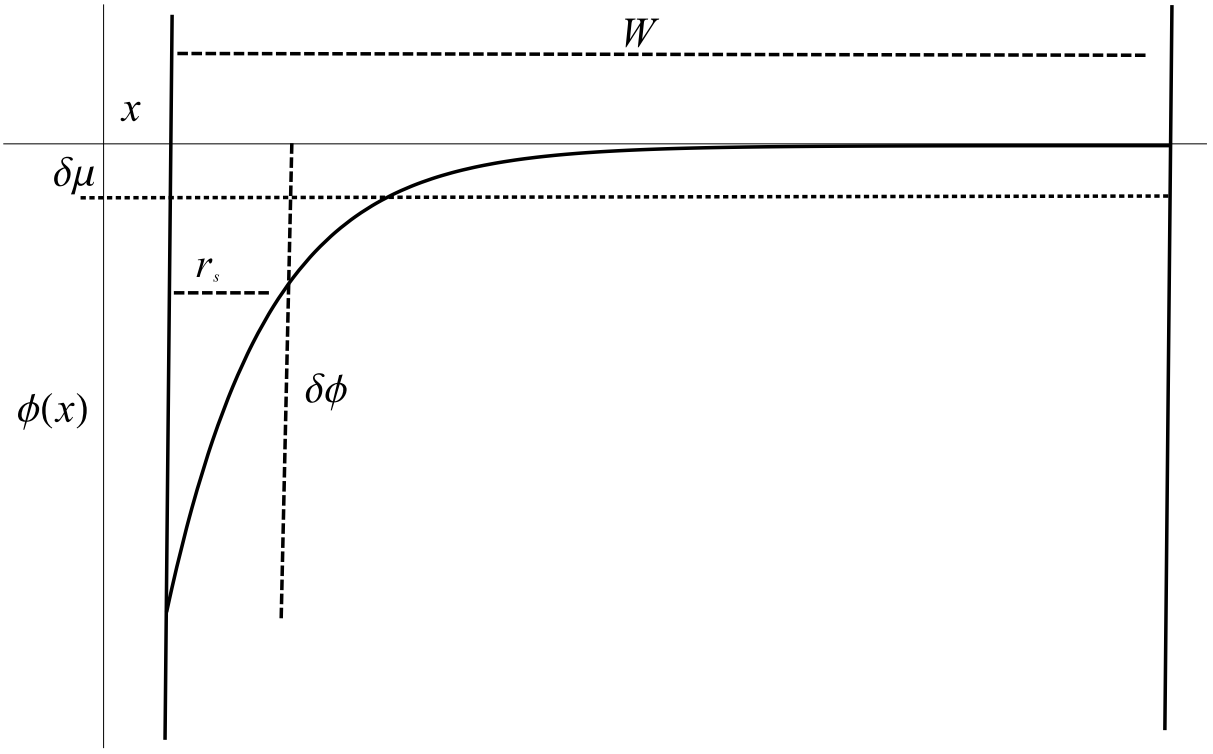

FIGURE C.1: Sketch of the electrochemical potential $\phi(x)$ as a function of position x in the transverse direction of the sample.

So the quantity that matters is not the electrochemical potential in the screening layer, but the electrochemical potential *averaged over the entire sample*, (or equivalently the zero transvere modes of the diffuson). Calling this average electrochemical potential $\delta\mu$, we have that

$$\delta\mu = \frac{1}{W}\int dx\, \delta\phi(x) = \frac{VC}{\nu_{3d}W}. \tag{C.8}$$

Combining the scaling $\delta\mu \sim T$ and Eq. (C.8) we obtain Eq. (C.6).

Appendix D

Hydrodynamics in the narrow resonance limit

The purpose of this supplementary section is to obtain explicitly express the parameters of the hydrodynamic description [Eqs. (2) – (3) of the main text]. We restrict ourselves to the two-dimensional case, $D = 2$, in the narrow resonance regime,

$$\eta \equiv \lambda\sqrt{n}\left(\frac{n}{m}\right)^{-1} \ll 1. \tag{D.1}$$

Moreover, we will consider the position of the resonance ε_b near the critical one ε_b^c as discussed in the main text.

We begin with the Hamiltonian density (1) of the main text, setting all the gauge fields to zero.

$$\begin{aligned}\hat{H} = b^\dagger\left(\frac{-\nabla^2}{4m} - \varepsilon_b\right)b + c_\sigma^\dagger\left(\frac{-\nabla^2}{2m}\right)c_\sigma \\ + \frac{\lambda}{2}\left[bc_{\sigma_1}^\dagger\tau^y_{\sigma_1\sigma_2}c_{\sigma_2}^\dagger + h.c.\right].\end{aligned} \tag{D.2}$$

As we are dealing with two-dimensional systems, all the observable quantities expressed via the bare parameters of the Hamiltonian contain logarithmic divergences, however, the relations between different observables are free of such divergences. To illustrate this point, we note that the quantity ε_b is not the observable location of the resonance. We may calculate the physical resonance E_r, by computing the correction to the energy of one b particle at zero momentum

due to the excitations of two virtual fermions:

$$\delta\Pi(\omega) = -\lambda^2 \int \frac{d^2k}{(2\pi)^2} \frac{1}{\frac{k^2}{m} - \omega} = -\frac{m\lambda^2}{4\pi} \ln\left(\frac{\Lambda}{\omega}\right), \tag{D.3}$$

where Λ is an unphysical high energy cutoff.

The physical location of the resonance is determined by the self-consistency equation

$$E_r = -\epsilon_b - \frac{m\lambda^2}{4\pi} \ln\left(\frac{\Lambda}{|E_r|}\right), \tag{D.4}$$

where Λ is some high-energy cut-off. The value of E_r is an observable position of the bound state at $E_r < 0$ and the position of the resonance at $E_r > 0$.

We proceed to calculate the properties of the ground in the in the saddle point approximation, which is valid in the narrow resonance regime. We take the spatially homogeneous ansatz

$$b = \Delta/\lambda \in \mathbb{R}. \tag{D.5}$$

and introduce the thermodynamic potential density so that

$$E_{GS}(n) = \Omega(\mu) - \mu\partial_\mu\Omega(\mu), \tag{D.6}$$

where $\mu(n)$ is found from

$$n = -\partial_\mu\Omega(\mu). \tag{D.7}$$

The the thermodynamic potential $\Omega(\mu)$ is found as the ground state of the mean-field version of the Hamiltonian (D.2)

$$\begin{aligned} \hat{H} = &-(2\mu + \varepsilon_b)\frac{\Delta^2}{\lambda^2} + c_\sigma^\dagger \left(\frac{-\nabla^2}{2m} - \mu\right) c_\sigma \\ &+ \left[\frac{\Delta}{2} c_{\sigma_1}^\dagger \tau^y_{\sigma_1\sigma_2} c_{\sigma_2}^\dagger + h.c.\right]. \end{aligned} \tag{D.8}$$

After Bogoliubov rotation of the fermion operators in Eq. (D.8), we have their spectrum for small k and small μ is

$$\begin{aligned} \epsilon(k) &= \left[\left(\frac{k^2}{2m} - \mu\right)^2 + \Delta^2\right]^{1/2} \\ &\approx |\Delta| - \frac{k^2\mu}{2m|\Delta|} + \frac{k^4}{8m^2|\Delta|}. \end{aligned} \tag{D.9}$$

Comparing (D.9) with Eq. (3b) of the main text we see that the critical point ϵ_b^c is determined by $\mu = 0$. Since we are investigating the vicinity of the region around this critical point we can restrict ourselves small μ limit.

The thermodynamic potential at zero temperature is given by,

$$\begin{aligned}\Omega(\mu,\Delta) &= (-\varepsilon_b - 2\mu)\frac{\Delta^2}{\lambda^2} \\ &+ \int \frac{d^2k}{(2\pi)^2}\left\{\frac{k^2}{2m} - \mu - \left[\left(\frac{k^2}{2m} - \mu\right)^2 + \Delta^2\right]^{\frac{1}{2}}\right\} \\ &\approx (-\varepsilon_b - 2\mu)\frac{\Delta^2}{\lambda^2} - \frac{m}{4\pi}\Delta^2 \ln\left(\frac{\sqrt{e}\Lambda}{\Delta}\right) + \mathcal{O}(\mu\Delta) \\ &= (E_r - 2\mu)\frac{\Delta^2}{\lambda^2} - \frac{m}{4\pi}\Delta^2 \ln\left(\frac{\sqrt{e}|E_r|}{\Delta}\right) + \mathcal{O}(\mu\Delta),\end{aligned} \tag{D.10}$$

where in the last line the physical resonance E_r from Eq. (D.4) is used to obtain the expression free of the logarithmic divergences.

Minimizing Eq. (D.10) with respect to Δ gives,

$$E_r - 2\mu = \frac{m\lambda^2}{4\pi}\ln\left(\frac{|E_r|}{\Delta}\right),$$

with the resulting expression for the fermionic gap

$$\Delta(\mu) = \Delta(0)\exp\left(\frac{8\pi\mu}{m\lambda^2}\right);\ \Delta(0) = |E_r|\exp\left(-\frac{4\pi E_r}{m\lambda^2}\right) \tag{D.11}$$

and the thermodynamic potential

$$\Omega(\mu) = -\frac{m}{8\pi}\Delta^2(\mu); \tag{D.12}$$

Varying μ and enforcing Eq. (D.7), we obtain

$$n = \frac{2\Delta^2(\mu)}{\lambda^2} \tag{D.13}$$

and the equation of states (D.6) as

$$E_{GS}(n) = \frac{mn\lambda^2}{16\pi}\ln\left(\frac{n\lambda^2}{2e\Delta_0^2}\right); \tag{D.14}$$

As noted above the critical detuning $\epsilon_b^c(n) = -E_r$ is defined by $\mu = 0$. Equations (D.11) and (D.13) give

$$\epsilon_b^c(n) = -\frac{m\lambda^2}{4\pi} \ln\left(\frac{\sqrt{2}\epsilon_b^c(n)}{\lambda\sqrt{n}}\right)$$

which with the logarithmic accuracy yields.

$$\epsilon_b^c(n) = \frac{m\lambda^2}{4\pi} \ln\left(\frac{2^{3/2}\pi}{\eta}\right) \tag{D.15}$$

The values of the remaining parameters entering into Eq. (3b), thus are [see Eq. (D.9)]

$$\Delta = \frac{\lambda\sqrt{n}}{\sqrt{2}},\ \alpha = \frac{1}{4m\Delta},\ \beta = \frac{1}{8m^2\Delta}. \tag{D.16}$$